ABSTRACT

Title of Document:    THE EFFECT OF COLLAGEN ORGANIZATION ON
                      TENSILE STRENGTH LOSS IN ANTERIOR
                      CRUCIATE LIGAMENT GRAFTS POST-
                      RECONSTRUCTION SURGERY

                      Team LEGS
                      Ayushi Chandramani
                      Matthew G. Costales
                      Benjamin C. Garbus
                      Joseph D. Hartstein
                      Kelley M. Heffner
                      Rupal S. Jain
                      Kelly M. Klein
                      Alicia N. McDonnell
                      Payal V. Patel
                      Victoria L. Stefanelli
                      Jenny Wang
                      Joseph T. Weinberg
                      Tina Zhang

Directed By:          Dr. Adam Hsieh, Bioengineering
                      Hyunchul Kim, Bioengineering

Grafts used for anterior cruciate ligament (ACL) reconstructions fall short of restoring native mechanics. This study investigated a morphological cause for tension loss by comparing native ACL and two common grafts, bone-patellar tendon-bone (BPTB) and semitendinosus/gracilis hamstring tendon (ST/G), in a cadaveric system. Tension loss during continuous passive motion was quantified via force transducer. Microstructural changes were assessed by measuring collagen crimp angles. No significant differences were found for rates of percent tension loss relative to total tension loss among grafts. However, all groups displayed exponential decay, implying rapid tension loss. The crimp angles for the unstressed grafts were significantly different from each other, suggesting innate differences. The percent

change experienced by stressed grafts, normalized to their unstressed baselines, showed that ST's crimp behavior was significantly different from that of ACL and BPTB, implying the BPTB graft is superior for ACL reconstruction because it better mimics the ACL's morphological behavior.

THE EFFECT OF COLLAGEN ORGANIZATION ON TENSILE STRENGTH
LOSS IN ANTERIOR CRUCIATE LIGAMENT GRAFTS POST-
RECONSTRUCTION SURGERY


By


Team LEGS

Ayushi Chandramani
Matthew G. Costales
Benjamin C. Garbus
Joseph D. Hartstein
Kelley M. Heffner
Rupal S. Jain
Kelly M. Klein
Alicia N. McDonnell
Payal V. Patel
Victoria L. Stefanelli
Jenny Wang
Joseph T. Weinberg
Tina Zhang


Thesis submitted to the
University of Maryland, College Park,
in partial fulfillment of the requirements of the
Gemstone Program,
University of Maryland
2012

Advisory Committee:
Dr. Adam Hsieh, Chair
Dr. Jae Kun Shim
Dr. Yu Chen
Dr. James C. Dreese
Dr. Robert C. Gillis
Andrew C. Merkle
Dr. Stephen Fahey

# ACKNOWLEDGEMENTS

# TABLE OF CONTENTS

# LIST OF FIGURES

# CHAPTER 1: INTRODUCTION

Each year approximately 175,000 anterior cruciate ligament (ACL) reconstruction surgeries are performed in the United States, costing over 2 billion dollars (Spindler & Wright, 2008). Despite the high incidence of ACL tears and high cost of ACL reconstruction, the surgical procedure for repair is far from perfected.

For a surgery that is so frequently employed, there is surprisingly no standard methodology. Many aspects of ACL reconstruction fall under the surgeon's discretion—for example, the graft material, fixation method, force and flexion angle during pre-tensioning, etc. (Woo, Wu, Dede, Vercillo, & Noorani, 2006). Therefore, there is no general consensus among doctors or researchers regarding the ideal ACL reconstruction procedure. As a result, surgical repair of the ACL leaves much to be desired, as it is unable to restore the normal range of movement, or laxity, in the knee (Woo et al., 2006).

There exists a direct correlation between *in situ* ACL graft tension and knee laxity. Therefore, when the tension in a patient's ACL graft decays, they will likely experience knee instability- the exact symptom which an ACL reconstruction surgery is intended to eliminate (Arnold, Lie, Verdonschot, de Graaf, Amis, & van Kampen, 2005). Knee instability is a serious medical issue that has a large influence on both athletic capabilities and the potential for further serious knee injury. The main purpose of the ACL is to restrain valgus torque and anterior translation of the tibia when the knee is fully extended. Without proper knee stability, this restraining mechanism cannot function optimally, preventing an athlete from executing movements as precisely as they would otherwise (Kakarlapudi & Bickerstaff, 2000).

More importantly, lack of proper restraint within the knee significantly increases one's chances of sustaining further knee injury. Notably, knee laxity associated with ACL deficiency has been shown to lead to chondral damage, meniscal tears, and subsequent laxity of other tendons and ligaments in the knee. These secondary injuries increase a patient's chances of developing osteoarthritis (Kakarlapudi & Bickerstaff, 2000).

Normally, the ACL's purpose is to prevent anterior-posterior translation in the knee joint during knee flexion. It functions in concert with the medial collateral ligament (MCL) and the posterior cruciate ligament (PCL) to ensure that the knee remains stable during a walking motion. The ACL is the most lax at around 40 to 50 degrees of flexion and is most tense at full flexion of the knee joint.

Injuries to the ACL, usually in the form of tears or ruptures, are more often seen in athletes. Sometimes damage to the ACL is accompanied by injury to surrounding knee ligaments as well. The classic clinical entity of O'Donoghue's "unhappy triad," for example, describes tearing to the medial meniscus and the medial collateral ligament, as well as the ACL (O'Donoghue, 1950; Shelbourne & Nitz, 1991). However, ACL injuries are the foremost cause of knee instability—the "giving-out" symptom seen in many knee injuries.

Most ACL injuries are due to a non-contact mechanism (70-80%), versus a contact mechanism, in which an injury occurs due to a force from another athlete (e.g. a tackle during football) (Boden, Dean, Feagin, & Garrett, 2000). ACL damage is usually caused by stress applied in a highly abnormal fashion in comparison to the normal functioning of the ligament. Non-contact stresses include abrupt deceleration

3

before a change in direction or landing motion, which results in axial compressive forces (Boden, Sheehan, Torg, & Hewett, 2010). Contact stresses occur during valgus strain and collapse of the knee, a deformity wherein the distal part of the leg is turned outwards from the midline of the knee (Boden et al., 2000).

In terms of demographics, females are more likely to suffer an ACL injury than their male counterparts in cutting and jumping sports (Dugan, 2005). They have a two- to eight-fold higher incidence of injury, with common injuries due to deceleration or valgus collapse (Toth & Cordasco, 2001; Quatman & Hewett, 2009, Dugan, 2005). The rationale behind the vulnerability of women to ACL injury is still unknown, though different sex hormones and neuromuscular imbalances have been considered (Dugan, 2005).

An important property of the ACL is that it does not change its length over the course of flexion and extension of the knee joint. This is an essential factor when determining the type of tissue that will be chosen to replace the ACL when it becomes damaged. The dominant criterion is that the graft tissue reproduce the stress-strain relationship of the ACL rather than mimic the exact spatial placement in the knee (Wheeless, 2011).

A material is defined as viscoelastic if it exhibits a different stress-strain relationship when it is being loaded as compared to when it is being unloaded (Appendix M: Glossary). The two main characteristics of viscoelasticity are viscoelastic creep and stress relaxation. Viscoelastic creep occurs when the strain in the tissue changes while the stress applied to the tissue remains constant. Stress relaxation occurs when there is a change in the stress in the tissue over time under a

constant situation of strain. Stress relaxation is more applicable to our study because once the ACL graft is implanted into the knee it does not stretch out significantly. Therefore, the strain remains fairly constant, but the stress decreases over time (Oza, 2006).

One of the properties that makes ligaments and tendons unique is their stress-strain loading profile. Rather than exhibiting a linear profile as in elastic tissue, the ligaments demonstrate a nonlinear concave "toe" region followed by a linear elastic region and concluding in a concave down region. The nonlinear toe region results from the crimped structure of the tissue. When the structure is unloaded, all of the crimps are wavy, but as it becomes loaded, the crimps begin to stretch, causing an increasing strain rate. This behavior ends when all the crimps have straightened out (Hansen, Weiss, & Barton, 2002).

At present, the factors responsible for the deficiency in biomechanical function in reconstructed ACL grafts are poorly understood. Prior studies have observed a dramatic loss of tensile strength in grafts post-reconstruction under cyclic loading, leading to excess knee laxity (Arnold et al., 2005). This phenomenon indicates that initial graft tension is expected to deteriorate. However, the extent of this degradation is insufficiently identified across different graft types. As such, the present study hopes to help bridge this gap in research and answer the following research question. In comparing the most common ACL grafts, namely bone-patellar tendon-bone (BPTB) and double-bundle semitendinosus and gracilis hamstring (ST/G), how does the rate of tension loss of each graft type compare to the normal tension loss of the native ACL under continuous passive motion (CPM)?

Our research assumes that the graft, which upholds tensile strength after mechanical loading, will prove to be the most viable option. Clinically, there are many perceived advantages and disadvantages to both the BPTB and ST/G grafts. Since the BPTB graft is taken from the middle one-third of the patient's intact BPTB, the advantage of such a graft is that it closely resembles the ligament that is being replaced. In addition, the graft can be easily attached to both bones where the ACL normally attaches. Such "bone to bone" attachment is believed to allow for more reinforced healing. However the disadvantage of using BPTB includes a high incidence of post-operative anterior knee pain during motions such as bending and kneeling (Rubinstein & Shelbourne, 1994).

The ST/G graft is comprised of two hamstring tendons that are bundled together, and hence avoids the removal of patellar tendon or bone. Whether the semitendinosus tissue is sufficient to construct the graft or whether gracilis tissue is needed as well falls to the judgment of the surgeon. Therefore, in this paper, the hamstring graft will always be referred to as ST/G to describe both possible forms. The anatomical advantage of the ST/G graft is that the tissue is taken from the posterior leg, reducing the amount of resulting anterior knee pain. However, the primary difficulty with ST/G is that it requires fixation of the graft to the bone tunnels, often using small interference screws (Eriksson, Anderberg, Hamberg, Olerud, & Wredmark, 2001).

Due to the lack of consensus, the type of graft falls under the surgeon's discretion, and the surgeon's choice often depends on their preferred procedure or the patient's situational factors. This study hopes to look at graft choice in a more

quantitative and objective manner through ranking the graft types by how well they retain tension and thus ensure stability of the knee.

This study also endeavors to address the lack of research focused on investigating the cause of tension loss in ACL graft tissues. Some studies have indicated that varying rates of tension loss may be due to differences in graft collagen organization. Collagen fibrils arrange in a crimping pattern along the longitudinal length of the ligament (Bontempi, 2009). While both ligaments and tendons have bundles of collagen fibrils grouped in a parallel fashion, the fibrils in ligaments are arranged in crisscrossed layers, which maintain integrity and reduce elasticity or tension loss. Tendons instead are composed of collagen fibrils that are parallel and twisting, allowing for greater movement compared to ligaments (Franchi et al., 2008; Franchi et al., 2009; Franchi, Ottani, Stagni, & Ruggeri, 2010).

These basic structural properties may provide a morphological basis for biomechanical performance. In a normal ACL, crimp elongation enables resistance to higher mechanical stress without permanent deformation (Freeman, 2009). Differences in crimp patterns among different graft tissues signify a relationship to the functional mechanical strength of connective tissue (Franchi et al., 2009). However, previous studies have not employed a loading procedure to model patient knee movement post-reconstruction surgery. Thus, we investigated how morphological differences in collagen crimping patterns relate to the observed differences in tension loss due to mechanical loading.

We hypothesized that the micro-structural organization of collagen was related to the rates of tension loss among the BPTB, ST/G, and ACL grafts. Collagen

organization was assessed by histological invasive and non-invasive imaging methods. Grafts with more extensive crimping were expected to maintain tension due to a greater ability to endure mechanical stress. Grafts with excess laxity after CPM were predicted to express a marked difference in morphology, such as an increase in crimp top angles and base lengths (indicating elongation).

In the following pages, the effect of collagen organization on the tension loss of grafts used for ACL reconstruction is evaluated. This study used a combination of biomechanical testing and imaging to study the structure-function relationship of ACL grafts, including native ACL, BPTB, and ST/G. As previously stated, the purpose of the biomechanical testing was to compare the rates of tension loss among graft types. After imaging sections of graft tissue, image analysis was used to correlate changes in crimp angle with the graft performance during testing.

The results of biomechanical testing showed no significant difference in rates of percent tension loss relative to total tension loss among the three graft types. However, all grafts displayed exponential decay, implying rapid tension loss. In regards to morphological analysis, the results suggest that BPTB grafts may perform better after reconstruction. BPTB grafts most closely mimicked the behavior of the native ACL when comparing normalized changes in crimp angle between the unstressed and stressed conditions. Furthermore, the ST grafts showed an increase in crimp angle, which implies that they may approach failure more quickly. We cannot draw any concrete conclusions, however, as the tissues were not stressed to failure in our experiment.

Throughout the process of completing our experiment, we experienced many

obstacles, particularly in the imaging methodology. The graft tissue was difficult to work with because the tissue was highly prone to shredding (fragmented, unusable slices of tissue). In addition, we experienced setbacks when it came to actually characterizing the tissue morphology using optical coherence tomography (OCT) and brightfield light microscopy (BLM). Although BLM turned out to be more promising than the less well understood OCT, the BLM images we obtained varied greatly in terms of how much crimping could be observed.

The document below reviews the relevant research literature related to ACL reconstruction surgeries, outlines the biomechanical and imaging methodologies, details the experimental results, and analyzes the results through the process of formulating conclusions. Finally, limitations and possible future directions of the overall study are presented.

# CHAPTER 2: LITERATURE REVIEW

The ACL is a major component of the knee that prevents excessive anterior translation of the tibia especially during flexion (Arnold et al., 2005). It is the major stabilizing ligament of the knee, connecting the femur to the tibia through the center of knee. However, it is prone to rupture and tear under abrupt twisting forces commonly experienced when pivoting or landing a jump in sports or during physical activity.

Without surgical intervention, a patient may suffer from persistent problems of instability due to the inability of the ACL to heal independently. In ACL reconstruction surgery, the damaged ACL is entirely replaced with a graft tissue. To date, this procedure has had many shortcomings, the primary inadequacy being the high likelihood of developing excess knee laxity due to the tension deterioration of the graft under mechanical loading (Arnold et al., 2005). In other words, the knee may become unstable again after reconstruction because the graft tissue loosens over time and loses its ability to regulate knee movement. For example, in a study of BPTB graft degradation during cyclic loading, graft tension was found to decrease dramatically by 41% during the first 500 cycles before finally leveling off at 46% after approximately 1500 cycles (Arnold et al., 2005). Determining the amount of tension loss in all graft types is essential for standardizing the ACL reconstruction procedure.

Prior studies have conducted limited comparisons of multiple grafts under direct loading or cyclic loading outside the reconstructed knee environment, focusing mostly on graft fixation procedures (Blythe, Tasker, & Zioupos, 2006; Gorios et al.,

2001).  Part of our study will test the BPTB and the ST/G grafts—the two preferred graft options for reconstruction of damaged ACLs—under continuous passive knee motion after reconstruction in a knee.  Currently, there is no consensus on which graft maximizes stability and minimizes morbidity post-reconstruction surgery (Biau, Tournoux, Katsahian, Schranz, & Nizard, 2006).  While the BPTB graft is considered the "gold standard procedure," the ST/G graft is gaining popularity as a common alternative at the discretion of the surgeon.  The main advantage for the BPTB graft is a faster rehabilitation time; this is mainly because initial attachment is stronger due to the presence of bone plugs within both the femoral and tibial bone tunnels.  However, BPTB grafts are also noted for causing a significant amount of donor site morbidity which results in sever pain and difficulty kneeling for several months following reconstruction surgery  (Rubinstein & Shelbourne, 1994).  Conversely, in a study conducted by Eriksson et al. (2001), the ST/G graft presented with lesser donor site morbidity and overall fewer short-term post-operative problems as compared to reconstruction with BPTB based on patient performance in the Lachman test and one-leg hop test.   In reviewing past and present literature, researchers have heavily debated the benefits of either graft type, leading to no definitive conclusions.

Since the ACL reconstruction methodology is highly variable, a singular optimal procedure must be chosen to allow a comparison between both graft types. Our literature review will discuss the basis for our decisions regarding procedural specifics.  One such mechanical variable that is usually under the surgeon's discretion is the pre-tensioning force applied to the ACL graft and the angle of knee flexion at which the force is applied.  Currently, surgeons in the field utilize a range of pre-

tensioning protocols ranging from 20 to 80 N at 0 to 25 degrees of flexion (Amis &

Jakob, 1998).  Pre-tensioning is required in order to restore normal knee laxity and

stability.  However, there are several differing opinions on how much tension should

be applied.  In accordance to the study testing ACL graft tension after cyclic knee

motion conducted by Arnold et al. (2005), this study chose to precondition the grafts

at 30N tension for 20 minutes.

### *ANATOMY & MICROSTRUCTURE OF THE ANTERIOR CRUCIATE LIGAMENT*
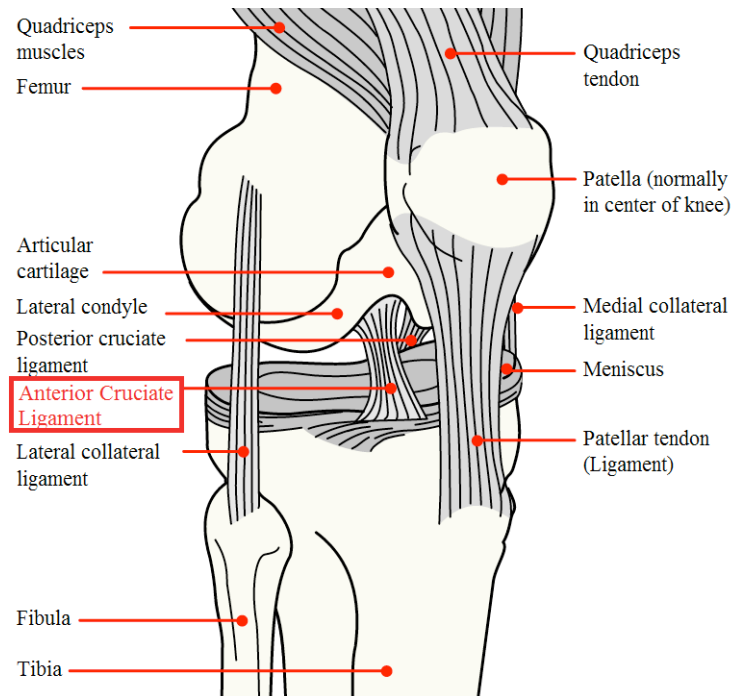


*Figure 1.* Basic anatomy of the knee. The ACL is highlighted in red.

The ACL connects the posterior aspect of the medial surface of the lateral

femoral condyle to the fossa in front of and lateral to the anterior tibial spine (Figure

1).  The tibial attachment is slightly wider and therefore, slightly stronger than the

femoral attachment.  In summary, the ACL travels through the joint in the anterior,

medial and distal directions from the femur to the tibia, before turning in a slight

lateral spiral (Arnoczky, 1982).  The spatial orientation of the ACL allows for the ligament to perform its main function: resisting anterior translation of the tibia with respect to the femur.

A synovial fold covers the ACL and provides vasculature yet the ACL is almost completely avascular and receives very little blood supply compared to other bodily tissues.  Thus, healing in the knee joint is considerably slower compared to the healing speed of more highly vascularized tissues in the human body.  The entire knee joint capsule is filled with synovial fluid, which acts as a lubricant to reduce friction between the articular cartilage of the tibia and femur during flexion and extension of the knee.
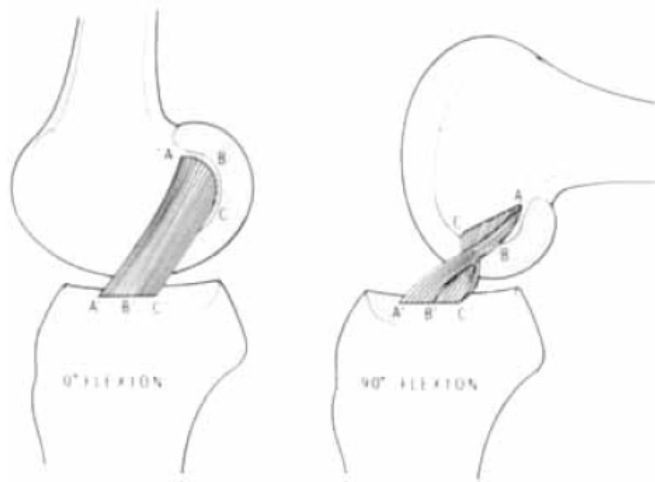


*Figure 2*. ACL during extension and then flexion of the knee.  A-A' is the AMB.  C-C' is the PLB (Arnoczky, 1982).

The ACL is composed of thick, wavy collagen fiber bundles sheathed in loose connective tissue, sometimes showing an alternating fascicular array that is either transverse or oblique to the long axis of the ligament.  These individual fascicles make up the ACL and can be divided into two basic bundles: the anteromedial band (AMB) and the posterolateral band (PLB).  This division is based on the general

function of the bundle during knee extension and flexion. In simple term, when the knee is extended, AMB is relaxed while the PLB is tight, and when the knee is flexed, the AMB tightens while the PLB is relaxed as seen in Figure 2 above. In any position of the knee, some portion of the ACL is under tension (Arnoczky, 1982). Thus, there is a certain amount of pretension in the ACL in its natural, healthy state within the body.

Two types of collagen fibrils exist in the ACL. Of the fibrils, 50.3% have a non-uniform diameter (25-85nm; peaks at 35, 50, 75 nm) and irregular outline. The other 43.7%, on the other hand, are characterized by a uniform diameter (45nm peak) and smooth margins. Wavy collagen bundles, arranged in various directions, predominate around the axis of the ACL and fibroblasts elongate in the direction of these bundles (Strocchi, 1992). The ACL is structured to withstand multi-axial stresses and tensile strains due to its varied orientation of bundles, complex ultra-structural organization, and abundant elastic system.

Due to the orientation of the fibers of the ACL, the ACL is weak against lateral rotational movements, which are common in many sports. These types of movements can strain and, more often, tear the ACL. A mid-substance ACL tear cannot heal like most other tendons and ligaments, and does result in a moderate to severe disability depending on the strength of the patient's surrounding supporting musculature.

The absence of the ACL can result in excessive translation of the tibia in relation to the femur, causing the knee to buckle and give way (Woo et al., 2006). This greatly increases the chance of further damage to other tissues within the knee,

especially the menisci and articular cartilage (Daniel et al., 1994).  ACL reconstruction is therefore highly recommended by surgeons.

## GRAFT TYPES



(A)                                                                          (B)
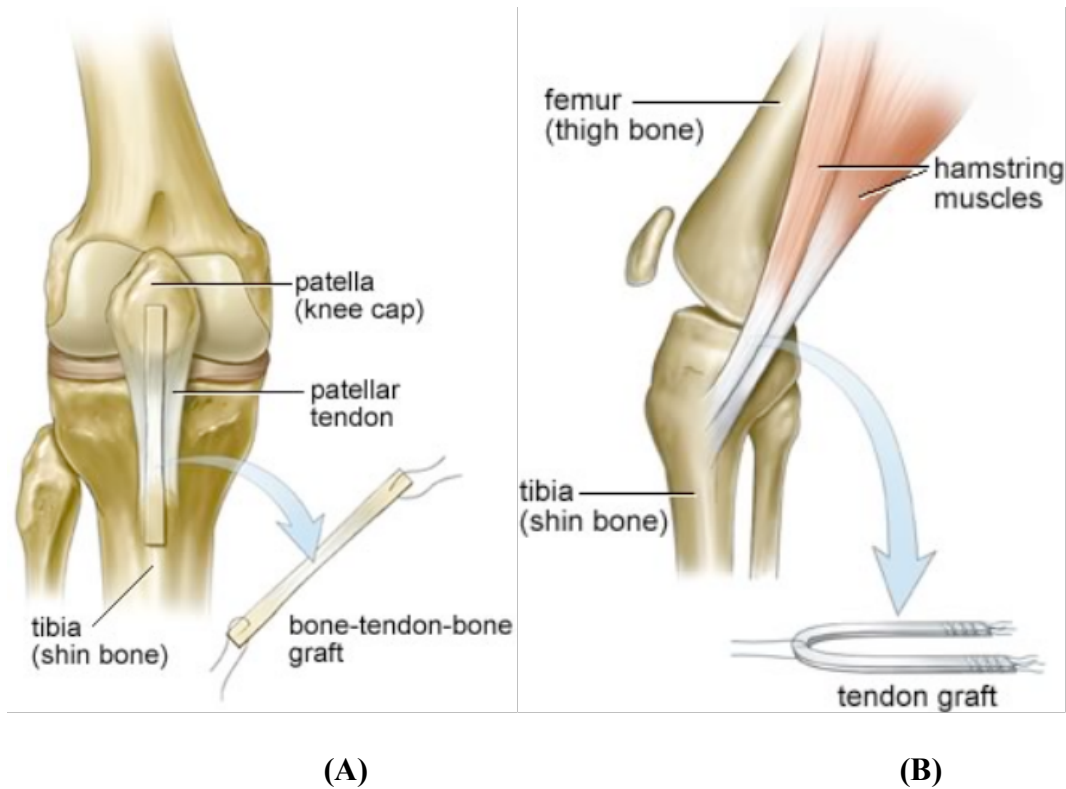
*Figure 3*. (A) Bone-patellar tendon-bone (BPTB) graft.  (B*)* Hamstring graft.  The hamstring graft is usually a bundle of semitendinosus and gracilis muscle (Sohrab, Smith, & West, 2011).

The most common grafts used in ACL reconstruction are the bone-patellar tendon-bone (BPTB) and the semitendinosus and gracilis (ST/G) hamstring grafts (Figures 3A and 3B, respectively).  The BPTB autograft was once referred to as the "gold-standard" for ACL reconstructions.  The normal function of the patellar tendon is to coordinate with the quadriceps and other various muscles to help extend the leg.

The graft harvest generally involves excising the middle third of the patellar tendon, including small portions of the bone at which the tendon is attached, called

bone plugs (Figure 4). These bone plugs allow for a much stronger graft fixation and lends to stronger overall graft strength. However, the excision procedure often results in patello-femoral-joint problems, patellar fracture, or even rupture of the patellar tendon (Liu, Kabo, and Osti, 1995).
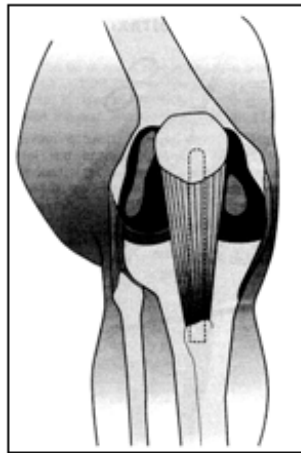


*Figure 4*. BPTB excision. Region of the BPTB to be excised in graft harvesting (Pinczewski, Roger, & Scranton Jr., 1998).

More recently, the ST/G hamstring graft has become increasingly popular since there is no resulting graft site morbidity found with the BPTB graft. In its normal location in the human body, the semitendinosus muscle acts in the back of the thigh as a part of the hamstrings to help extend the hip joint, flex the knee joint, and medially rotate the knee. The gracilis muscle, also part of the hamstrings, helps with much of the same movements as the semitendinosus muscle such as flexing the knee and medially rotating the leg when the knee is flexed.

To obtain the ST/G graft, the semitendinosus and gracilis tendons are taken from the hamstring muscle and braided together to form a strong ACL graft (Figures 5A and 5B). However, the ST/G hamstring graft does not have the advantage of possessing bone plugs and thus, has weaker graft fixation strength (Liu, Kabo, and

Osti, 1995). In addition, loss of knee flexor strength is very common after reconstruction with an ST/G grafts.
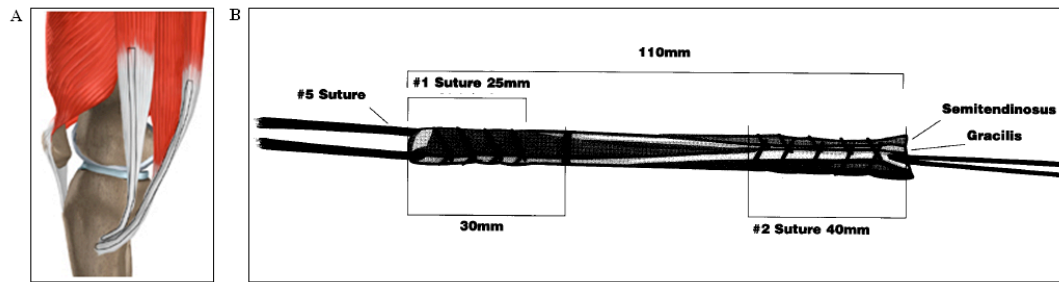


*Figure 5.* ST/G excision. (A) Locations of the ST/G tendons for extraction, and the (B) Resulting hamstring graft (Pinczewski et al., 1998).

Nonetheless, most surgeons have made the shift from BPTB to ST/G grafts to avoid the complications of graft site morbidity. And in response to this shift, many efforts have been made to improve the strength of the ST/G grafts, such as the quadrupled ST/G autograft (Woo et al., 2006).

## GRAFT ATTACHMENT METHODS

A review conducted by Dargel, Gotter, Mader, Penning, Koebke, & Schmidt-Wiethoff (2007) compared graft attachment methods and concluded that using interference screws is a commonly accepted procedure for both hamstring and patellar tendon grafts. Interference screws were shown to provide the strongest attachment and are therefore the preferred method for securing patellar grafts in both the tibial and femoral bone tunnels.

For hamstring grafts, washer-plates or sutures were found to be the preferred attachment method in the tibial bone tunnel, though the ultimate failure load for interference screws with hamstring grafts in the tibial tunnel was shown to be 776N. This load is significantly higher than those that will be incurred in this study,

indicating that the interference screw method for hamstring grafts is still feasible (Dargel et al., 2007).

The use of interference screws for both BPTB and ST/G grafts allowed for a uniform graft fixation procedure for this experiment, eliminating graft attachment method as a variable for tension loss. This study focused on biomechanical properties as the possible cause for tension loss in grafts.

## CADAVER KNEE SPECIMEN PREPARATION

In order to accurately replicate the interior environment of the knee joint, it is essential to keep intact as many of the surrounding soft tissues as possible. Connective tissues like ligaments and tendons are especially important as they directly impact the biomechanics of the joint. Other soft tissues such as fat, synovial membranes, and skin are integral for maintaining a fluid balance within and around the ACL, which in turn can affect the ligament's viscoelastic properties. By mimicking the natural state of the knee, this study's findings would be more applicable to a clinical setting.

Necessities of the mechanical testing protocol, however, rendered this ideal of maintaining soft tissue structures throughout the length of the cadaver leg impractical. One basic requirement of the materials testing system (MTS Systems Corporation, Eden Prairie, MN) is a method for obtaining firm fixation of the test specimen to the apparatus without damaging the specimen itself. A low-cost and simple strategy for accomplishing this with human cadaver legs is through the use of bone cement around the distal ends of the appendage. As implied by its name, bone cement

adheres optimally to bone material, and so this fixation process required the removal of soft tissues within the fixation region.

This elicited the following question: how much soft tissue could be removed while still maintaining a realistic environment around the knee joint? Several previous *in vitro* experiments demonstrated varying degrees of importance placed on different soft tissue structures. Studies conducted by Arnold et al. (2005) and Fukubayashi, Torzilli, Sherman, and Warren (1982), took an extreme approach of removing most soft tissues and muscles, which were deemed extraneous. Care was taken to preserve certain structures deemed important for knee stability. Specifically, Arnold et al. (2005) chose to reserve all capsuloligamentous structures, the smaller ligament-like entities grouped around various joints, which provide structural support. Fukbayashi et al. (1982) kept the joint capsule, patella, and distal one third of the iliotibial band intact.

Most other *in vitro* studies kept a larger portion of the soft tissue structures intact. This was accomplished holistically by setting exact length requirements for the preferred amounts of soft tissue that should be maintained. Both Wascher, Markolf, Shapiro, and Finerman (1993) and More and Markolf (1988) resected soft tissues to within ten centimeters of the joint line.

Yet studies by Woo et al. (2002) and Markolf, Wascher, and Finerman (1993) took more cautious approaches, maintaining soft tissues and muscles within twenty and twelve centimeters of the joint line, respectively. These studies noted prevention of dehydration as the major rationale for maintaining such large proportions of the soft tissue structure. For that purpose, More and Markolf (1988) included the

additional measure of wrapping their knees in moistened plastic bags throughout the experiment as a further preventative precaution against moisture loss.

Dr. Bennett, the supervisory orthopedic surgeon for this study, was in concordance with these latter researchers with the need to maintain the majority of soft tissues surrounding the knee (C. Bennett, M.D., personal communication, August 8, 2011).  His assertion was that the precise minimal amounts of soft tissue maintenance required would differ from leg to leg depending on overall size and structure.



**(A)**          **(B)**
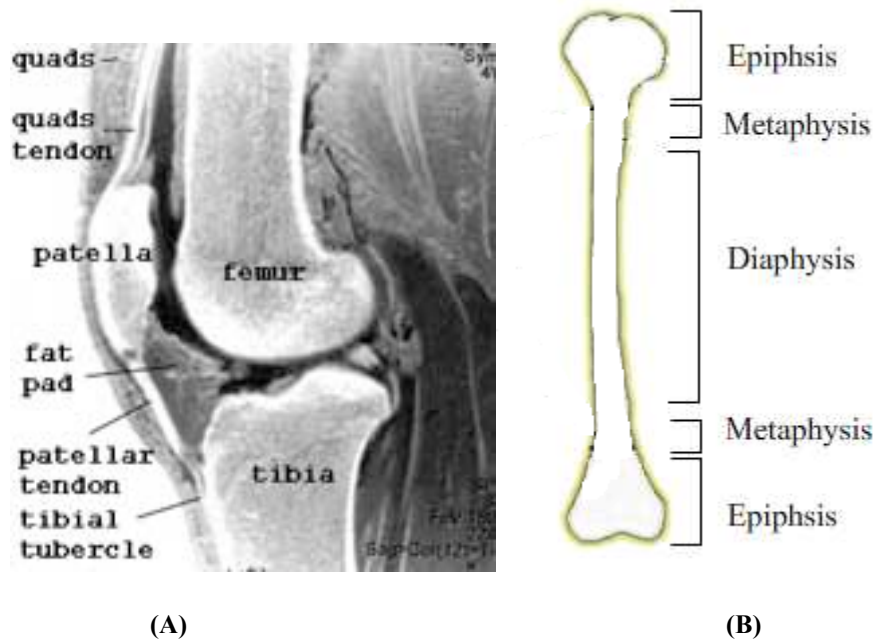
*Figure 6.* Human knee. (A) An MRI image of a human knee, and (B) Drawing of a human femur depicting the relative locations of different bone structures.

His recommendation was that the cut-off points for soft tissue removal should be established based on the location of certain bone structures.  Specifically, within the proximal portion of the femur, enough soft tissue should be maintained so that all of the metaphysis, and at least part of the diaphysis of the femur was covered (Figure 6A).  For the proximal portion of the tibia, tissues up to ten centimeters below the

tibial tubercle should also be maintained (Figure 6B). Beyond these cut-off points, any additional soft tissues maintained would be superfluous, though not detrimental if included.

## BIOMECHANICS OF SOFT BIOLOGICAL TISSUE

### BIPHASIC NATURE

An important concept in describing the viscoelastic nature of soft tissues such as ligaments and tendons is accurately accounting for their biphasic nature. Essentially, tendons and ligaments consist of two separate phases. There is the solid phase, the main components of which are collagen and elastin. There is also the liquid phase in the form of interstitial fluid, which is a mix of water and electrolytes (Holzapfel, 2000; Olberding & Suh, 2006; Özkaya, Nordin, & Leger, 1999). The co-existence and interaction of these two distinct phases is what makes soft tissues biphasic.

The presence of two separate phases must be taken into consideration for a biomechanical analysis, since it has been well established that solid and liquid phases possess fundamentally different responses to mechanical stress. Solid phases typically have an elastic response where the stress is directly proportional to strain, and both of these quantities are time independent. Conversely, fluids possess a viscous nature so that instead of deforming a finite amount in response to stress, they continuously deform, or flow. A particular fluid's viscosity is a measure of how well it resists flow, or its stress response to strain rate, an *ipso facto* time-dependent quantity (Munson, Young, & Okiishi, 2009; Özkaya et al., 1999).

The interaction of the solid and liquid phases within a soft tissue is very complex, with many factors potentially affecting the overall mechanical properties of the tissue. Generally, the solid phase serves as a porous skeletal matrix. The fluid phase flows through this porous matrix, the rate of which is dependent upon the solid's permeability, porosity, and amount of deformation. Of course the viscosity of the fluid itself serves to introduce drag forces into the system. The two phases may be considered immiscible for all intensive purposes, and so altogether, at the microscopic level, soft tissues possess a very heterogeneous makeup (Olberding & Suh, 2006; Wolfgang & Bernd, 2001).
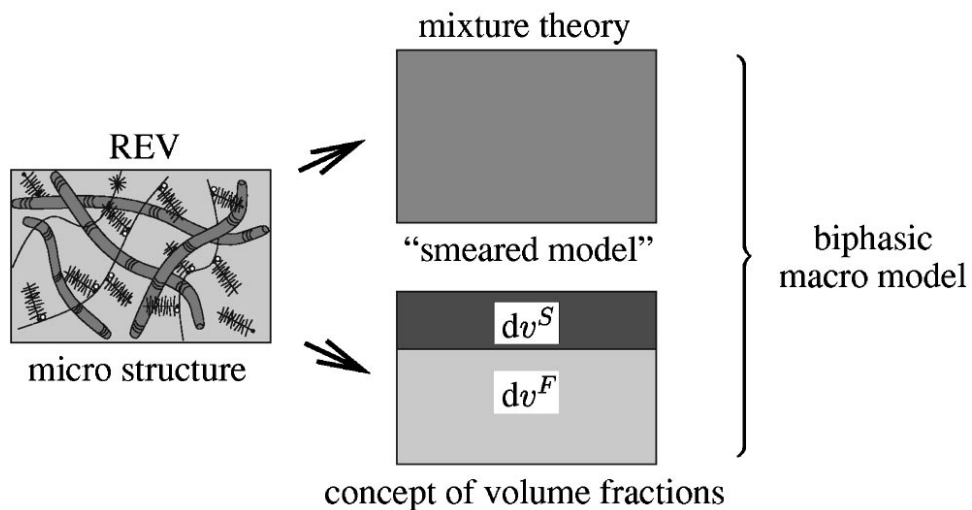


*Figure 7.* Soft tissue properties. Diagram illustrating how the biphasic macro model approximates the properties of soft tissues by averaging the properties of components of the tissue microstructure (Wolfgang & Bernd, 2001).

To accurately describe the mechanical properties of such a heterogeneous system at the macroscopic level, it is therefore necessary to adopt a theory that accounts for soft tissues' biphasic nature. One such theory is called the Biphasic Poroelastic Theory, or the Theory of Porous Media (Figure 7). This theory specifically describes immiscible, non-deformable superimposed continua with

internal interactions that can be defined through a combination of theories used for mixtures, fluid dynamics and volume fractions. Basically, for any given representative volume element, this theory aims to establish an average of constituent properties based on the densities and volume fractions of the given constituents. The result is a homogenized or smeared model of mechanical properties which applies only to the given volume element (Olberding & Suh, 2006; Wolfgang & Bernd, 2001).

A key take-away from Biphasic Poroelastic Theory is its dependence on the volume fractions of each constituent. The mere presence of water in the system effectively raises the osmotic pressure, therefore increasing the overall mechanical stiffness of the tissue. It should be noted though, that while the overall amount of the solid phase in soft tissues may be constant, the volume of the fluid phase is much more dynamic, which can significantly shift the overall ratio of the volume fractions. Sources of variation in tissue fluid volumes include innate tissue composition, the health of the tissue itself, and environmental factors. Geometrical considerations such as tissue orientation and positioning also affect fluid content, as fluid loss occurs most quickly at the surface of a tissue, compared to at its interior (Olberding & Suh, 2006; Wolfgang & Bernd, 2001).

In summary, the fluid content of a tissue determines the comparative volume fractions of its constituents, which in turn allows for an averaging of intrinsic mechanical properties for the development of a homogenous model, which can then be used in the macroscopic description of that tissue's deformation. Specifically, this implies that higher water contents in soft tissues are generally correlated with stiffer

mechanical properties.  Therefore, to accurately compare the mechanical properties of any two soft tissues, it is essential to keep their hydration levels as consistent as possible (Özkaya et al., 1999).

**EFFECTS OF THE FREEZE-THAW CYCLE ON BIOMECHANICS**

Many biomechanical studies use cadaveric specimens and tissue for use in procedures.  The main method for preserving tissues is by freezing them for storage and thawing them before use.  However, the use of frozen storage on tissues in biomechanical studies is important, since freezing may affect essential properties of the tissue in question.  Therefore, the effect of freezing and thawing cycles on the elasticity and tensile strength is significant for any study in biomechanical analysis of any tissue.

A study by Goh et al. (2010) tested the effects of frozen storage temperature on tendon elasticity in mice.  Two common temperatures, -20°C and -80°C, for freezing were tested.  Mechanical properties of frozen tendons in the tail of the murine model (C56BL6 mouse) were investigated.  The maximum stress ($\sigma$), stiffness (E), strain ($\varepsilon$), strain energy density (u), and strain energy density until rupture ($u_P$), were the specific variables examined.  In comparison to the control tissue, the tendon frozen at -20°C revealed no effect on any variables.  On the other hand, the tendon that was frozen at -80°C resulted in higher values for maximum stress, stiffness, and strain energy density.  The values for strain and strain energy density until rupture remained unaffected.  The implications from this report was that if under the correct conditions, not under -20°C, then frozen tissue would maintain its bioelasticity and stiffness after being thawed from its frozen state (Goh et al., 2010).

A study by Huang, Zhang, Sun, Zhang, and Tian (2011) examined the effect of multiple cycles of freezing and thawing on the biomechanical properties of human tendons. The tendons in this study were the flexor digitorum superficialis and the flexor pollicis longus, both of which originate in the forearm and are used for flexing of the fingers. Freezing was done at the temperature -80°C for four days and thawed at room temperature for 6 hours. Groups underwent freeze-thaw cycles of either 1, 2, 3, 5, or 10 multiples, which was then followed by testing using a materials testing machine. The results showed that groups that underwent 3 or less cycles had similar performance to the fresh control group.

However, the tendons that underwent 5 cycles or greater displayed smaller ultimate loads, stiffness, stress and Young's modulus. Young's modulus is a measure of stiffness that is defined as the ratio of uni-axial stress over uni-axial strain for the range of stress that follows Hooke's Law. This study suggests that repetitive freezing-thawing cycles of greater than five cycles would have a deleterious effect on the structural and viscoelastic properties of human tendons (Huang et al., 2011).

Instead of tendons, Jung et al. (2011) studied the effect of multiple freeze-thaw cycles on the bone-patellar tendon-bone allograft. The BPTB graft is one of the frequently used grafts for ACL reconstructions. Three groups were put under 1, 4, or 8 freeze-thaw cycles at -20°C for more than six hours and 22°C for at least six hours. Afterwards, specimens were exposed to cyclic loading between 50N and 200N for 100 cycles and then loaded to failure. The results revealed similar properties of creep, tangent modulus, and ultimate load between the freeze-thaw groups and the fresh control groups. Therefore, there would be little measurable effect between the

frozen and unfrozen BPTB grafts in their biomechanical properties under the correct care (Jung et al., 2011).

Another study attempted to evaluate the mechanical modifications brought on by freezing and thawing on human tendons in vitro. Both the BPTB and STG autografts were tested. After being taken from fresh cadavers, half of the samples were tested immediately and the others were deep-frozen and then thawed. Using a materials testing machine, a relaxation test and uniaxial tensile test were performed. These tests were used to obtain the ultimate tensile failure and the elastic modulus of the each pair of tissues. It was found that freezing had no influence on the tendinous relaxation of the tendons. However, there was a large change between the frozen and unfrozen pairs of tendons in the ultimate tensile failure and Young's modulus. (Clavert et. al., 2007).

## ANTERIOR CRUCIATE LIGAMENT REPLACEMENT SOURCE VARIABLES

In performing a biomechanical comparison of patellar tendons and hamstring tendons, the overall goal is to compare intrinsic tissue properties such as elasticity, tensile strength, and ultimate strength. To objectively analyze these properties, however, it is important to recognize that they may potentially be influenced by outside variables such as age, gender, activity level, and disease state of the person from which the tendons were taken. In an ideal experimental protocol, each of these variables would be controlled. Since this is not always feasible, however, it is therefore important to understand how tendon biomechanical properties may be dependent upon each of these variables.

**AGE**

Up through twenty years of age, humans are still considered to be in a maturation stage from a biomechanics perspective. During this time, the quality and amount of cross-links within and among the collagen molecules composing tendons and ligaments tends to increase. These cross-links are directly correlated to tissue strength, and so throughout this maturation phase, human tendons and ligaments develop a greater overall tensile strength (Hashemi, Chandrashekar, & Slauterbeck, 2005; Nordin & Frankel, 2001).

Once matured, collagen's biomechanical properties become consistent and remain that way until old age, at which point tissue tensile strength and elasticity may decrease. It is possible that this late-life mechanical decline is influenced by cardiopulmonary, vascular, and osteoarthitic medical conditions. Generally though, when the ACL from healthy donors of average age 30 are compared to ACLs from healthy donors of average age 65, it is found that there is no statistical significance in the variation of mechanical properties, such as tissue strength, elasticity, and strain (Nordin & Frankel, 2001).

Several studies of the patellar tendon in particular have shown that there is no significant correlation between donor age and the tendon's mechanical properties. In one study, 82 freshly frozen bone-patellar tendon-bone grafts from 25 different persons aged 17 to 54 were uni-axially stressed until failure. It was found that for multiple different strain rates, there was no correlation between age and mechanical properties, including that of tensile strength, failure mode, and elastic modulus (Blevins, Hecker, Bigler, Boland, & Hayes, 1994).

Another study compared mechanical properties of the patellar tendon from donors aged 18 to 55 using a 10% strain rate. While it was noted that there was a small decline in tendon tensile strength in older donor specimens, no significant correlation between age and mechanical properties, including elongation, failure stress, tensile elastic modulus, and tensile stress was found (Flahiff, Brooks, Hollis, Vander Schilden, & Nicholas, 1995).

## GENDER

Hashemi, Chandrashekar, and Slauterbeck (2005) tested twenty unmatched human patellar tendons from ten men and ten women for tension in an attempt to examine relationships between gender and mechanical properties. No evidence of gender-derived differences was found for ultimate tensile strength, strain energy density, or elastic modulus (Hashemi et al., 2005).

## HEALTH FACTORS

A variety of health conditions have been shown to influence the mechanical properties of collagen-based structures in the human body. Patients with diabetes mellitus have been shown to possess stiffer tendons, a fact which would most directly influence mode of tendon failure (Nordin & Frankel, 2001).

Long-lasting corticosteroids can hinder the collagen synthesis process and therefore negatively impact tendon failure strength, stiffness, and energy absorption. Conversely, non-steroidal anti-inflammatory drugs (NSAIDs) have been shown to increase tendon mechanical strength. Examples of NSAIDs include acetaminophen, aspirin, and indomethacin (Nordin & Frankel, 2001).

Finally, there is a correlation between renal failure and tendon degradation. Long-term hemodialysis patients have been shown to have hyperlaxity and excessive elongation in both tendons and ligaments (Nordin & Frankel, 2001).

## ACTIVITY LEVEL

Similarly to bone, both ligaments and tendons are dynamic in the sense that they are capable of responding to mechanical demands placed upon them and restructure accordingly. Generally, a person who is active places high mechanical demands upon their tendons and ligaments, and the soft tissue structures respond by becoming stronger and stiffer. Conversely, immobilized persons tend to possess tendons and ligaments that are weaker, less stiff, and elongate more easily (Nordin & Frankel, 2001).

In an example of extreme immobilization, primates were placed in body casts for eight weeks. Afterwards, they were shown to have a 39% decrease in maximum ACL failure load, and a 32% decrease in the amount of energy stored until failure (Nordin & Frankel, 2001). Similar patterns of degradation may be seen in other extreme immobility instances including that of bed-ridden patients and paralysis patients.

## INFLUENCE OF TISSUE CADAVERIC SITE

In order to make real-world conclusions from a cadaveric biomechanics study, it is imperative to understand the differences that exist between cadaveric and healthy *in vivo* ligaments and tendons. The main relevant factors are the differences of vascularization as well as the ability of a live human body to mount an inflammatory reaction to outside disturbances and subsequently remodel a damaged area.

Following reconstruction surgery, there is an attempt by the body to incorporate the ACL graft into the body and to restructure it so that it is optimized for its new biomechanical function. Such a process is referred to as "ligamentization" (Amiel, Kleiner, Roux, Harwood, & Akeson, 1986). In this study, Amiel et al. (1986) performed both a time-dependent histological and biochemical analysis of rabbits that had undergone ACL reconstruction surgeries with bone patellar autografts. The changes in the autografts post surgery were very gradual, occurring over a period of thirty weeks. In this time, cell morphology became increasingly more ligamentous, a microscopic similarity with normal ACL cells. Further, the concentration of type III collagen, which is not normally found in bone patellar tendons slowly increased to 10% of the total collagen concentration—this is the same frequency seen in native ACLs. It was suggested that these changes were initially fueled by nutrients from the knee synovial fluid and later from revascularization, which generally began six weeks post-operatively.

A follow-up study by Marumo, Saito, Yamagishi, and Fujii (2005) extended the Amiel et al. (1986) study to an analysis of human bone patellar, semitendinosus, and gracilis autografts used in ACL reconstruction surgeries. A total of fifty patients underwent arthroscopic ACL reconstruction with either bone patellar or semitendinosus and gracilis tendons. It was found that total collagen content and crosslink content within collagen molecules increased within four to six months in patients with semitendinosus and gracilis autografts and within 11 to 13 months for patients with bone patellar autografts. These results are synonymous with the process of ligamentization described by Amiel et al. (1986). Autografts increase in

mechanical strength and adapt to become more similar to ACL within one year of the surgery (Marumo et al., 2005).

The essential fact to note with regards to the ligamentization process is that it is a very gradual process occurring over 30 weeks in the Amiel et al. (1986) study and from four to 13 months in the 2005 Marumo et al. (2005) study. So while this process is certainly capable of changing the mechanical properties of tendons, these changes are only measureable after a significant amount of post-operative time. Conduction of mechanical tests on cadaveric tissues immediately following reconstruction surgery, in a time frame of at most two hours following surgery, minimizes any discrepancy that may been seen in a live specimen in the same timeframe due to the ligamentization process.

Another major difference between living and cadaveric tissue is their respective states of vascularization. Autografts typically undergo four main phases of transformation following implantation: 1) avascular necrosis, 2) re-vascularization, 3) cellular proliferation, and 4) remodeling. A decrease in mechanical strength is typically observed during the vascular necrosis stage, although this is largely believed to be due graft fixation techniques.

A study by Rupp, Sell, Kohn, and Muller (2000) examined this exact phenomenon through an *in vitro* mechanical comparison of post-mortem human BPTB specimens obtained within 24 hours of death. BPTB grafts came from 11 different pairs of human knees and were treated according to a vascularized or non-vascularized protocol. It was found that vascularity did not have a significant effect on mechanical properties such as maximum force, stiffness, or elastic modulus of the

tendons. Viscoelasticity in avascularized grafts, however, was shown to be significantly different from vascularized counterparts. Specifically, avascularized specimens showed a significant increase in stress relaxation (Rupp et al., 2000). This phenomenon may be responsible for often observed graft laxity post surgical reconstruction.

While avascularity may significantly affect the viscoelastic properties of tendon grafts, it is essential to remember that the re-vascularization process, like the ligamentization process, is not instantaneous in live human ACL reconstructions. The graft begins to undergo the re-vascularization process at two or four weeks, respectively, in rabbits and dogs (Rupp et al., 2000). The process generally does not begin until about six weeks post-reconstruction surgery in humans (Amiel et al., 1986). Therefore, if mechanical testing is performed immediately following reconstruction surgery, the avascularity is expected to be comparable to that of an autograft of a live human.

### TENSION TRANSDUCER

In order to measure graft tensile strength, a study conducted by Arnold et al. (2005) made use of a tension transducer which measures tensile forces in soft tissues. This tension transducer was implanted in the graft, midway between the femoral and tibial attachment sites by making a small incision. The transducer was then reinforced with sutures.

The device's probe is the shape of an ellipse and is inserted into the tissue so that the long arcs of the ellipse are aligned with the tissue fibers (Figure 8). As these fibers are pulled in uni-axial tension, they squeeze the wings of the probe and, in

doing so, change the intrinsic resistance of the probe. This change of resistance allows a new voltage to be produced from the small current that runs through the probe. It is this voltage value that is relayed to a signal amplifier and software program, which produces a loading profile in real-time (MicroStrain, 2011). Changes in tensile strength of each graft were then compared using data collected during mechanical loading.
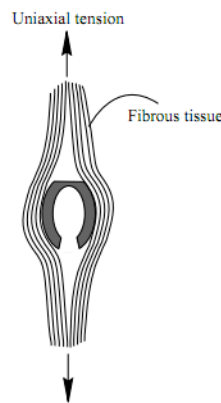


*Figure 8.* Tension transducer. An illustration of tension transducer alignment with respect to tissue fibers (MicroStrain, 2011).

Use of an implantable force probe is a relatively new development, so the reliability and accuracy of such probes have just begun to be investigated. Fleming, Peura, and Beynnon (2000) have previously described variability of sensor output with successive tests using the same implantation site. This variability was attributed partially to the settling or reorientation of the sensor in the graft over time (Fleming et al., 2000).

Another study showed that slit length has an effect on transducer output (Tohyama et al., 1994). Herzog, Hasler, and Leonard (1996) have reported voltage changes of up to 100% for small angular deviations in the sensor placement. Fleming

et al. (2000) have demonstrated errors ranging from 3.7-109.4% due to sensor removal and re-implantation in the same location. Their range of error increased to 1.5-202.8% when re-implanted at a second location (Fleming et al., 2000).

These results suggest that particular attention should be given to sensor placement so that slit length and sensor orientation may be kept constant for all implantations. More importantly, re-implantation of the sensor should be avoided where possible for accurate comparison of different test data.

It should be noted that while the applied tension in this study acts uniaxially within the ACL or ACL graft, these forces are pushing on the force probe transversely. This is certainly a limitation of the probe in that absolute force readings may not coincide with true uniaxial forces. There is also the possibility that transverse forces may partially be a function of tendon cross-sectional area, therefore allowing two tendons of different thicknesses to produce different readings from the same uniaxially applied force.

Nevertheless, a study by Fleming, Peura, & Beynnon (2000) showed that probe specificity was not affected by tissue cross-sectional area. This same study acknowledged that its range of specimen cross-sectional areas was relatively small and so further study on this issue may be needed. These results show that the probe is still an effective tool for investigating percent tension loss even though absolute tension values may contain some error (Fleming et al., 2000).

Use of this implantable probe certainly has its limitations. Nevertheless, currently available methods of measuring in situ tension are also very limited. Most studies that investigate ligament and tendon biomechanics utilize an MTS machine,

which requires removing the tissue specimen from its host and then clamping the ends into specialized MTS machine grips (Freed & Todd, 2005; Blevins et al., 1994; Dargel et al., 2007; Fukubayashi, Torzilli, Sherman, & Warren, 1982). This method, however, does not mimic natural movements of a joint, and therefore it cannot accurately simulate the *in situ* forces that would be expected during such movements.

Woo et al. (2002) devised a more unique method of measuring *in situ* forces knee forces. This method involves placing distal ends of the tibia and femur into a robotic/universal force-moment sensor testing system (UFS). The UFS is capable of up to six degrees of freedom, and it can measure the orthogonal forces and moments of the knee. From these measurements it is able to infer the *in situ* forces of a knee ligament (Woo et al., 2002). This method is significantly more complex than an implantable force probe, and even still, true *in situ* force values must be inferred from indirect measurements.

Traditionally, site-specific force measurements have been taken through the use of strain gauges, which have been developed over a long period of time and have been shown to be very accurate. They may be constructed of a variety of metals and placed in a range of configurations to optimally obtain an accurate strain measurement. If the elastic coefficient and dimensions of the metal used within the gauge are known, then it is possible to accurately calculate force from the measured strain. These gauges, however, require firm mounting on a sturdy, and typically flat surface, and such is not the case in biological studies (Clark, 2010). MicroStrain Inc. (2011), who manufactures the AIFP, is the first company to have configured strain gauges inside of an electronic device that is meant to be inserted within biological

components.  Therefore, while the AIFP certainly possesses limitations, it is currently the most accurate and direct method of measuring *in situ* forces of soft biological tissues while they remain inside natural joint structures.

## *MECHANICAL TESTING OF THE INTACT ANTERIOR CRUCIATE LIGAMENT*

### **ANTERIOR TIBIAL DISPLACEMENT AND *IN SITU* FORCE TESTING**

There have been many studies that have investigated the load-elongation curve using uni-axial testing to obtain stiffness, ultimate strength, and stress-strain data of ACL specimens.  The tools used typically to measure such properties are buckle transducers or load cells, but most traditional tools come into contact with the ACL.  Ideally, forces in the ACL would be best measured while still intact and attached to the tibia and femur.

For the first few months post-reconstruction, the ACL graft is not an integrated part of the body and thus, not receiving any significant amount of blood supply.  As such, researchers have justified using cadaveric knees and donor graft tissue to perform experimental studies.

In one study, a human cadaveric knee was mounted on a robotic testing system.  As seen below in Figure 9, the flesh and soft tissue was kept intact around the knee while the tibia and femur were potted, allowing a robotic manipulator to extend and flex the knee to replicate normal knee motion (Woo et al., 2006).
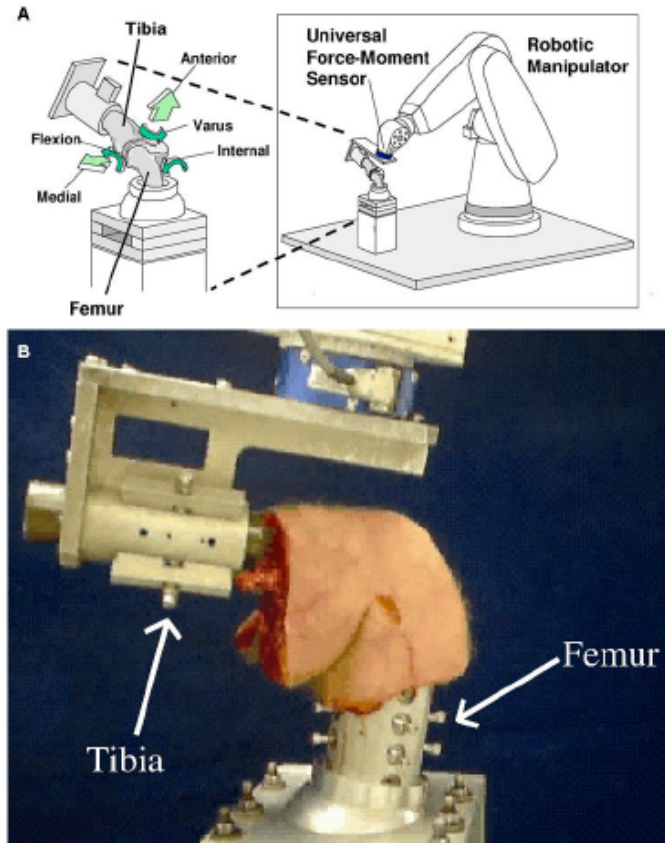
*Figure 9.* Universal force-moment sensor. (A) The robotic/UFS testing system, and (B) The human cadaveric knee specimen mounted on the robotic/UFS system (Woo et al., 2006).

The universal force-moment sensor (UFS) allowed the measurement of *in situ* force vectors of the ACL, which the researchers used to obtain a more thorough understanding of the anteriomedial band and lateromedial (LMB) band. In Figure 10 below, the magnitude of the *in situ* forces of the intact AMB and LMB as well as the ACL are graphed against the flexion angle of the cadaver knee specimen.

One particularly significant finding was that under combined rotator loads of valgus and internal tibial torques, the AMB and posterolateral band (PLB) shared the load evenly at 45 degrees of flexion. Depending on the magnitude of the load, the angle at which the AMB and PLB share the load evenly varies. However, the

presence of this phenomenon implies that the PLB plays an important role in controlling rotary stability of the knee as well tibial translation (Woo et al., 2006).
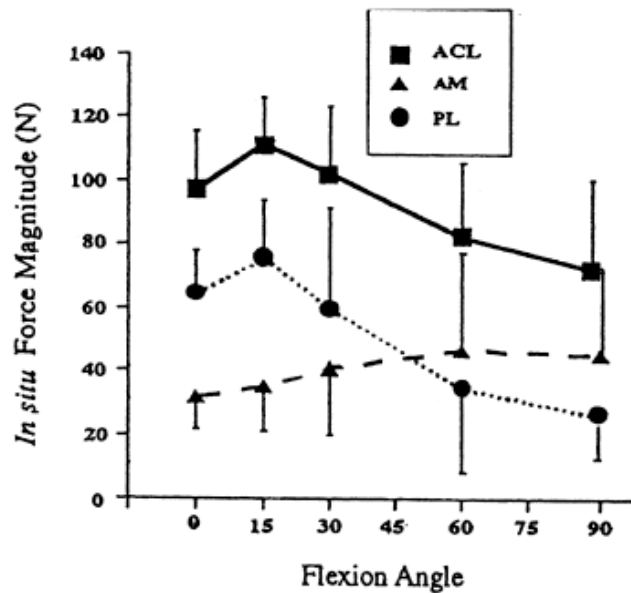


*Figure 10. In situ* forces. A 110 N anterior tibial load was applied at varying flexion angles of the knee, and the resulting *in situ* force was measured (Woo et al., 1998).

In addition, the graph of *in situ* forces in the PLB more closely resembles that of the ACL. This would indicate that ACL reconstruction in which the graft is placed to mimic the PLB would more accurately restore normal knee function and movement. But this data suggests that the ideal method would be to select a graft capable of mimicking both the AMB and PLB, such as a double-bundle graft (Woo et al., 1998).

## MECHANICAL TESTING OF THE RECONSTRUCTED KNEE

### ANTERIOR TIBIAL DISPLACEMENT AND *IN SITU* FORCE TESTING

In addition to testing the intact ACL, Woo et al. (1998) tested reconstructed human cadaveric knees using the quadruple semitendinosus and gracilis (QST/G)

38

graft and then the bone-patellar tendon-bone graft. The reconstructed knees were mounted on the robotic/UFS testing system and resulting *in situ* forces and anterior displacement were measured in response to varying anterior loads and knee flexion angles. Below, in Figure 11, a graph illustrates the percentage of anterior displacement experienced by the reconstructed knees as compared to an ACL-deficient knee (Woo et al., 1998).
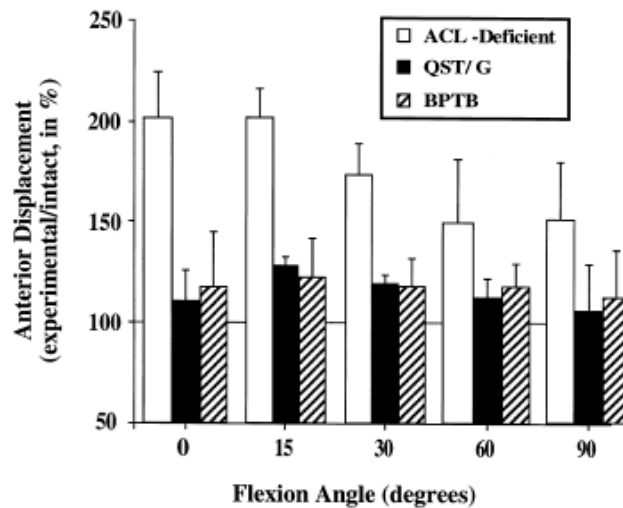


*Figure 11.* Anterior displacement. Anterior tibial displacement expressed as a percentage of the anterior displacement of intact knee, as a function of knee flexion angle (Woo et al., 1998).

From Figure 11, the data suggests that both the QST/G and BPTB grafts perform equally in restraining anterior tibial displacement to normal levels. However, Figure 12 suggests otherwise when comparing the *in situ* forces of the grafts after ACL reconstruction. At low flexion angles, both grafts had similar *in situ* force magnitudes, but at flexion angles greater than 30 degrees, the force magnitudes of the grafts severely decrease.
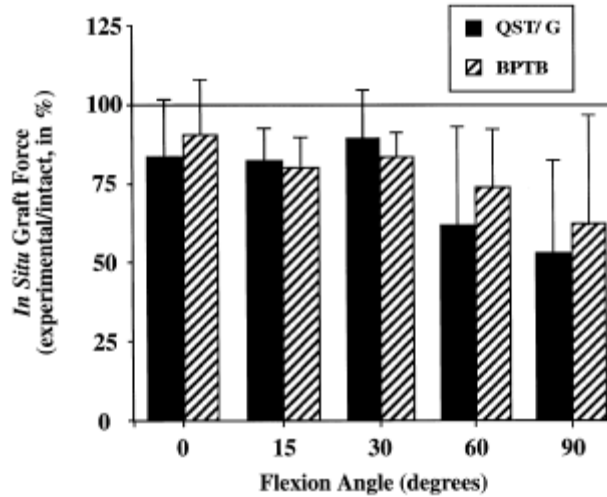
*Figure 12. In situ* forces vs. flexion angle. Magnitude of *in situ* forces expressed as a percentage of the intact ACL, as a function of knee flexion angle (Woo et al., 1998).

Overall, the QST/G graft had *in situ* forces close to those of the intact ACL for a larger range of knee flexion angles but neither grafts had stellar performances. Ideally, an ACL graft should be designed to almost perfectly mimic the intact ACL's function in the knee regarding anterior tibial displacement and rotation restraint as well as *in situ* forces responding to applied tibial load.

## CYCLICAL LOADING TESTING

In a study conducted by Arnold et al. (2005), human cadaver knee specimens were reconstructed with BPTB grafts and mounted in a cyclical flexion-extension motorized rig for 1500 cycles to investigate the graft tension after ACL reconstruction in normal knee motion. A small tension transducer was inserted into the graft at the time of surgery.

The study observed a dramatic loss of tensile strength in grafts post-reconstruction, which causes excess knee laxity. The graft tension was found to

decrease dramatically by 41% during the first 500 cycles, finally leveling off at 46% after approximately 1500 cycles as seen below in Figure 13 (Arnold et al., 2005).
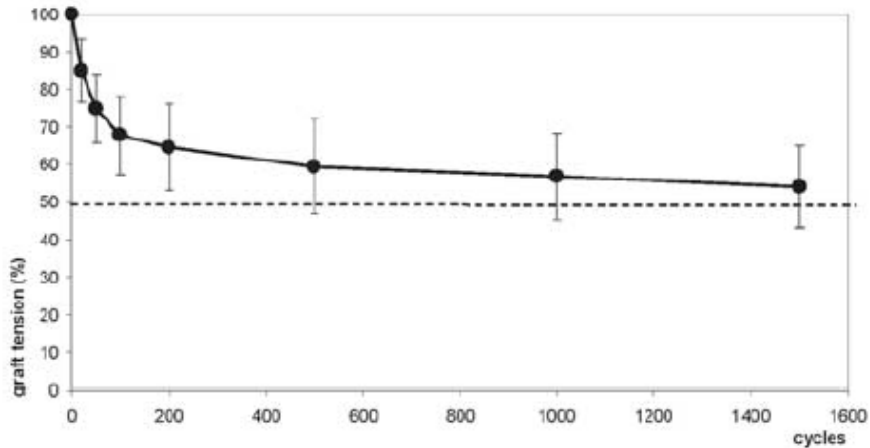


*Figure 13.* Graft tension vs. cycles. Graft tension expressed at a percentage of the initial tension as a function of cycles (Arnold et al., 2005).

This behavior indicates that the initial graft tension at time of surgery is directly related to knee laxity and therefore is a crucial factor in improving the success rate of ACL reconstruction (Friederich & O'Brien, 1998). Determining the extent of tension loss in grafts is essential for standardizing the ACL reconstruction procedure. However, this study did not measure the tension loss in ST/G reconstructed knees or in intact ACL, and from a fairly extensive literature search, no study has yet.

## COLLAGEN CRIMPING

### MORPHOLOGY

The second goal of this experiment is to investigate the cause of ACL graft tension degradation post-reconstruction. Crimping has been observed in collagen fibers from multiple sources. Several studies have indicated that the morphology of

connective tissue, specifically collagen crimping pattern, is related to its biomechanical strength. Collagen fibrils, the structural unit of ligaments and tendons, exhibit a sinusoidal pattern known as crimping which allows a ligament to resist higher mechanical stresses without yielding. Upon closer examination, some studies have described these crimps less as a pure sine curve and more like a zigzag pattern (Diamant, Keller, Baer, Litt, & Arridge, 1972).

Studies involving rotation of collagen fibrils while using polarized light microscopy have shown that crimps are two dimensional, mostly confined to a single plane and not due to fiber twisting. The crimp angles in rat-tail tendon were measured to be between 13.6 and 15.0 degrees and crimp segment lengths were measured to be between 40 and 52 microns (Shah, Jayson, & Hampson, 1979). Another study measured similar crimp angles between 12 and 20 degrees (Diamant et al., 1972).

However, more extensive studies on the collagen fibril patterns show that the microfibrillar arrangement of connective tissue is even more specific and dependent on whether the tissue is subject to multidirectional or unidirectional forces. In the case of tendons and most ligaments, the collagen fibrils are thick (100-300nm) and capable of withstanding a large unidirectional load. Therefore, the collagen fibers mostly run parallel along the direction of stress, but show irregular undulations, or "knots" in some regions of the collagen fibers (Franchi et al., 2010). These knots are formed when the fibrils change direction due to sudden flexion.

Although similar in many ways, there are some differences in the anatomy of ligaments and tendons. These differences were found when the subfibrillar

arrangement of the tissues were studied.  Ligaments tend to have less packed fibrils and also contain some smaller fibrils than tendons.  Whereas larger fibrils in tendons and ligaments have straight subfibrillar arrangement, these smaller fibrils only found in ligaments can have a helical subfibrillar arrangement.  It is thought that these helical subfibrils may be present in ligaments to help the ligament withstand rotation forces that are not seen in tendons.  The differences are logical due to the fact that tendons exist primarily to transmit forces from muscles to bone whereas ligaments connect bones in order to limit motion and may face multidirectional forces (Franchi et al., 2008).

Three-dimensional analysis of the crimping in the large and poorly flexible collagen fibrils of tendons and ligaments shows that the collagen fibrils must "first twist leftwards with respect to the main fibril axis, changing the plane of their running, and then bend, changing the direction of their course in the new plane" (Franchi et al., 2010).  However, it is not yet understood if these knots are a result of a local morphological deformation or whether the undulating region serves as a more flexible region of the otherwise rigid fibril.

## BIOMECHANICAL PROPERTIES

It is believed that this collagen crimping in tendons and ligaments functions in absorbing and transmitting loads as well as in guiding the recoil of collagen fibers (Franchi, Trirè, Quaranta, Orsini, & Ottani, 2007B; Franchi et al., 2008; Raspanti, Manelli, Franchi, & Ruggeri, 2005).  During loading, the crimped fibrils straighten and then return to their original shapes after the stress is removed.  Hansen, Weiss, and Barton (2002) also found that straightening of crimps differed based on crimp

location, with crimp extinction being reached on the outside of the fascicle prior to the inside.

The point where the crimp completely straightens is called the point of crimp extinction (Hansen et al., 2002). Before the point of crimp extinction is reached, a non-linear "toe region" can be observed in the stress-strain curve. Most normal function occurs within this region (Hansen et al., 2002). While in this region, there is less likelihood of injury, because the collagen crimps can absorb sudden changes in tension. However, when the crimps are straight, there is more risk of tearing.

The behavior seen in the toe region can be described mathematically using a model known as 'elastica.' The behavior is dependent upon the modulus of elasticity, the crimp segment length, the crimp angle and the diameter of the fibers (Shah, Jayson, & Hampson, 1979). Studies have found that the elastic behavior of the crimping as seen in rat-tail tendon is reversible at strains under 4%. It was found that at strains over 4% the crimping pattern was affected (Diamant et al., 1972).

Therefore, a minimal amount of crimping is disadvantageous for the ligament as it quickens the progression toward plastic deformation (Franchi et al., 2009). Excessive amounts of strain in human grafts may result in permanent elongation and a perceived loosening of the ligament (Blythe et al., 2006).

Age is another factor that may affect crimp morphology in tendons and ligaments. Several studies have determined that crimp length increases and crimp angle decreases with age in rat-tail tendon. It is thought that there may be a constant crimp frequency in these tendons but that the crimps elongate as the tendon grows longer. Therefore, crimp morphology and biomechanical properties may be

somewhat different based on both the age of an organism and the individual collagen fibril (Diamant et al., 1972).

A study using Sprague-Dawley rats showed that the morphological structures of tendons and ligaments are related to their biomechanical properties (Franchi et al., 2009). Franchi et al. (2009) used polarized light microscopy (PLM) to analyze crimping patterns by determining crimp number, crimp top angle, and corresponding crimp base length in tendons and ligaments.

By staining with Picrosirius Red to stain for collagen, morphological variations in different ACL graft tissues pre- and post- CPM can be analyzed and the underlying causes of their biomechanical performances can be determined.

## OPTICAL COHERENCE TOMOGRAPHY

However, in PLM, specimen preparation compromises the tissue integrity and therefore cannot be conducted before mechanical testing of the grafts (Franchi et al., 2009). As such, a noninvasive imaging modality is required to analyze tissue morphology on grafts to be reconstructed and mechanically loaded. In a study conducted by Hansen et al. (2002), OCT was used to study rat-tail fascicles. The purpose of this study was to evaluate the feasibility of analyzing crimp patterns and to observe changes in crimping with applied stress. Fascicle crimping was observed and the crest and trough of each crimp could be seen in real-time, which allowed the successful measurement of a crimp's period length (Hansen et al., 2002).

OCT is an imaging technique that creates an image by measuring the echo delay and magnitude of light reflected back (Fujimoto, 2003). Though similar to ultrasound, OCT has a higher resolution and depth (Andrews et al., 2008; Li et al.,

2009).  The image resolution of OCT ranges from 1-15μm: standard resolution is 10-15μm, while laser light sources can provide an image resolution of 1-5μm.  OCT generates cross-sectional images of tissue limited to a depth of 2-3mm (Fujimoto, 2003).  In order to visualize tendon morphology at multiple levels of specificity, OCT will be used to analyze fascicle collagen crimping while PLM will allow measurement of collagen fibril crimping in graft tissues.

OCT is a relatively new medical imaging technique with current application especially in the fields of ophthalmology and dermatology. The first *in vitro* OCT images were presented in 1991 (Huang et al., 1991A). Shortly after, the same group determined the diagnostic potential for OCT in distinguishing between atherosclerotic plaque and a normal coronary arterial wall (Huang, Wang, Lin, Puliafito, & Fujimoto, 1991B). Currently the most widespread use of OCT in medical imaging is in visualizing structures of the eye including the cornea, sclera, iris, and lens anterior capsule (Izatt et al., 1994). OCT is now able to measure the retinal thickness, "the anterior chamber depth, the anterior chamber angle, the radii of curvature of the cornea, the corneal refraction power, the corneal thickness, and the thickness of the epithelial layer," which can be used to diagnose pathologies of the eye (Fercher, 1996).

In recent years, OCT application has been expanded to soft tissue studies pertaining to our research interest in tendons and ligaments of the knee. As soft tissue abnormalities are difficult to detect with current medical imaging modalities, OCT was used in a study to detect anatomical changes of the cochlear soft tissue in hearing impaired mice (Gao et al., 2011). This study however used freshly excised mouse

cochlea to visualize several structures that could not be studied *in vivo* with OCT. Although the study verified that measurement of lengths and angles of the tympanic membrane was possible with *in vitro* OCT, the visual hindrance of the cochlea due to surrounding otic bone suggested that *in vivo* imaging would be difficult even with surgical access. In addition to blocking visual accessibility, the otic bones are also highly scattering, impacting the quality of OCT image produced (Gao et al., 2011).

In another pioneering study applying OCT to more widespread fields of medicine, Chen et al. (2009) investigated OCT as a future neuroimaging tool to detect hemodynamic changes in response to somatosensory stimulation in rats. The limitation of OCT *in vivo* as a human medical diagnostic tool is again demonstrated as preparation of the rats involved "thinning the skull with a dental burr until transparent (Chen et al., 2009)."

The combined results of brightfield microscopy and OCT will allow for a comparison between pre- and post- mechanical loading images in order to determine how crimping changes simultaneously with tension loss. As it is a relatively new imaging technique, OCT has not yet been implemented to analyze collagen crimp patterns in the ACL, BPTB or ST/G grafts in relation to orthopedic research.

## *LIMITATIONS*

As OCT is a relatively new imaging technique in the medical field, and moreover in the orthopedic field, our OCT results were largely inconclusive. Our study was limited by accessibility the intact ACL due to the anatomy and location of the ACL within the knee. Despite our effort to expose the ACL with a medial parapatellar athrotomy, only a segment of the intact ACL was exposed due to

interference from the fat pad, femur, tibia and surrounding ligaments. Since OCT has roughly a depth of 2-3mm, it was necessary for the OCT probe to reach the ACL by means of removal of surrounding fat. Although we aimed to use OCT as a non-invasive technique to compare collagen crimping pre- and post- loading, visualizing the ACL required compromise of the structural integrity of the knee.

In addition to the problems experienced with OCT, analyzing images obtained from brightfield microscopy proved to be difficult. Our goal was to view crimp patterns with brightfield microscopy, but what we realized after looking at the images was that it was hard to distinguish exactly what parts of the images were crimps. Some images also looked like they contained no crimping patterns, so they could not be used for our analysis of the crimp angles.

Slides that were created by sectioning blocks embedded with tissue were used for microscopy, so the issues that arose with the images were probably derived from the initial tissue processing and fixation methods. The grafts were cut into small pieces for blocking, and this cutting was not regulated in terms of plane or angle. Where the pieces were cut along the length of the grafts was also not regulated, which may be the reason why crimping was differentially present in different slides. The grafts were fixed in formalin both before the cutting process and after they were cut into smaller pieces for three weeks total and then placed in ethanol until the tissue was ready to be blocked. Both under-fixation and over-fixation can be harmful to tissue and can actually prevent the tissue from maintaining its original morphology. Although we chose to fix for three weeks based on fixing recommendation and

previous literature, there may have been a possibility that the fixing may be the cause of some tissue damage.

Following fixation, the tissue was processed.  If tissue is fixed incorrectly, it can turn hard and brittle after processing, which can ultimately result in poor sections. During many of the instances in which we sectioned the tissue, we noticed that the tissue was shredding and quite brittle.  This may have been due to inadequate fixation.  Something could have also gone wrong in the tissue processor machine, since we cannot manually control what substance the tissue is placed in and for how long.

Many of the steps taken before the imaging portions of our experiment may have contributed to the poor images we obtained from brightfield microscopy.  Even though we tried to troubleshoot various portions of the procedure in order to produce the best outcomes, our images still did not turn out ideally in some cases. Nonetheless, some tissue has produced promising images that we can use for our analysis of crimping.

# CHAPTER 3: METHODOLOGIES AND METHODS

## *OVERVIEW OF EXPERIMENTAL METHODOLOGY (APPENDIX A)*

Starting materials consisted of ten human cadaver legs, which were divided into five sets of matched pairs. A matched pair is a right and a left leg belonging to the same person, and for all intents and purposes, the condition and structures of each leg in a matched pair should be close to identical. In addition to these ten legs, five matched pair bone-patellar tendon-bone grafts and five matched pair semitendinosus and gracilis hamstring grafts were obtained, excised, and created from cadaver legs provided by the Musculoskeletal Transplant Foundation (MTF). All tissue grafts were also grouped into sets of matched pairs.

All starting materials were divided into two groups: the control and the experimental group. Divisions were purposefully made so that one half of each matched pair went into each group. Careful attention was also made towards ensuring that the splitting of each matched pair was randomized so that the right and left halves of a matched pair had equal chance of being assigned to the control or experimental group.

Once all the starting materials were split, ACLs were immediately removed from the legs in the control group so that these ACLs were never stressed. They served as baseline measures. The ACLs in the experimental group were kept inside of the legs while the legs were stressed. Only after this stress by the MTS machine were the ACLs removed.

All ten of the cadaver legs had had their ACLs removed, and they were therefore ready for reconstruction surgeries. The legs were again divided into two groups so that half of the legs were reconstructed with ST/G grafts and the other half were reconstructed with BPTB grafts. The grafts were similarly randomized for the split between the control and experimental groups as the ACL. This meant that the left or right half of the matched pair had an equal chance of either being reconstructed in the leg, to be stressed, or to be left unstressed as a baseline. Following each reconstruction the leg would be stressed, and following this stress, each ACL graft—either ST/G or BPTB—was removed.

At this stage of the methodology there existed a total of thirty tissue specimens, half of which had been stressed and half of which had never been stressed. All tissue specimens were then subjected to an identical imaging methodology that consisted of two separate modalities. The first imaging modality consisted of OCT, which is a very non-destructive imaging method in that it does not damage or change the structure of the tissue being imaged in any way. Following OCT each tissue sample was analyzed via light microscopy. Light microscopy is a very destructive imaging method because the tissue must first be fixed and then sliced; due to this tissue damage the light microscopy imaging modality came last in the experimental methodology.

Standard operating procedures (SOPs) of the methods described below can be found in Appendix F.

## EXPOSING THE ANTERIOR CRUCIATE LIGAMENT

A medial parapatellar arthrotomy was performed to expose the intact ACL. An anterior midline incision approximately 15 to 20 cm in length was made above the patella, cutting through the skin and subcutaneous tissue. This incision exposed the patella, patellar tendon, quadriceps tendon and vastus medialis oblique. The arthrotomy then began with an incision on the medial border of the quadriceps tendon, approximately 3 to 5 cm from the top of the patella. This incision continued parallel to the medial border of the patella, and to the medial border of the patellar tendon, approximately 5-10cm from the bottom of the patella. Special care was taken to avoid damaging the ACL.

Once past the patella, the incision through the medial border of the patellar tendon was bone-deep. The infrapatellar fat pad was then removed, and the patella was shifted to the lateral side of the leg, exposing the inside of the knee joint. Finally, the ligamentum mucosa was removed to fully expose the intact ACL. All intact ACLs were imaged via OCT before undergoing either brightfield light microscopy or mechanical testing.

## MATERIALS TESTING SYSTEM ATTACHMENT & FIXTURE CONSTRUCTION

A materials testing system consists of a piston, which can move up and down repeatedly in a vertical motion. It is possible for the experimenter to control the amount of piston displacement, the rate of that displacement, and the force with which the piston moves with a great amount of precision.

In order to utilize such a machine for the purpose of this study, several design requirements were necessary so that the relevant forces experienced by the ACL

during mechanical loading could be analyzed. First, the leg needed to be loaded and secured into the MTS machine. Second, the leg needed be able to bend in such a way that it mimicked the motion of a knee placed in a continuous passive motion machine, as used by patients after reconstruction surgery. Though the CPM machine is no longer a standard of care post-surgery in recent years, surgeons and physical therapists do encourage patients to exercise the leg in a similar fashion (J. Dreese, personal communication, March 31, 2012).



*Figure 14*. MTS machine fixture. Photograph of a test leg loaded into the MTS machine fixture and attached to the MTS machine at a moment of flexion during the mechanical loading protocol.

In order to translate the vertical motions of the MTS machine into a biomechanically accurate knee-bending profile, it was necessary to create a novel MTS machine attachment fixture (Figure 14). This fixture was dimensioned so that each half could rigidly be fixed into the model of MTS machine that existed in the lab. The fixture itself consists of two pinned joints attached to the distal ends of the tibia and femur that act as hinges between these ends of the leg and the MTS machine.

Loading of a leg into the fixture requires first potting the distal ends of the femur and tibia in bone cement. This method of attachment also serves to prevent the concentration of stress on a single location of the bone ends. The bone pots are what needed to be mounted to the top and bottom of the MTS machine load cells in a manner that permitted free rotation.

Although several designs were considered, the simplest option that still achieved the desired loading motion was chosen. This design consisted of placing a rod through the bone cement, and rotating the bone around that rod in the form of a pinned joint. The rod was the key part of the apparatus, as it allowed the bone pot to rotate while also connecting the bone pot to the MTS machine attachments at the top and bottom.

When designing and implementing the MTS machine fixture, the top and bottom MTS machine attachments needed to coordinate with the locations of the screws at the top and bottom load cells. Additionally, the bone pots necessitated room to rotate through their full range of motion. The material chosen for the fixture was Ultra-High Molecular-Weight polyethylene (UHMWPE), a material commonly

used in orthopedics because of its high strength-to-weight ratio and its ability to self-lubricate (Ridout Plastics, 2011).

The top and bottom attachments were U-shaped and composed of a 3"x4" base plate and two 3"x3" side plates (Figure 15). The holes that matched the MTS machine screw holes were drilled first. Next, the side plates were attached with L shaped brackets on the inside of the U. To ensure that the attachments were flush with the MTS machine, the edges of the screw were often cut and sanded down. To allow the bone pots to rotate without friction, two ball bearings were set into each side-plate of the U-shaped attachment, a square inset was milled out of UHMWPE, and ball bearings were glued in.
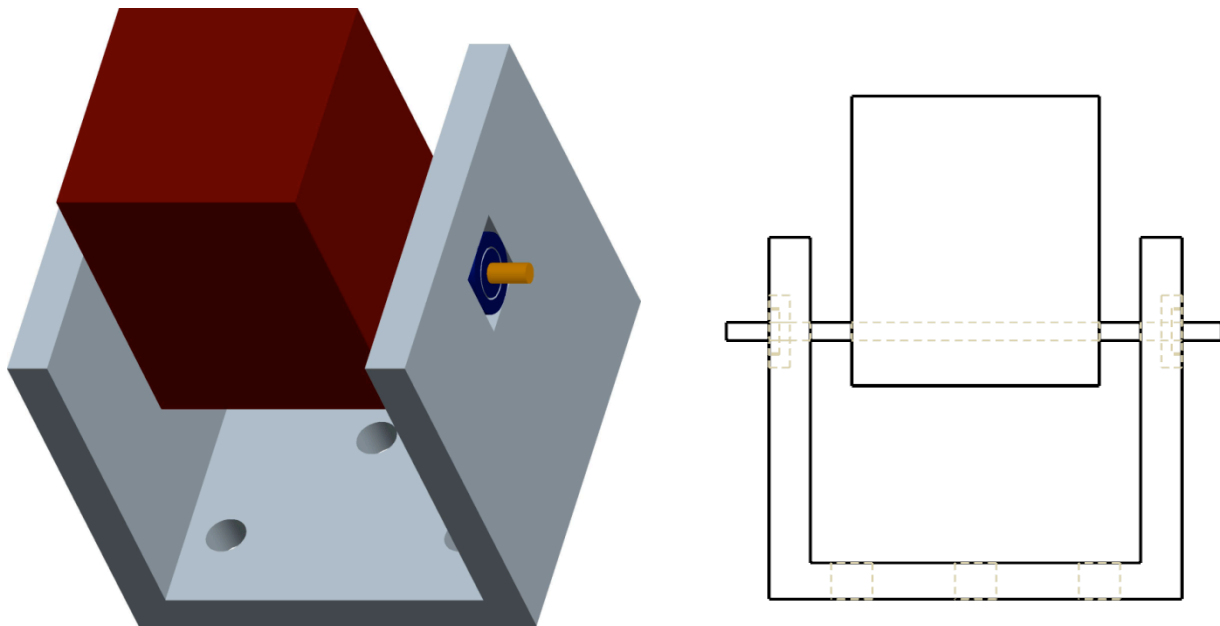


*Figure 15.* Fixture assembly. Angled computer-angled design (CAD) drawing of MTS machine fixture assembly with bone pot shown in red, U-shaped fixture in grey, rod in gold, and ball bearing in blue (left). Front view of this same MTS machine fixture assembly (right).

## POTTING PROCESS

In order to keep the leg fixed while being tension tested with the MTS machine, the legs were secured with bone cement. First the 3"x3" bone cement mold was assembled using tape to seal all cracks, so the liquid phase of the cement would not pour out. A rod was inserted into a metal sheath that was placed in the bone cement mold through a hole drilled in the side. The femur end of the leg was then placed into the 3"x3" bone cement mold.

Using an approximately 1 gram to 15-milliliter ratio of Fastray™ white powder to water, a slurry was made. This slurry was then poured into the cement mold, which contained the femur end of the leg. The amount of bone cement used varied during the testing process. When the first legs were potted, approximately 15 scoops, or 15 grams of bone cement powder were used. As the testing procedure progressed there was a shortage of bone cement so it was necessary to decrease the amount of slurry used to pot. This was accomplished by placing spacers on both sides of the mold flanking the anterior and posterior ends of the bone, thus reducing the length of the bone cement block while retaining the area of contact for the bone cement. For the later legs a total of 9 scoops, or 9 grams, of bone cement powder were used.

A vice was used to hold the tibia end of the leg immobile while the bone cement was being dispensed into the mold. The cement was then allowed 20-30 minutes to air dry to let the bone cement solidify. The tape was taken off of the 3"x3" cement mold which facilitated the removal of the bone cement mold and the rod that had been placed in the bone cement.

Some difficulties arose when removing the rod from the hardened bone cement.  During the hardening, the bone cement compressed the metal sheath that surrounded the rod causing a great deal of resistance when the rod was being pulled out of the sheath.  In order to fix this problem in subsequent potting procedures, the metal sheath was discarded in favor of greasing the metal rod.  The grease reduced the friction of the rod in the bone cement tunnel and facilitated easy removal of the metal rod.

The femur leg in bone cement was then placed into the top attachment of the fixture and subsequently installed onto the upper load cell of the MTS machine. Using the MTS machine, the leg was lowered into liquid bone cement and allowed to dry for another 20-30 minutes.

While the bone cement was hardening it was very important to ensure that the tibia was twisted as little as possible with respect to the femur.  If the tibia was set in a fashion that placed it at an angle to the femur, the MTS machine motion would be effectively simulating walking with feet directed inward or outward, which would not be physiologically relevant.

To ensure optimal rotation of the second bone pot, the angle of the tibial end was stabilized by hand until the bone cement was hard enough to keep the bone in place.  At this point, the dry bone cement was placed into the bottom attachment of the jig and a rod was placed through the side of the bone pot.

## *ARTHROSCOPICALLY IMPLANTABLE FORCE PROBE INSERTION*

Using a scalpel, a tiny slit was made in the center of the medial portion of the ACL or of the ACL graft for the tension transducer. The slit was in line with the

longitudinal positioning of the tissue fibers. In the case of ST/G grafts, which were looped and therefore consisted of two separate strands of tissue, the slit was made in the thicker of the two strands.

The Arthroscopically Implantable Force Probe (AIFP) was placed into this slit using a pair of tweezers so that the wings of the transducer were aligned with the fibers (Figure 16). A suture was placed at the top and bottom of the slit as close to the transducer as possible to ensure that the transducer was snugly placed inside the slit and that it could not fall out or rotate.

Following insertion of the transducer, the skin and subcutaneous tissues of the knee were sutured back together using a baseball stitch to preserve moisture content in the knee during mechanical testing. The AIFP cord was then taped to the side of the cadaver knee to ensure that it was not subject to dislodging forces during the testing.



(A)                                    (B)
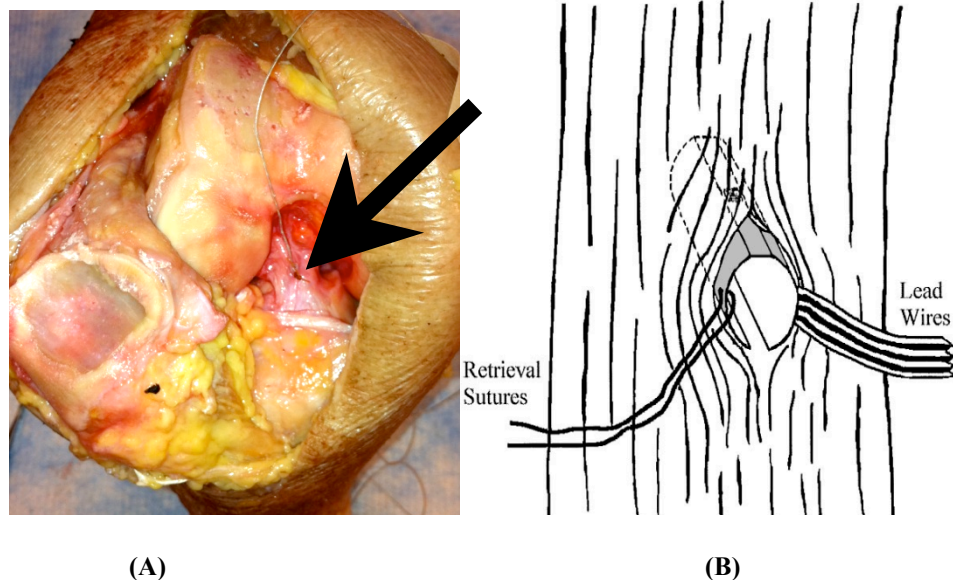
*Figure 16.* AIFP. (A) Insertion point of AIFP force transducer is indicated by the arrow, and (B) Diagram shows proper sensor positioning with respect to tissue fiber (Microstrain, 2011).

In order to make practical sense of voltages produced by the AIFP, it was necessary to correlate them to a precise amount of applied force or tension. This correlation was established by first calibrating the sensor according to the gross calibration method recommended by the MicroStrain Corporation (MicroStrain, 2011).
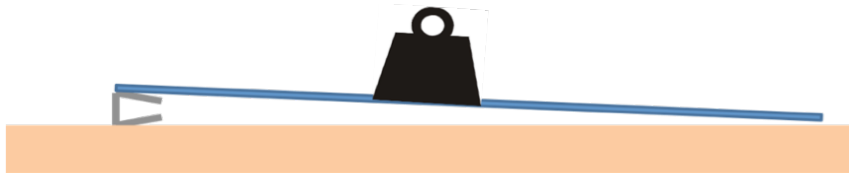


*Figure 17*. Gross calibration. Illustration of the AIFP being subjected to the gross calibration protocol.

Gross calibration consisted of placing the sensor on a flat surface and then placing a series of different weights on top of it as seen in Figure 17 above. Since the values of the weights placed on the sensor were known, the force produced by each of these weights, equal to mass times acceleration due to gravity (F=m*a), was also known. These forces would then be compared to the resultant voltages and a trend line or calibration curve was produced.
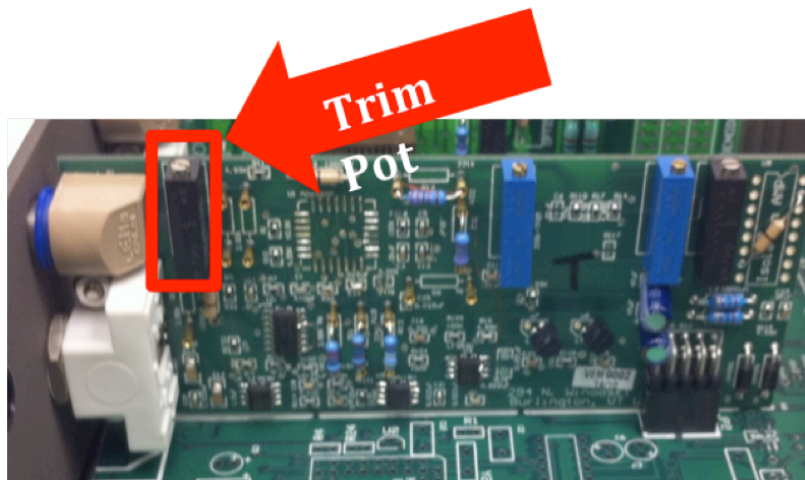


*Figure 18*. Trim pot. AIFP signal conditioning card with trim pot highlighted in red.

59

An advantage of the AIFP sensor is that it works in conjunction with a signal conditioning card, pictured in the top of Figure 18. This card possesses a type of variable resistor called a trim pot, which allows the experimenter to adjust the sensitivity of the sensor.

Figure 19 is a graph that depicts one of the calibration tests. Essentially, a single weight was placed on the sensor, and without changing the weight at all, the trim pot was adjusted so that the voltage correlated to that the specific weight started to change with each turn of the trim pot.

In this manner it was possible to adjust the sensitivity of the AIFP output. The importance of adjusting the sensitivity of the sensor is so that the sensor could be provided with the proper sensitivity range. This allowed the probe to accurately read the full range of force values expected to be produced during the mechanical stress protocol.
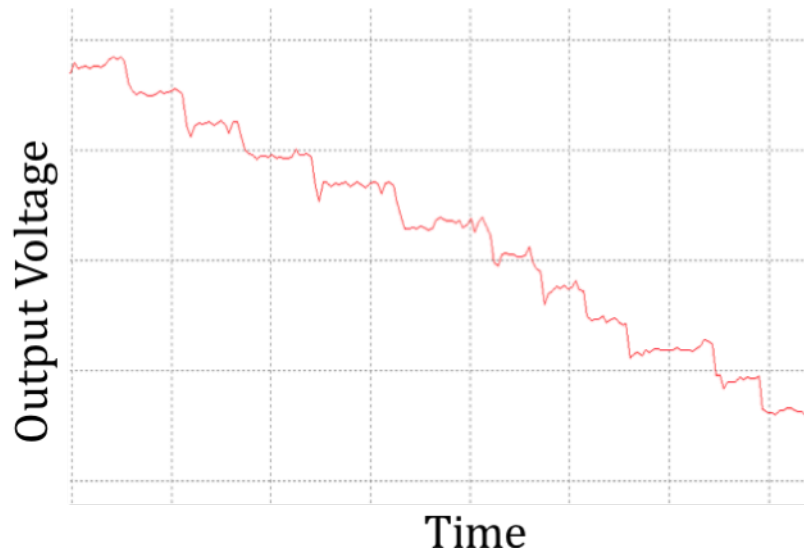


*Figure 19.* Trim pot adjustment. Graph of AIFP output voltage with respect to time as the trim pot was adjusted.

## *S*EMITENDINOSUS*/G*RACILIS *G*RAFT *S*URGICAL *C*ONSTRUCTION

Semitendinosus and gracilis tendons were located in the area of the medial popliteal fossa. A 2cm transverse skin incision was made and tissue was dissected until the popliteal fascia was seen. The fascia was incised longitudinally, at which point muscle tissue on the gracilis could be seen, while the semitendinosus was solely tendon (Arthrex, 2010).

A right angled clamp was used to retrieve the semitendinosus and a suture was placed around the tendon. The tendon was pulled proximally and distally away from surrounding tissue. Once free, the fascial attachments were resected. The Minimally Invasive Graft Harvester® was advanced proximally while pulling distally on the tendon, until the tendon was released. The muscle was cleaned off the tendon and was stitched using the #2 FiberLoop® (Arthrex, 2010).

The Minimally Invasive Graft Harvester® was advanced towards the tendon insertion while the tendon was being pulled proximally, until the tendon was completely freed from the tibial cortex. If necessary, the gracilis tendon was also harvested, found superior to the semitendinosus. The same technique was used for the removal of the gracilis, at which point the incision was closed (Arthrex, 2010).

The RetroButton® Drill Pin II was used was used to drill through the medial portal of the femoral socket (Appendix D, Figure 1). The intraosseous distance was measured by reading the depth marking on the pin closest to the femoral notch. This was done by pulling back on the pin until it became caught in the femoral cortex (Appendix D, Figure 2) (Arthrex, 2010).

Using Low Profile Reamers, the femur was drilled to a depth equal to the amount of graft desired in the socket. With the tibial tunnel created, the suture was passed through the tibia (Appendix D, Figure 3) (Arthrex, 2010).

The semitendinosus and gracilis tendons were attached to a button and placed at the end of a Graft Sizing Block. The tendons were marked twice, first, on the implant, at a distance equal to the intraosseous length from the button and second, on the graft, at a point equal to the depth of the femoral socket or desired amount of the graft in the socket (Appendix D, Figure 7) (Arthrex, 2010).

The blue suture was passed through the tibia and out the femur. The button was pulled through the femur until it exited the lateral cortex. The graft was pulled on in order to confirm fixation, which was indicated when the mark on the implant reached the femoral socket (Appendix D, Figure 4) (Arthrex, 2010).

The marked strands were retrieved from the implant through the medial portal. The graft was advanced and pulled on, in order to put tension on the shortening strands. The right placement of the graft was indicated when the mark on the graft reached the femoral socket (Appendix D, Figure 5) (Arthrex, 2010).

The graft was pulled on firmly in order to confirm full fixation. Shortening strands were tightened as necessary. No additional force was placed on the shortening strands once the graft stability was verified, as excessive force could break the strands. After confirming fixation, the shortening strands were cut with an arthroscopic #2 FiberWire cutter (Appendix D, Figure 6) (Arthrex, 2010).

## *BONE-PATELLAR TENDON-BONE GRAFT SURGICAL CONSTRUCTION*

A 9.5mm trapezoidal saw guide was placed over the patella bone to allow for precise harvesting of the 25mm length bone block. Two 2 mm diameter pins were inserted through the guide block into the patella to stabilize the guide block and create suture holes in the bone block for later use. A bone saw with a 7mm depth self stop blade was used in conjunction with a 10mm parallel knife blade to remove the block. The procedure was repeated to remove the bone block on the tibia bone. The resulting Bone-Patellar Tendon-Bone graft was marked with a methylene blue line to designate the tendon-bone junction. The bone blocks were threaded with #2FiberWire® in preparation for fixation (Appendix E, Figure 1) (Garrett, 2011).

After graft preparation, the knee was placed at 90 degrees of flexion, and a Target POP Marking Hook attached to an Adapteur C-Ring was inserted through the anteromedial portal. The marking hook was placed against the PCL by its base, with the guide angle adjusted to have the guide sleeve 1 cm above the pes anserinus and 2.0 cm medial of the tibial tubercle to ensure sufficient tibial tunnel length. A 2.4 mm Drill Tip Guide Pin was placed through the Guide Pin Sleeve. To prevent movement upon drilling, the drill was initiated before contact with the bone. The marking hook ensured a 7 mm distance between the guide pin and the PCL. The guide sleeve, marking hook and guide were removed to confirm correct pin position (Appendix E, Figure 2) (Garrett, 2011).

A Coring Reamer was used to create a tibial tunnel with a round-bone graft (Appendix E, Figure 3). Next, a Headed Reamer with a diameter 1 mm larger than the Coring Reamer was drilled to a depth of 1 cm. The guide pin was then removed and

replaced with a Collared Pin. A Coring Reamer was placed over the Collared Pin and drilled through the predefined hole placed by the Header Reamer. The Coring Reamer was slowly drilled through the tibia creating a smooth tibial tunnel. The reamer was pulled back through the tunnel and the bone core was removed (Appendix E, Figure 4) (Garrett, 2011).

A tibial cannula was then placed in the tibial tunnel and a 7mm Transtibial Femoral ACL Drill Guide (TTG) was selected, in order to create a 10mm tunnel leaving 1-2mm backwall. The TTG was inserted into the tibial cannula and the tip placed against the over-the-top position. The 2.4mm guide pin with suture eyelet was drilled through, exiting the lateral thigh. The guide pin was extracted using a Jacob's Chuck Handle (Appendix E, Figure 5). A Headed Reamer was inserted through the tibial tunnel and past the PCL. A drilling depth of 30mm was confirmed using the 5mm graduated markings to fully accommodate the 25mm length of bone block (Appendix E, Figure 6) (Garrett, 2011).

Next, a notch was created in the femoral socket using a Tunnel Notcher. This was necessary to ease interference screw placement. The notcher was inserted through the tibial tunnel and tapped lightly with a mallet until the depth mark was flush with the rim of the femoral socket (Appendix E, Figure 7). The prepared graft was then selected and the #2FiberWire sutures previously attached to the bone block were placed in the suture eye of the graft passing guide pin and the pin was pulled. The graft was pulled into the femoral socket through the tibial tunnel with the help of the guide pin and a probe. The graft was pulled until the methylene blue line was flush with the femoral socket rim. The tendon fibers were oriented posteriorly

(Appendix E, Figure 8). The knee was placed at 120 degrees of flexion to allow access to the femoral tunnel through the anteromedial portal. A 1.1 mm diameter guide pin was placed through the guide tunnel and moved flush with the notch created by the Tunnel Notcher. The bone block was inserted into the femoral tunnel up to the demarcated second laser line of the guide pin. This step ensured that the bone block was placed at the appropriate depth in the femoral tunnel (Appendix E, Figure 9) (Garrett, 2011).

Next a sheathed PLLA round head Bio-Interference screw was inserted into the anteromedial portal. The sheath was oriented as to protect the PCL from damage during fixation and the sheath window was positioned superiorly to provide clear visualization of the screw insertion. A cannulated Ratcheting Screwdriving Handle was inserted over the guide pin and into the sheath to engage the screw. The screw was inserted until the head was slightly countersunk into the femoral socket. The guide pin, screwdriver and excess FiberWire were then removed (Appendix E, Figure 10). After femoral fixation, the knee was cycled through a full range of motion to ensure proper graft condition and confirm graft position in the femur. The knee was placed at approximately 0-20 degrees of flexion and the graft was fixed in this position. The screw was sunk until complete fixation was confirmed. The knee was again put through a full range of motion to confirm proper attachment (Appendix E, Figure 11) (Garrett, 2011).

## MECHANICAL CONTINUOUS PASSIVE MOTION TESTING

A 25kN axial/torsional materials testing system (MTS Systems Corporation, Eden Prairie, MN) was used to simulate continuous passive knee motion. The potted

cadaver knee specimen was mounted onto the MTS machine using the earlier constructed attachment devices. The U-shaped attachment pieces were fixed to the top and bottom load cells of the MTS machine via hex bolts.

The potted ends of the cadaver knee specimen were then connected to the U-pieces via metal rods, taking care to prevent the knee joint from directly supporting the weight of the potted ends. The MTS machine was then programmed to cycle at 0.3Hz, bring the knee from 20 to 70 degrees of flexion for 1200 cycles. Force data from the AIFP was collected at a rate of 100 degrees per minute throughout the entire duration of the test.

### GRAFT EXCISION

When removing the grafts and native ACL tissue from the cadaver knees, it was necessary to ensure that as much of the tissue was retained intact as possible. It was easier to retain the whole graft tissue because it had been secured artificially by the surgeon and thus could be removed at its attachment points.

ACL grafts had to be removed by slicing in areas that were accessible by scalpel. The bone-patellar tendon-bone and the semitendinosus and gracilis grafts were attached to the knee through screws and pins. In some cases, it was possible to cut the cords that attached the graft to the pins; in other cases, it was necessary to completely unscrew the interference screws that secured the grafts in the bone tunnels.

After the attachment points were severed it was possible to manually pull the grafts through the bone tunnels. After removal, the grafts and native ACL tissue were cleaned with phosphate buffered saline (PBS) and were placed in formalin fixative.

## *BRIGHTFIELD LIGHT MICROSCOPY*

### TISSUE HARVESTING

The intact ACL or graft substitute was excised from the leg.  Excess fluid, like blood, was washed with PBS and 70% ethanol.  Excess tissues, like fat, were trimmed from the tissue with a scalpel.  The tissue was then fixed in formalin and stored at 4°C for approximately three weeks, one week as whole tissue and two weeks as cut up tissue.

To cut up the tissue, the whole tissue was severed at approximately 1cm lengths with a scalpel.  Creating smaller sections of the whole tissue allowed for more surface area to be exposed to the formalin, resulting in more efficient and effective fixing.  Following the three-week fixation period, some tissue sections were removed for processing; the remaining tissue was moved into 70% ethanol for storage.

The length of fixation time was lengthened occasionally depending on the quality of the tissue post-tissue processing. If the tissue began shredding during the sectioning process (described below), the stored tissue in 70% ethanol was moved back into a container of formalin. Generally, the tissue stayed in formalin for another week before it was re-processed and its quality was evaluated.

### TISSUE PROCESSING

Samples not exceeding 1cm in length were placed in labeled tissue cassettes for easy manipulation in the LEICA TP 1020 (Leica Microsystems, Wetzlar, Germany), the automated tissue processor (Figure 20). Tissues were first dehydrated in two washes of 70% ethanol, two washes of 95% ethanol, and two washes of 100% ethanol.  Each wash lasted for 2.5 hours, which is lengthier than common protocols

because the tissue is relatively large.  Specimens were cleared in xylene for 1.5 hour before being infiltrated with paraffin, a wax-like substance, for two 1.5-hour washes.

All solutions were vacuum pumped to ensure lack of contamination.  The total time required for tissue processing was approximately 28-29 hours.



*Figure 20.* Tissue processor. Leica Microsystems tissue processing machine.

**EMBEDDING**

Tissues were embedded in paraffin blocks using the LEICA EG1160 Paraffin Embedding Station (Leica Microsystems, Wetzlar, Germany) and TissuePrep Paraffin (melting point 56-57 degrees Celsius).  Embedding in paraffin blocks is desirable because it allows for thin sections to be cut in order to observe detailed morphology.

To make the blocks, samples were placed in metal trays, onto which a plastic block mold was placed.  To ensure that no piece of the sample protruded too far into the mold, the specimen was held as close to the bottom of the metal tray as possible with a pair of forceps.

Hot wax was then poured into the tray and around the specimen. Care was taken to ensure that enough paraffin had been added for the attachment of the block to the mold. Blocks were then cooled on the cold plate for one hour until paraffin solidified to form a paraffin block. The blocks were then stored at room temperature until they were to be sectioned.

Two to three blocks were created per tissue type. This provided sufficient material for sectioning. Some blocks would yield no sections because the tissue was shredding as the blade sliced. In those cases, there were still one or two extra blocks of the same tissue type available, precluding the necessity for repeating the length tissue processing procedure.

**SECTIONING**



*Figure 21.* Tissue sectioning. MICROM HM 355S microtome machine.

The MICROM HM 355S microtome machine (Thermo Fisher Scientific Inc, Walldorf, Germany) was cleaned, ensuring that all dust and wax shavings were removed from the cutting surface to prevent any disturbance to the delicate sectioning

process (Figure 21). To cut slices of tissue, a newly sharpened blade was secured in the machine. The sharpness of the blade was important for producing the ideal thin, flat sections that were free of gaps or sheared tissue.

After a blade was inserted, the paraffin block containing the tissue was clamped into the specimen holder. The block was inserted either horizontally or vertically. The initial orientation of the block was determined by the type of tissue to be sectioned or the desired directionality of the slice. Care was taken to slice along the crimping longitude rather than cutting into the undulating patterns.

Once the block had been secured, the blade and the paraffin block were positioned at an appropriate distance from one another. This was accomplished by moving the blade-stand forward until the sharp edge was flush with the surface of the paraffin. The blade stand was then locked into place. The block was sectioned by cranking the handle on the side of the machine, which allowed the block to be cycled up and down while being pushed forward against the blade. Adjustments to the angle of the blade stand were made depending on the directionality of the slices, e.g., if only parts of the block were being cut.

At first, the slices were composed entirely of paraffin because the tissue had been embedded deep within the block. After the upper paraffin layer was removed, the block was cooled by placing a cold, PBS-soaked Kimwipe on the surface of the wax for several minutes. Cooling ensured that the wax and the specimen were at a compatible level of hardness, which was crucial for obtaining good tissue sections. Otherwise, sections were shredded or bunched.

The feed on the machine was set between six and eight, which corresponded to the specimen thickness of each slice in micrometers.  By experimenting with various thicknesses and determining the ideal setting, the feed was set to yield the best slices.  The slices could not be too thin or the tissue would shred, but they also could not be too thick or the collagen patterns were laid over each other during imaging, thus making it difficult to discern the crimping. Once the tissue was broached by the blade, slicing should be done more slowly and carefully to avoid generating a thick slice that contains all the usable tissue.

The workable tissue sections were immediately placed in a 37°C water bath for approximately 20 minutes, which smoothed out the wrinkles in the paraffin.  Once the wax was smooth, a microscope slide was moved under and up the sections so that they laid flat against the glass.  The slide was then heat fixed, allowing the tissue to adhere completely to the glass.

An effort was made to take sections from the beginning, middle and ends of each tissue block to provide a representative sample of each tissue type.  Multiple slides of sections were created per tissue type so that many images could be taken and analyzed.  The slides were subsequently stained with Picrosirius Red and imaged via brightfield microscopy.

## STAINING

The previous steps of tissue processing generated thin slices of tissue attached to glass slides.  Prior to staining, the slides were transparent.  Thus, the Picrosirius Red stain was used to highlight the collagen crimping pattern.  Picrosirius Red is the optimal stain employed by researchers to study collagen organization because it has

the ability to detect the thin collagen fibers that are not visible using other staining methods (Rich & Whittaker, 2005).

Examples of alternative stains include the van Gieson and the trichrome stains, which combine multiple anionic dyes that bind differentially to tissue components depending upon the dye molecules' size and physical structure of the tissue (Rich & Whittaker, 2005). These properties result in stains that fail to reveal thin collagen fibers, thus causing collagen content to be underestimated. Another disadvantage of these stains is that they fade quickly. Therefore, due to its superior advantages, Picrosirius Red was used to visualize collagen organization for all slides prepared.

The Picrosirius Red stain kit was obtained from Fisher Scientific. The kit contains 1) picric acid, which is a dye that is small, anionic, and hydrophobic, and 2) Sirius Red, which is a dye that is large, hydrophobic, and combined with a metal complex (Polysciences, 2010). This combination creates the Picrosirius Red stain mechanism for detecting collagen fibers.

Collagen is stained with a red hue that is controlled by the size of the dye molecule. Various factors affect the quality of the stain such as temperature, time, thickness of sample, pH, and fixation time (Polysciences, 2010). Fixatives that increase staining rates result in a redder section, whereas thick sections stain more yellow than thin sections.

The staining protocol was provided by Polysciences, Incorporated (Polysciences, 2010). First, slides to be stained were collected and dipped in Weigert's hematoxylin for 10 minutes. Subsequently, slides were washed in a

container of distilled water for 10 minutes to remove the stain.  Next, the slides were dipped in Picrosirius Red stain for 1 hour.  After the collagen stain, slides were rinsed twice by dipping in a container of distilled water for 10 minutes each to remove the stain.  After the final rinse, slides were removed from the container and excess water was allowed to drip off the slides.

Slides were next dehydrated by performing three quick washes in 100% ethanol; each wash was rapid and lasted less than 5 seconds.  Finally, the slides were cleared by washing each into a container of xylene.  A drop of permount mounting medium was added to each slide, which was subsequently covered with a coverslip. This ensured that stain quality was preserved until imaging, allowing for long-term storage of the slides at room temperature.  See Figure 22 for before and after images of stained slides.
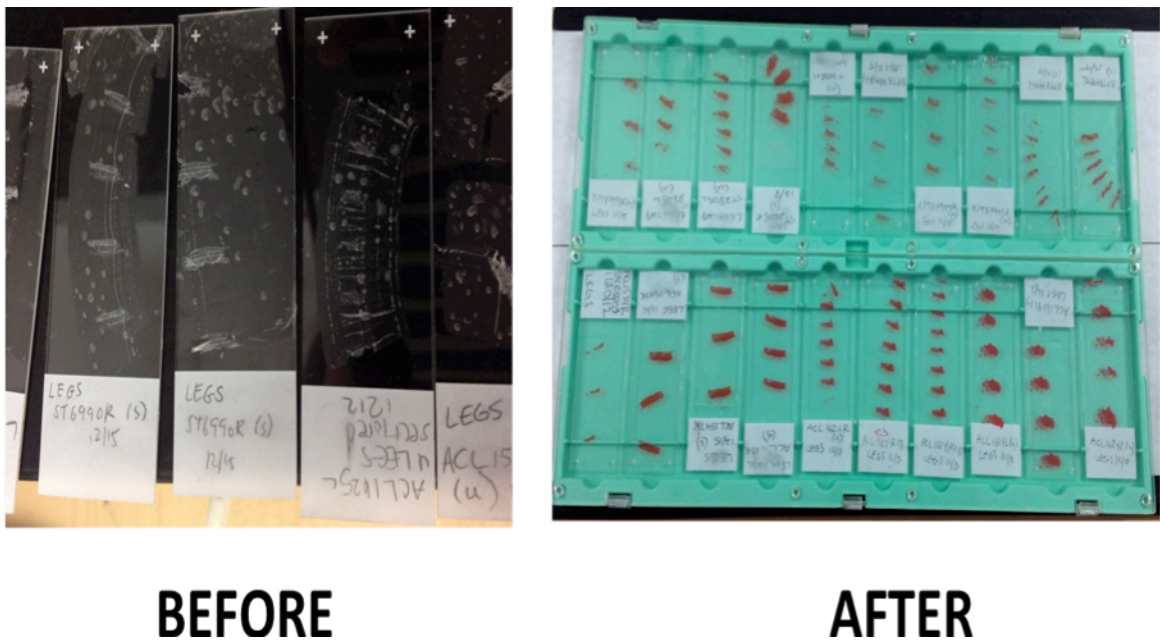


**BEFORE**          **AFTER**

*Figure 22*. Staining. Slides shown before (left) and after (right) staining with Picrosirius Red.

**MICROSCOPY**

Brightfield microscopy was performed on all imaging sections (Figure 23). After slides were prepared and stained, they were imaged using QCapture Pro software. QCapture Pro provides computer control of all camera functions for preview, capture, and save, as well as for functions such as binning, region of interest, and live histogram optimization of dynamic range (QImaging, 2012). This program was used for obtaining images because its color correction algorithms ensure that color imaging is accurate.
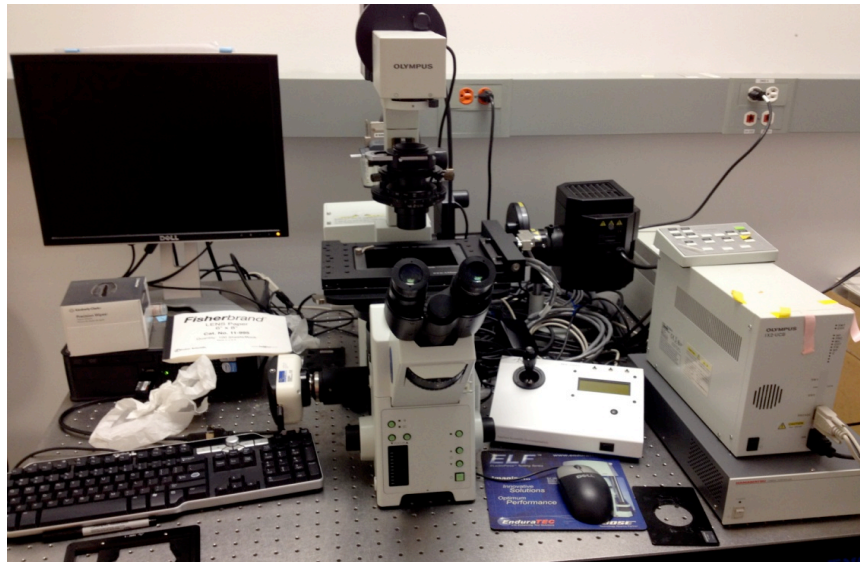


*Figure 23.* Imaging. Brightfield microscope used for tissue imaging.

A slide was first placed on the microscope stage and the section to be imaged was centered above the light illuminator. Clips were used to secure the slide in place. The QCapture Pro software was opened and an imaging preview option was selected. This allowed the user to get a visual of the slide on the computer screen and avoided using the eyepiece of the microscope. The image was first sharpened at low magnification (total magnification of 40X image size) to locate the general area of the

tissue.  The coarse and fine adjustment knobs were rotated until the image became clear on the computer screen.  A joystick was used to move different portions of the slide into the frame.

Crimping patterns were not visible at the lowest magnification, so the magnification of the microscope was increased to a total magnification of 100X image size.  Again, the coarse and fine adjustment knobs were rotated until the image became clear on the computer screen.  This adjustment was quick, because the image was already focused at the lower magnification.  The final magnification selected to observe crimping was 400X.

After sharpening the image, a snapshot was obtained by selecting the snap option on QCapture Pro software.  Once the image was obtained, it was saved and transferred to another computer for image analysis.  The entire procedure was repeated multiple times for each slide to obtain images representative of the entire sample.  Images were obtained from multiple users to eliminate bias. For representative pictures of good and bad images for each tissue type (ACL, ST/G, & BPTB) see Appendix L.

### IMAGE ANALYSIS

All images were analyzed using ImageJ, free software provided by the National Institutes of Health (NIH).  Before analyzing samples, a calibration was first performed to obtain accurate length measurements.  An image of a hemocytometer, a device used to count cells, was obtained with QCapture Pro at a total magnification of 400X image size.  The hemocytometer has known dimensions so it can be used to

relate pixel length (a dimensionless property of the image) to measurement length (in standard length units).

After opening ImageJ, the image of the hemocytometer was selected. Then, the set scale function from the toolbar was selected to calibrate the length scale. An arrow was drawn across a known distance, which in this case was 1/4 mm for a square on a hemocytometer. The software was then able to set the measurement scale for all images to be analyzed. This calibration had to be performed every time the software was reopened to accurately correlate the pixel dimensions to a standard length.

After setting the length scale, an experimental image was opened. The angle tool was used to approximate the angle of the crimp. This measurement was repeated for multiple crimps on the same image. The straight-line selection tool was then used to approximate the length of the crimp. This measurement was provided in standard length units that were calibrated as described previously. The length measurement was also repeated for multiple crimps on the same image. To eliminate bias, multiple users analyzed the same image and the results shown are an average of the measurements.

Analysis was randomized across the different users, with three different users analyzing images for each tissue type. Each user took five crimp angles for each tissue type. After obtaining measurements for the angle, the measurements were averaged across images and subsequently for each graft type. Statistical analysis was performed to determine confidence intervals for the measurements. This allowed for

a determination of statistically significant differences in crimping between graft types.

The method used to measure crimp angles has been previously reported (Shah, Jayson, & Hampson, 1977).  In this method, a horizontal line was drawn tangent to the lowest point, or trough, of the crimp pattern.  This line runs parallel along the direction of the crimps and connects the lowest point of two troughs of the crimp pattern.

Then another line is drawn from the horizontal to the peak of the next crimp, such that an angle, denoted θ in Figure 24, is formed between the lines.  This angle is used to characterize the crimp pattern.
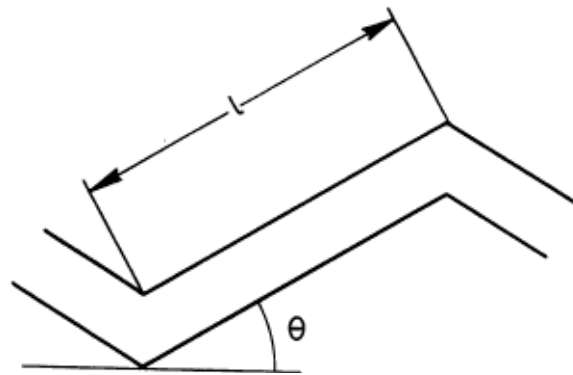


*Figure 24.* Crimp angle measurement. Method used to define the crimp angle for image analysis.  In the figure, *l* represents the length of the crimp (taken as the distance between the base and peak of the crimp pattern) and θ represents the crimp angle (Shah, 1977).

## STATISTICAL ANALYSES

For the imaging statistical analyses, six comparisons were made with mean crimp angle as the dependent variable.  First, a one-way ANOVA was used to compare stressed versus unstressed values within each graft type (e.g. BPTB stressed vs. BPTB unstressed).  Second, a one-way ANOVA was used to compare across all graft types with the stressed and unstressed data combined.  Third, a one-way

ANOVA was used to compare between the stressed and unstressed conditions irrespective of graft type. Fourth, a one-way ANOVA was used to compare across the stressed conditions for each graft type. Fifth, a one-way ANOVA was used to compare across the unstressed conditions for each graft type. Finally, a two-factor ANOVA was used to test for an interaction between the stressed/unstressed conditions and the graft type.

An additional comparison was made using percent change in crimp angle as the dependent variable. The percent change was calculated for every matched pair of each graft type, using the following equation: (stressed crimp angle-unstressed crimp angle) / unstressed crimp angle. The percent change values were then averaged for each graft type and a one-way ANOVA was used to compare across the groups. For the biomechanics statistical analyses, a one-way ANOVA was used to compare between the logarithmic decay coefficients for each graft type. For all results, post hoc testing, in the form of Scheffe and Tukey HSD comparisons, was used whenever appropriate to interpret the meaning of statistical significance. The level of significance for all tests was set at $p < 0.05$.

# CHAPTER 4: RESULTS

## *MECHANICAL CONTINUOUS PASSIVE MOTION TESTING*

As a result of MTS machine testing, plots of percentage relative tension loss vs. number of cycles were obtained for each tissue type. The percentage of relative tension loss was measured in order to control for variability between tissues and normalize the data set.

### INTACT ACL

Figure 1 of Appendix H shows the percent relative tension loss of each of our five intact ACL cadaver specimens during mechanical CPM testing. In general, the intact ACL reached equilibrium after cyclic loading for 1500 cycles. Also, the intact ACL tended to reach 50% relative tension loss by around 200 cycles. As seen in Figure 1, Appendix H, two legs portrayed the logarithmic decay behavior expected, the ACL pilot test leg and also 1617R. These legs both started at 100% tension and then gradually reached 0% tension as it underwent more cycles.

In the case of the other legs, other patterns were seen. In 1574L, the leg exhibited an increase in tension, as opposed to the expected decrease. The plot conforms to a polynomial, rather than a logarithmic fit, since it increases and decreases to around 69% to 34%, before steadily increasing to 100%. This difference is likely due to misalignment of the tension transducer or loss of fluid in the tissue during the mechanical CPM test. Cadaveric tissue should not gain tensile strength over time under cyclic loading and therefore, the data for 1574L is not accurate.

Similar to 1574L, the results of biomechanical testing for 1624R show an increase in tension. Another thing to note about the plot of 1624R is the lack of complete testing, as there was only data recorded to 400 cycles as opposed to the full 1500 cycles seen in the other tests. Like specimen 1574L, there is no real explanation for cadaveric tissue showing a gain in tensile strength over time under cyclic loading other than faulty data collection. Therefore, the test for specimen 1624R can be considered as failed and its data is not accurate and therefore should not be considered in our conclusions.

Lastly, specimen 1603R shows a flat curve, indicating that the tension within the intact ACL remained approximately the same during the mechanical CPM testing. This may be either due to the fact that the relative tension does not have the same magnitude or the AIFP voltage reading maxed out. In addition, the plot of 1603R starts at below the expected tension with data points that may have been faulty due to misalignment or faulty connection of the transducer. The curve then decreases slowly from 100% to approximately 96% relative tension after approximately 1200 cycles.

## ST/G GRAFTS

In Figure 2 of Appendix H, the ST/G grafts exhibited similar behavior to the intact ACL testing. Both the ST/G grafts in 1574L and 1603L exhibited logarithmic decay behavior. The point of 50% tension loss occurred at approximately 200 cycles, similar to the Intact ACL. It should be noted that the graft for 1603L was composed of only semitendinosus tendon because it was thick enough to be an ACL graft without combining it with a gracilis tendon.

The ST/G graft in 1625L showed an initial increase, then a gradual decrease, followed by a steady increase again. Once again, this exponential growth behavior of 1625L indicates that this test was failed either due to instrumentation or human error. Overall, the ST/G graft behaved very similarly to the Intact ACL with regards to tension loss per cycle.

**BPTB GRAFTS**

Figure 3 of Appendix H shows the percent relative tension loss of the BPTB grafts during mechanical CPM testing and fitted logarithmic data. A strong logarithmic decay behavior was observed in specimens 1574R, 1624L, and 1625R with $R^2$-values greater than 0.9. In specimens 1603R and 1617R, the $R^2$-values were greater than 0.8, indicating that the logarithmic decay behavior is still strong despite being weaker than the three previously mentioned specimens.

For the five BPTB specimens, 50% of the relative tension loss occurs between 100 to 300 cycles. However, equilibrium was not reached by any of the specimen.

**COMPARISON OF EXPERIMENTAL GROUPS**

Data from failed tests in which the plot exhibited tension gain rather than loss was excluded. The data for intact ACL, BPTB and ST/G grafts were then each respectively averaged and a logarithmic curve was fitted for each of the experimental groups as seen in Figure 25 below.
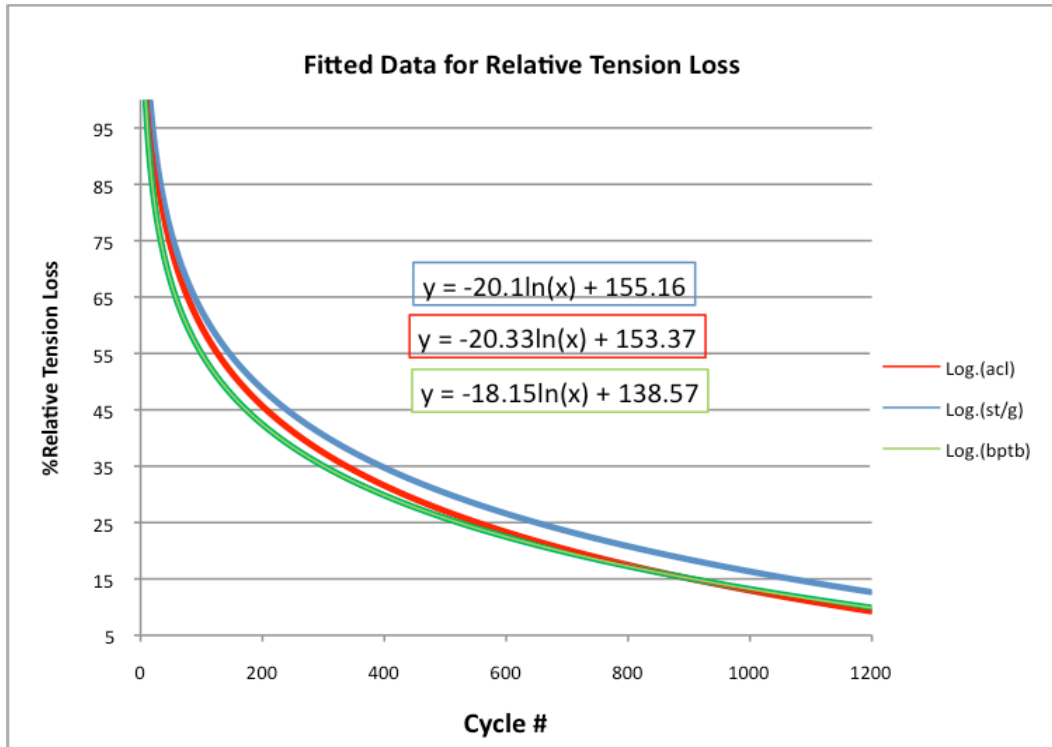
*Figure 25.* Relative tension loss. This figure shows the logarithmic curves fitted to % tension loss relative to the total tension loss of intact ACL and BPTB and ST/G grafts during mechanical CPM testing. The red, blue, and green lines indicate the fitted curve for % tension loss relative to total tension for the intact ACL, ST/G grafts, and BPTP grafts, respectively.
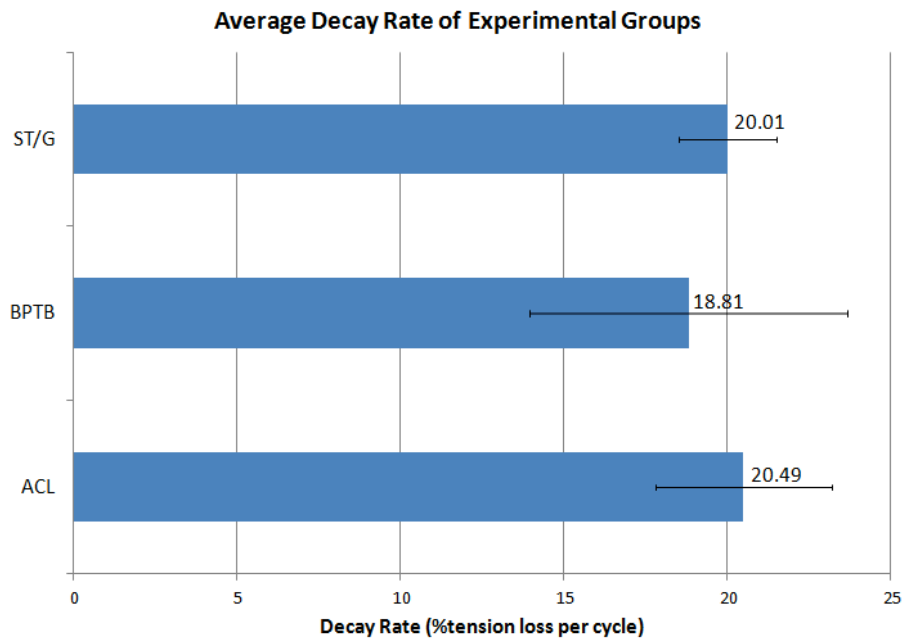


*Figure 26.* Average decay rate of experimental groups. No significant difference was found between the graft types on the dependent variable of decay rate (logarithmic decay coefficient).

Of the three groups, BPTB grafts had the highest rate of tension loss while ST/G had the lowest. Despite the fact that BPTB grafts had a higher rate of tension loss than the intact ACL, the former appears to approach equilibrium faster than the latter as cycle number approaches the thousands. There was no significant difference between the graft types on the dependent variable of logarithmic decay coefficient ($F(2,6)=0.14$, $p>0.05$) (Figure 26). Overall, the rate of tension loss does not vary between intact ACL and ACL grafts or between either ACL graft types.

## TISSUE CRIMP ANGLE
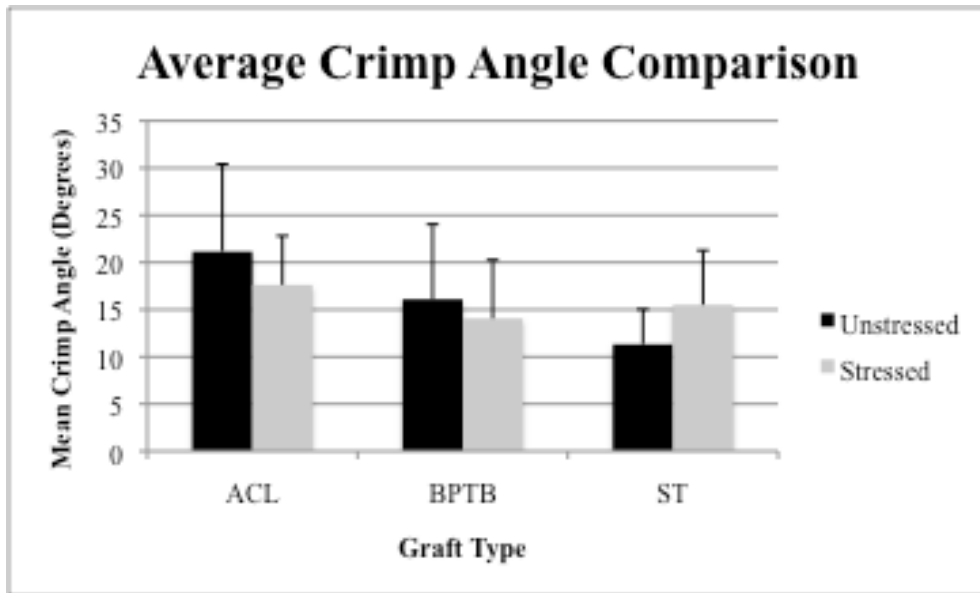


*Figure 27.* Mean comparisons of crimp angle. This figure shows the means and standard deviations in crimp angle for each type of tissue across the stressed and unstressed conditions.

All the crimp angles measured for each graft through Image J analysis were compiled into a large table as depicted in Appendix J. The means for each graft type and corresponding condition (stressed vs. unstressed) are shown in Figure 27.

Data was successfully collected from five unstressed ACL tissues, which have an overall mean crimp angle of 21.15° and a standard deviation of 9.26°. Data was

collected for five stressed ACL tissues, which have an overall mean crimp angle of 17.62° and a standard deviation of 5.19°. Data was collected from five unstressed BPTB tissues, which have an overall mean crimp angle of 16.10° and a standard deviation of 7.93°. Data was collected for four stressed BPTB tissues, which have an overall mean crimp angle of 14.06° and a standard deviation of 6.20°. Data was collected from five unstressed ST tissues, which have an overall mean crimp angle of 11.32° and a standard deviation of 3.71°. Data was available for four stressed ST tissues, which have a mean crimp angle of 15.51° and a standard deviation of 5.77°.
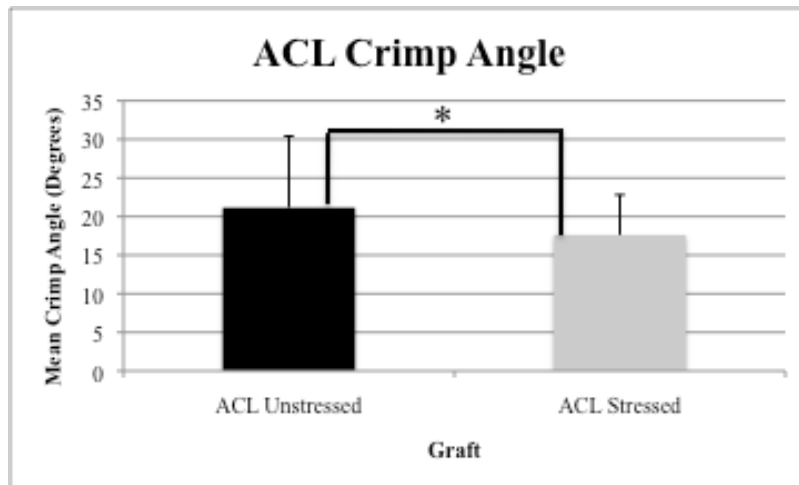


*Figure 28*. Mean comparisons of ACL crimp angle. A significant difference was found between the ACL unstressed and ACL stressed crimp angles. The error bars represent +/- 1 standard deviation, which was determined from the variance of the measured angles. An asterisk represents significance as determined by an ANOVA, where p < 0.05.

After completing the statistical analyses outlined in the methodology section, the following results were obtained. There was a significant difference between the ACL stressed and unstressed tissues on the measure of crimp angle ($F_{(1,148)}=8.26$, $p<0.05$) (Figure 28). The crimp angle for ACL unstressed (M=21.15°) is significantly greater than ACL stressed (M=17.62°). There were no significant differences between the BPTB stressed versus unstressed on the dependent variable of crimp angle

(F(1,133)=2.71, p>0.05) (Figure 29). There was a significant difference between the ST stressed and unstressed tissues on the measure of crimp angle (F(1,133)=26.08, p<0.05) (Figure 30). The crimp angle for ST stressed (M=15.51°) is significantly greater than ST unstressed (M=11.32°).
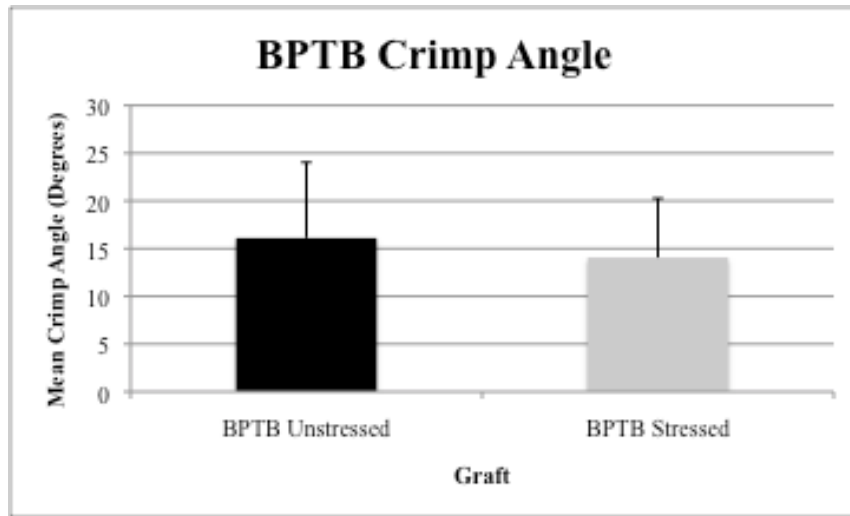


*Figure 29*. Mean comparisons of BPTB crimp angle. No significant difference was found between the BPTB unstressed and BPTB stressed crimp angles. The error bars represent +/- 1 standard deviation, which was determined from the variance of the measured angles. An asterisk represents significance as determined by an ANOVA, where p < 0.05.
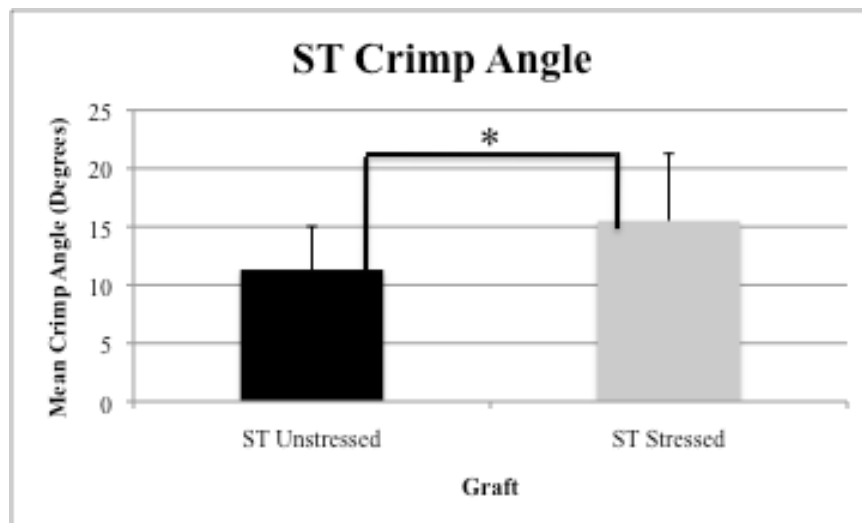


*Figure 30*. Mean comparisons of ST crimp angle. A significant difference was found between the ST unstressed and ST stressed crimp angles. The error bars represent +/- 1 standard deviation, which was determined from the variance of the measured angles. An asterisk represents significance as determined by an ANOVA, where p < 0.05.
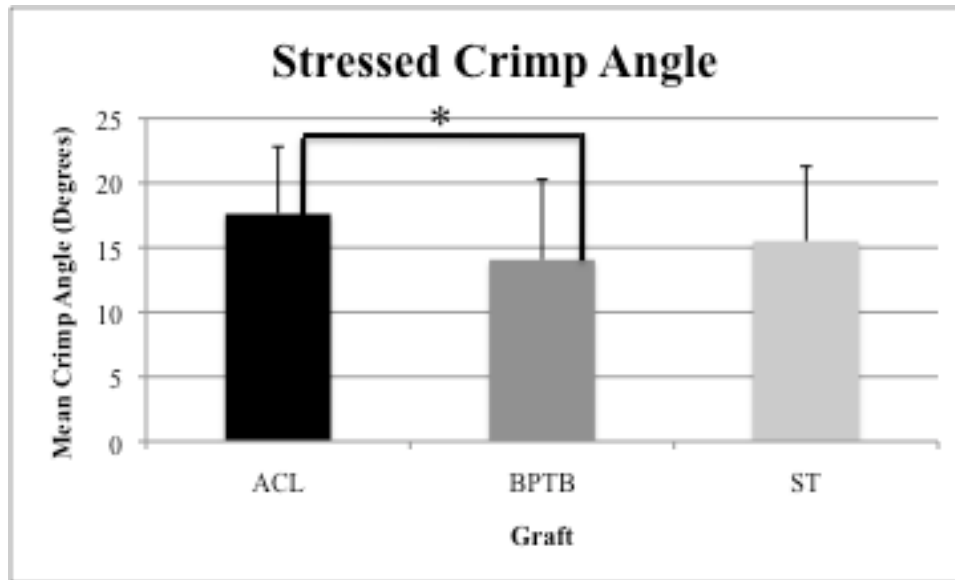
*Figure 31*. Mean comparisons of the stressed crimp angles. A significant difference was found between ACL stressed and BPTB stressed. The error bars represent +/- 1 standard deviation, which was determined from the variance of the measured angles. An asterisk represents significance as determined by an ANOVA, where p < 0.05.

When comparing ACL vs. BPTB vs. ST irrespective of condition, a significant difference on the dependent measure of crimp angle was found ($F_{(2, 417)}=30.81$, $p<0.05$). Post hoc testing revealed that ACL (M=19.38°) is different from BPTB (M=15.20°) and ST (M=13.19°), but that BPTB and ST are not significantly different from one another. Upon comparison across conditions (not considering graft type) no significant difference was found ($F_{(1,373)}=0.17$, $p>0.05$). When comparing ACL stressed versus BPTB stressed versus ST stressed on the dependent measure of crimp angle, a significant difference was found ($F_{(2, 192)}=6.70$, $p<0.05$) (Figure 31). Post hoc testing revealed that ACL stressed (M=17.62°) is different from BPTB stressed (M=14.06°), but that ACL and ST (M=15.51°) are not significantly different from one another, nor are BPTB and ST. The comparison between ACL unstressed versus BPTB unstressed versus ST unstressed on the dependent variable of crimp angle yielded a significant result ($F_{(2,}$

222)=33.43, p<0.05) (Figure 32). Through post hoc testing, it was revealed that each

type of unstressed tissue is significantly different from the other two.
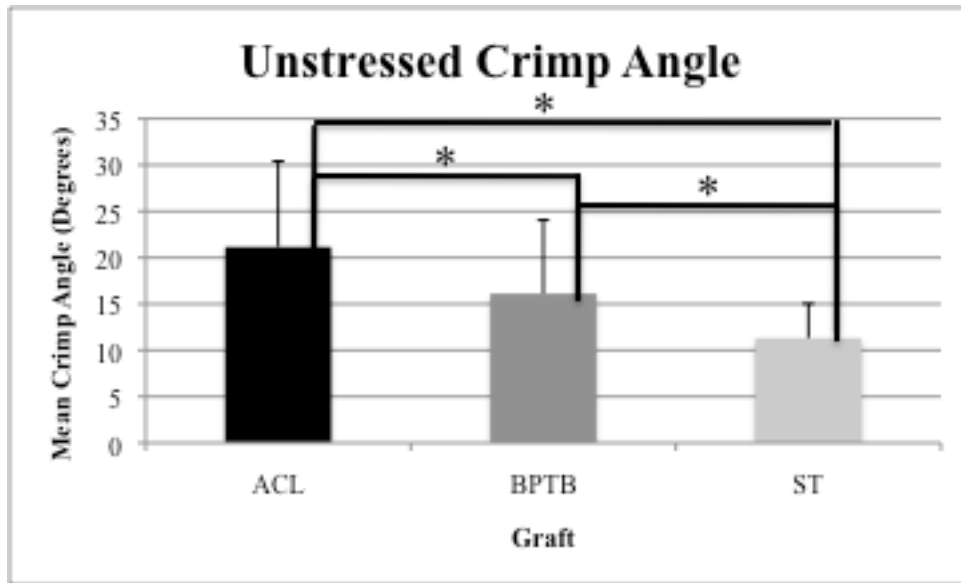


*Figure 32.* Mean comparisons of the unstressed crimp angles. A significant difference was found
between all three graft types. The error bars represent +/- 1 standard deviation, which was determined
from the variance of the measured angles. An asterisk represents significance as determined by an
ANOVA, where p < 0.05.
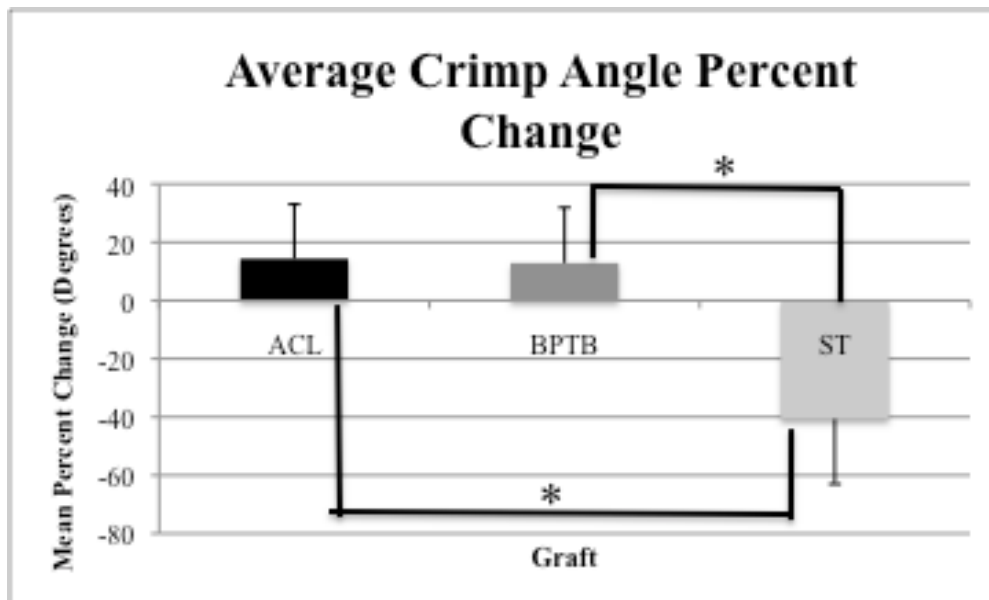


*Figure 33.* Average crimp angle percent change. A significant difference was found between ACL and
ST and BPTB and ST. The error bars represent +/- 1 standard deviation, which was determined from
the variance of the measured angles. An asterisk represents significance as determined by an ANOVA,
where p < 0.05.

Upon completion of a two-factor ANOVA to test for interaction effects, the following results were obtained. The main effect for the stressed vs. unstressed conditions was not significant ($F_{(1, 414)}=0.51$, $p>0.05$). The main effect for tissue type (BPTB vs. ACL vs. ST/G) was significant ($F_{(2, 414)}=30.78$, $p<0.05$). There also was a significant interaction observed ($F_{(2, 414)}=13.12$, $p<0.05$). For percent change in crimp angle, significant results were found ($F_{(2,10)}=10.31$, $p<0.05$) (Figure 33). Post hoc testing revealed that ACL (M=14.38) and ST (M= -40.66) are significantly different from one another, as are BPTB (M=12.88) and ST. ACL and BPTB are not significantly different from one another. For a more complete presentation of the statistical results, please see Appendix K.

# CHAPTER 5: DISCUSSION

## *MECHANICAL CPM TESTING*

As seen in Figure 23, there was no statistical significance in the difference of rate of tension loss or the percent total tension loss among the experimental groups consisting of intact ACL, BPTB, and ST/G grafts.  This outcome may be attributed to either the low applied forces utilized in the CPM protocol or the fact that the sample size was too low to provide any statistical significance.   For the former scenario, it is essential to note that absolute values for peak in situ ACL forces experienced during mechanical testing were on the order of about five Newtons.  A series of studies by Morrison (1970) estimated that about 169 Newtons are applied to the ACL during normal human walking, and 445 Newtons are applied when descending stairs (Dargel et al., 2007).  These comparatively high in situ forces indicate that the CPM protocol certainly qualified as a passive process.   Tendons and ligaments are capable of sensing and responding to biomechanical stresses, especially during developmental periods. These tissues are known to restructure themselves so that they may optimally withstand such stresses (Nordin & Frankel, 2001).  Therefore, if the normal in situ forces experienced by the knee are on the order of 169 Newtons, then it is not surprising that all three tissue specimens were able to withstand and perform similarly when subjected to a significantly smaller stress.

Numerous studies have investigated intrinsic differences in mechanical strength among the different tissue types and found statistically different results.  All of these studies, however, tested the tissues to failure, which required applied forces or strains much higher than that generated in this study or even in everyday knee

motion. Woo, Chan, and Yamaji (1997) found that the ultimate failure load for the native ACL in a young cadaveric specimens was 2160 Newtons. Liu, Cabo, and Osti (1995) measured the ultimate failure load of a BPTB grafts at 663 Newtons. Hamstring tendon ultimate failure loads have been reported to range from 419 to 930 Newtons, depending on the attachment method chosen during reconstruction surgery (Dargel et al., 2007). The CPM protocol utilized in this study did not stress any tissue specimen to failure, and therefore it is not possible to make any conclusions regarding overall differences in mechanical properties of the tissue types. We may only conclude that the in situ forces generated during passive knee motion are not sufficient to cause any significant differences in mechanical performance among tissue types. Of course, this does raise the question of at what level of applied force do the mechanical performances of these tissue types start to differ. More importantly, would this level of applied force have any clinical relevance?

Certainly, the limited sample sizes utilized in this study must be taken into consideration when interpreting the validity of the results. The sample size of the experimental groups was extremely small (n=5 for BPTB, n=2 for intact ACL, n=2 for ST/G), especially after data from failed tests were excluded. Within this small sample size, a variety of variables including age, health, and activity level of the persons from whom the ACL grafts were obtained could have possibly confounded the results further (Blevins et al., 1994; Nordin & Frankel, 2001). In addition, the data collected from the AIFP implantable force transducer included a large amount of noise, indicating some inherent fluctuations or error in the measurements taken. These fluctuations are most likely due to the delicate nature of the relationship

between the alignment of the AIFP and the accuracy of its measurements. Even the insertion of the sensor itself may have influenced the results, since both slit length and angular orientation of the sensor have been shown to produce voltage changes up to 100% (Herzog et al., 1996).

Another consistent observation for all three tissue types was a logarithmic decay behavior of in situ force. Previous scientific literature has indicated that BPTB grafts display this behavior under cyclical loading so these results were somewhat expected (Arnold et al., 1995). Possible causes for this behavior may be attributed to unnatural graft attachment methods, the cadaveric state of the tissues, or viscoelastic phenomena. The majority of studies investigating post surgical graft laxity have focused on methods of graft attachment (Dargel et al., 2007). However, graft laxity due to attachment failure is usually observed as a sudden drop in force rather than the gradual decline seen in logarithmic decay, indicating that attachment methods did not significantly influence the results of this study. Further, the pull-out strength for interference screws immediately following surgery can be as high as 50% of the graft strength itself (Frank & Jackson, 1997). Again, since the forces applied to the knee in the CPM protocol were relatively low, it is unlikely that they were able to disturb the graft attachment sites in any significant way.

The most surprising aspect of these results was that the intact ACL also exhibited a tension loss, since one would expect an intact specimen to be able to withstand low levels of stress without decay of tension. Thus, it is possible that this exponential decay behavior in all three tissue types may actually be a property of the cadaveric states of the tissues. Notably, cadaveric tissues are avascularized; the

vascularization process does not begin until six weeks post-operatively, and so our model of immediately post-operative biomechanical stresses remains valid (Amiel et al., 1986). A study by Rupp et al. (2000) examined this exact phenomenon through an in vitro mechanical comparison of postmortem human BPTB specimens obtained within 24 hours of death. BPTB grafts came from 11 different pairs of human knees and were treated according to a vascularized or non-vascularized protocol. It was found that vascularity did not have a significant effect on mechanical properties such as maximum force, stiffness, or elastic modulus of the tendons. However, viscoelasticity in avascularized grafts was shown to be significantly different from vascularized counterparts. Specifically, avascularized specimens showed a significant increase in stress relaxation (Rupp et al., 2000).

Therefore, the viscoelastic nature of the three different tissue specimens may be able to account for their consistent logarithmic decay behavior. Tendons and ligaments consist of two separate phases. There is the solid phase, the main components of which are collagen and elastin. There is also the liquid phase in the form of interstitial fluid, which is a mixture of water and electrolytes (Holzapfel, 2000). The presence of both the liquid and solid phases makes tendons and ligaments biphasic, which means their mechanical deformation will follow some sort of intermediate profile between that of an elastic solid and a Newtonian fluid (Wolfgang & Bernd, 2001). A fluid's flow, or its response to a force input is a time-dependent quantity. Therefore, it is well-established that mechanical profiles of viscoelastic materials are also time-dependent (Özkaya et al., 1999). To conclude that the logarithmic decay seen in this study is a result of the tissues' viscoelastic natures, it

92

would therefore be necessary to observe the mechanical stress protocols at different strain rates. Any change decay profiles due to strain rate variations would indicate that the logarithmic tension decay is a viscoelastic phenomenon.

One of the more pertinent characteristics of viscoelastic materials is their tendency to exhibit stress relaxation whereby the in situ stress will decrease over time when the tissue is subjected to a constant strain (Özkaya et al., 1999). The peak cyclic strain in this study remained constant over all 2400 cycles of CPM, and so it is likely that the overall decrease of in situ stress measured over the course of mechanical testing may have simply been stress relaxation. Typically, viscoelastic tissues that exhibit stress relaxation are capable of regaining their initial levels of stress once the strain is removed. Subsequent decay of stress during re-application of the strain is called hysteresis and would be a true indicator of permanent tension loss (Özkaya et al., 1999). Our study did not conduct multiple sessions of cyclic loading and so we cannot conclude whether or not any hysteresis occurred in our tissue samples. This would be an interesting future of study, however, and if differing levels of hysteresis were to be observed, then this would seem to recommend a cyclic loading protocol in the future for ACL grafts prior to implantation during reconstruction surgery.

Another important factor to a cadaveric tissue state is that moisture levels within the tissue specimen may not be maintained or replenished without artificial measures. As biphasic materials, both tendons and ligaments contain water, and the mere presence of water effectively raises osmotic pressures within the tissue, therefore increasing the overall mechanical stiffness of the tissue (Wolfgang & Bernd,

2001).  While soft tissues immediately surrounding the cadaveric knees were kept in place, this did not completely prevent water loss.  Every time the knee was flexed, the fibers of the ACL or ACL graft would be pulled in tension, during which time a small amount of water may have been forced out.  The knee joint itself was only partially enclosed by soft tissues, held together by a spaced out baseball stitch, during the course of CPM, which possibly allowed some moisture to evaporate.  Therefore, it is likely that the volume fraction of water within the ACL and ACL grafts decreased during the course of mechanical testing which would have decreased the intrinsic value of the tissue's elastic coefficient.  Lower elastic coefficients would linearly correspond to decreased in situ forces, and so it is very likely that part of the logarithmic decay may also be attributed to moisture loss that occurred during the course of CPM.

Lastly, we compared the relative tension loss and not the absolute tension loss of three experimental groups during mechanical CPM testing.  Thus, while all three tissue types may have similar rates of tension loss, one might have had a smaller total absolute tension loss, making it more favorable as an ACL graft.  However, this was outside the scope of this experiment as we were interested in the rate of tension loss rather the absolute total tension loss.  In addition, the absolute tension of the graft depends greatly on the thickness of the graft.  This value would not be easily calculated for the ST/G graft since this graft is composed of two tendons bundled together and doubled over, unlike the ACL and BPTB graft where no such preparation is necessary.  As such, the results of this experiment indicate that there is no better performing graft between BPTB and ST/G in terms of rate of tension loss,

but prior scientific literature has concluded that BPTB is stronger in absolute tensile strength. Thus, BPTB may be the graft that should be preferred if one is only considering the strength of the tissue and the rate of tension loss.

## *BRIGHTFIELD MICROSCOPY*

This study aimed to examine the crimping structure of the different graft types as well as the change in crimping caused by stressing the tissues. Results showed that the crimp size of all three unstressed tissue types were significantly different. The ACL showed significantly larger crimp angles before stress, meaning that the crimping in the ACL was tighter than the BPTB or ST/G grafts. BPTB had the second highest crimp angle and ST/G grafts had the smallest crimp angle. This means the ST/G graft started off with the most relaxed crimping pattern. Because these observed differences in crimping were found in the unstressed forms of all three tissue types, they must be due to innate tissue differences.

These findings are consistent with previous studies that have shown innate differences in tendons and ligaments. Amiel, Frank, Harwood, Fronek, and Akeson (1983) studied biochemical and histological differences in tendons and ligaments in rabbits. Despite appearing grossly similar, tendons and ligaments exhibit differences in several properties including: presence of type III collagen, DNA content, metabolic activity, and total collagen.

Franchi et al. (2008) examined the subfibrillar arrangement of tendons and ligaments and found that ligaments contain some smaller fibrils with a helical subfibrillar arrangement not seen in tendons. These fibrils help ligaments respond to multidirectional forces better than tendons. Additionally, ligaments and tendons have

different jobs within the body, which helps explain their variation in structure (Franchi et al., 2008; Amiel et al., 1983). Tendons exist to transmit motion between muscles and bones, while ligaments function to limit motion between bones (Franchi et al., 2008). The significant difference observed in initial crimp angle between the native ACL and the two tendon grafts in this study is likely related to differences in the innate functions of ligaments versus tendons.

Amiel et al. (1983) concluded that there was variation even within a specific tissue type. For example, differences in structure were observed between collateral and cruciate ligaments and patellar and Achilles tendons studied in rabbits. These differences were smaller than those seen between tendons and ligaments, but still measurable (Amiel et al., 1983). Furthermore, even if the tissues started out the same, previous research has shown that the unique experience of each tissue can alter its properties (Shadwick, 1990). Shadwick (1990) found that the digital flexor and digital extensor tendons found in pigs are identical at birth, but develop differently depending on the stress each tendon type experiences. Changes in elastic properties occur naturally in these tendons with age and growth, but that change is amplified in a tissue that has been exposed to more severe loads (Shadwick, 1990).

Due to the differences in location within the leg, the hamstring and patella tendons are likely to have experienced different load ranges. The reported differences found within a specific tissue type align with our finding of a statistically significant difference between the unstressed BPTB and ST/G grafts. Differences in composition and previous stress may explain why this study found significant initial crimp differences between the unstressed tendons.

Although our study found inherent morphological differences among the unstressed ACL, BPTB, and ST/G grafts, the crimp patterns of each graft type were not significantly different from each other after stressing, except for between the ACL and BPTB. The difference between ACL and BPTB does not seem particularly meaningful, as each tissue had different baseline measurements in terms of their initial crimp angle prior to stress. Instead, the differences between stressed and unstressed tissue must be analyzed in a normalized manner. Thus, the raw stressed data is meaningless except in the context of their starting points.

Another goal of our study was to compare the difference between the initial and final crimp angles for each of the types of tissue. Figure 33 displays a comparison of percent change, i.e., change relative to their initial state, between the three tissue types. We expected the stressed tissue to have larger crimp angles than the unstressed tissue. Significant differences were found between ACL and ST, as well as between BPTB and ST tissues. The data showed that ACL and BPTB behaved similarly and in a manner according to our hypothesis. Their crimp angles had an overall increase, causing their crimps to flatten in response to stress. ST, on the other hand, behaved in a completely opposite manner.

Contrary to our hypothesis, the trend for the ST tendon showed that the collagen crimp angle got tighter after mechanical stress rather than flattening out as expected. The response of tissue to stress is to extend its length, or increase strain. Originally, we had thought that after immense stress, the crimps would not be able to recoil back to their original shape once the stress had been removed, and that this loss of elasticity was ultimately responsible for the decreasing tensile strength of the

tissue: the tissue can no longer extend as far when new stress is applied. However, our data suggests that the ST tendon had been stressed to the point where collagen fibers were moving relative to each other to enable fiber extension.

Collagen molecule sliding has been found as a mechanism for fibril elongation (Purslow, Wess, & Hukins, 1998; Screen, Lee, Bader, & Shelton, 2004). This phenomenon allows the tendon to better resist stress at lower loads by extending the fibril. When the mechanical stimulus is removed, the fibers slide back into their original position by way of the proteoglycan crosslinks connecting them. However, at high loads, the sliding fibers fail to snap back into position and contribute to irreversible failure of the tissue. Screen et al. (2004) hypothesize that this observation is because the crosslinks reach a threshold for failure, and the fibers can no longer resume their prior shape.

Because the collagen fibers are moving against each other, they are eventually moving outside the fibril sheath. Because the fibers have escaped their bundles, the crimps that used to be compressed can now recoil more since the constraints are no longer present. This may explain the smaller crimp top angle seen in our data.

Because we see this phenomenon long after the mechanical stimulus is removed, our data suggests that the ST tendon's crosslinks have actually broken, thus preventing the collagen molecules from sliding back into their original formation. This would also imply that given the same mechanical stress load, the ST tendon approaches failure more quickly than either the ACL or the BPTB tissues. We cannot make sweeping generalizations about morphology during mechanical failure as our methodology did not stress the tissue to that extent.

Nonetheless, Kondo et al. (2012) found that precautions should be taken following ACL reconstruction with ST grafts, as they experience necrosis and are weakened after surgery. This study was performed in live sheep, which differed from our cadaveric model system. However, the clinical implications of their study match that of ours: vigorous activity with a knee reconstructed with an ST graft may not service the patient as well as BPTB graft reconstructions.

Further evidence of this clinical implication is that the ACL and BPTB's morphological behaviors were not significantly different from each other, though they were both significantly different from ST. Regardless of what graft is used in reconstruction, neither can be perfect because tendons are used as substitutes for ligaments. They cannot recreate the complex nature of the native anterior cruciate ligament. As Franchi et al. (2008) and Amiel et al. (1983) have shown, the functions of ligaments and tendons differ, and thus their morphology is arranged to best accommodate those functions.

The BPTB graft was considered the gold standard of ACL reconstruction surgery for its comparative strength. ST/G grafts were found to have 49-70% of the initial strength of the ACL versus the BPTB grafts, which showed 159-168% (Noyes, Butler, Grood, Zernicke, & Hefzy, 1984). Though the hamstring graft has also risen in popularity, primarily for its lack of post-operative complications and pain, many researchers and surgeons still find bone-patellar tendon-bone to be the better choice (Li et al., 2010).

Recent studies have also shown that reconstruction with BPTB offers more stability to patients as compared to hamstring (Anderson, Snyder, & Lipscomb, 2001;

Hospodar & Miller, 2009). Paterno, Weed, & Hewett (2012) showed that there was more anterior-posterior knee laxity when the hamstring autograft was used. Beynnon et al. (2002) found that in the criteria of knee laxity, pivot-shift grade, and strength of the knee flexor, the BPTB replacement showed superior results over the STG graft. For example, in post-operative procedures such as the KT-1000, Lachman, and pivot tests, the BPTB showed more favorable results that indicated higher knee stability (Li et al., 2010).

The results of our study agree with the aforementioned conclusions and offer a rationale behind the objectively better performance of the BPTB graft in ACL reconstruction. We hypothesized that the graft tissue with behavior most similar to that of the native ACL should be considered the graft tissue that is best suited as its substitute. In other words, which tendon is best able to traverse the innate differences between itself and ACL? On a criterion of crimp angle alone, BPTB seems to mimic the native ACL's morphological behavior the best. This may suggest that clinically, the BPTB graft should be preferred in ACL reconstructions.

## *LIMITATIONS*

There are several limitations in our experimental methodology that could be corrected in the future, the primary of which being a more controlled environment. There were many outside sources of variability that we could not manipulate for this study.

Ideally, the cadaveric legs and the graft tissue would also have similar conditions, e.g., age, sex, weight, cause of death, etc., in the future. Fortunately, the tissues for this study did not have causes of death that directly related to

biomechanical performance. It is unlikely that future studies would be able to standardize such a condition, so non-biomechanically related causes of death may be as close to ideal as possible. However, a more representative study would use tissue from people of similar ages. Specimens from younger people would be more applicable, as they are generally the ones who undergo ACL reconstruction. Additionally, the sexes should either be uniform, all male or all female, or have an equal representation of each since females have a higher tendency to suffer from ACL injuries than their male counterparts (Dugan, 2005). The underlying cause for this skew in demographic is as of yet unconfirmed. There is speculation that the lower center of gravity and wider hips may contribute to this difference in ACL injury occurrence between the male and female sexes. Thus, tissues from males versus females may not be comparable.

Though we tried to ensure identical treatments for all tissue, oftentimes tissues underwent differing amounts of freeze-thaw cycles. More problematic still is that they went through more than one freeze-thaw cycles. Previous studies have had mixed conclusions about the effect of multiple freeze-thaw cycles on the biomechanical performance of tissue. Some found the effect negligible on the tissues in question for this study, e.g., the BPTB and ST/G (Jung et al., 2010; Clavert et al., 2007). Others found that there was a measurable difference under certain conditions (Goh et al., 2010; Huang et al., 2010). Regardless, in the future, we hope to limit the number of freeze-thaw cycle to one for each tissue: freezing for storage and thawing only when the leg or tissue is ready for reconstruction followed by continuous passive motion mechanical testing.

Additionally, in regards to the freeze-thaw cycles, we would hope that in future studies, all tissues underwent the same number of cycles and the same amount of time for freezing as well as thawing. To ensure this, future studies should perform reconstruction and mechanical testing on all specimens within the same few days. Unfortunately, this study separated out the mechanical testing of specimens sometimes by weeks or months, as we were constrained by the functionality and availability of various equipment, e.g., the tension transducer, the MTS machine, the OCT apparatus, etc. The uniformity in freeze-thaw cycles and their respective times would lend less uncertainty as to whether the biomechanical performance and morphological differences were a function of the tissues innate nature or whether temperature had played a part.

A more standardized method of sampling tissue should be employed in the future. Because the tissue was often uncooperative during sectioning, this study gathered as many samples as possible regardless of its relative position in the full-length tissue and its relative position to the tension transducer during mechanical testing. However, tissue near the tension transducer may be damaged due to the insertion of the device, and tissue in the center versus tissue at the edges may not be comparable. This study did separate out center versus edge fragments of tissue, but the apportionment was vague rather than specific. During sectioning, samples were taken anywhere from the fragment length. Thus, in the future, tissue dye should be applied to the length of the tissue to mark where it had been exactly, and to sample tissues that are in more or less the same location. Additionally, more care should be

taken when sectioning to take samples from the beginning, middle, and ends of the tissue fragment.

Another potential confounding variable was the calibration of the tension transducer. Gross calibrations were performed on the device to ensure that the voltage outputs could be correlated to more meaningful force data. However, gross calibration was limited and inconsistent due to the nature of the AIFP transducer. The shape and size of the transducer made it difficult to capture absolute tension values. In addition, different transducers were used over the course of this experiment because the delicate nature of the transducer caused the device to malfunction several times. In the future, we would try to locate a different transducer that could measure force data with greater precision and durability than the AIFP.

There was also much difficulty with the placement of the transducer within the intact ACL and the ACL grafts before mechanical testing. In order to implant the transducer, an incision had to be made and sutures were required to keep the transducer from slipping during the mechanical CPM testing. Due to the variations in tissue properties across the grafts and native ACL, it is possible that the incision and addition of sutures could have affected the readings from the transducer. In the future, the effect of an incision and subsequent suturing should be evaluated. In order to better characterize the confounding effect of sutures, future calibrations could be run on the tissue with sutures placed at differing distances from the transducer. Such a design would allow future force data to be adjusted based on the distance from the sutures to the force probe.

The surgical procedure for the ST/G reconstruction also varied in this study. Depending on the suitability and sufficiency of the ST tissue, the surgeon occasionally chose to construct a graft of just semitendinosus and other times constructed a graft with both semitendinosus and gracilis. This difference could have affected the biomechanical performance of the ST versus STG grafts relative to each other.

Previous research has shown that the gracilis tendon has a comparatively higher fibril-to-interstitium ratio as well as a higher density of collagen III fibers while the semitendinosus tendon has a higher density of blood vessels and collagen I fibers (Hadjicostas et al., 2008). Hadjicostas et al. (2008) concluded that given the same thickness, the gracilis tendon would be able to provide 15% more collagen than the semitendinosus tendon, which could "play an important role for better biomechanical stability of the gracilis tendon." Since morphology is often thought to be linked to function, there likely exist differences in the abilities of ST versus STG grafts to resisting stress. Additionally, if the gracilis tendon is more capable of providing biomechanical stability, its collagen may have been preferentially stretched as compared to the semitendinosus tendon. The morphology of the ST tissues in ST versus ST/G grafts may also not be an accurate representation of how crimping changes.

The choice of ST versus STG grafts is likely common in real-life surgical situations, if the surgeon finds the patient's semitendinosus insufficient for creating an autograft, and thus this study accurately reflects that realistic situation. However, for creating a more controlled environment, future studies should all construct an STG

graft to minimize confounding variables during the reconstruction process. Though every ST may not be insufficient, it probably also will not hurt to have the gracilis tendon as a participant in the graft.

As to tissue processing, future studies should standardize the amount of time the tissue specimen is fixed in formalin, both as whole tissue and as fragmented tissue. Though we attempted to maintain the tissue whole for one week and cut for an additional two weeks, this was often not possible. In some instances, we hoped to analyze the tissue using the OCT modality and thus were forced to keep the tissue whole until the OCT machine was available for use. OCT analysis of 1cm fragments would hardly have given us any useful crimping patterns. For some tissues, the three total weeks of fixation did not seem sufficient as it began to shred when sectioned. We were then forced to fix the tissue for longer periods of time for better quality paraffin blocks.

Fixation period is considered a major cause of variation in the reproducibility of immunohistochemical staining (Werner, Chott, Fabiano, & Battifora, 2000). Although this study does not employ immunohistochemistry, the inconsistency of fixation could have resulted in unforeseen confounding variables. The morphology of the tissue samples could have been affected by the time period spent in the formalin, and thus the collagen crimp angles may not have been reflective of the actual tissue. Thus, in the future, an absolute minimum time should be established for tissue fixation—a period of time wherein all the different types of tissues could definitely be sectioned without any trouble. From experience, this time period could be four to five weeks if erring on the side of safety. Additionally, if the OCT modality is

available immediately after mechanical testing, that would mean the tissue could be cut into fragments immediately. This would mean the tissue has more surface area to be fixed at the onset, allowing for more efficient tissue processing and hopefully better results.

Future studies should strive for a greater sample size. This study was constrained financially and by mechanical failures, so the final *n* ranged from three at the very least to five at the very most. Possession of a large sample size may help to diminish influences of such variables as gender, age, and disease state. Eliminating such variability would make the average dependent values obtained more representative of the experimental groups and would allow trends to be more easily visualized. Most importantly, a larger sample size would allow us to have greater confidence in the accuracy of our results, so that a more concrete discussion could be formulated.

## *FUTURE DIRECTIONS*

Concerning the OCT machine, in the future, studies should confirm crimping for OCT. What this means is that a control experiment should have been performed on tissue to confirm what crimping looked like under the OCT modality. Hansen et al. (2002), for example, examined a piece of tissue under OCT and then stretched the tissue so that the crimping should have stretched out until it disappeared from the output image. They noted that when the sheep tendon had been stretched, the dark vertical banding was smoothed out and thus that must have indicated the crimping troughs. In this study, we relied on Hansen et al.'s (2002) methodologies and results to assume that vertical banding was in fact evidence of crimping while the horizontal

banding was simply superfluous birefringent banding. Future studies should perform the experiment anew to provide an accurate baseline for what is being seen for OCT.

OCT should also be performed on the same piece of tissue before and after mechanical testing. In this study, the OCT construct was not available immediately before or after mechanical testing, and thus we were forced to make use of the matched pair tissue. In other words, tissue A and B are a matched pair, and tissue A stayed unstressed while tissue B would be stressed. A "pre-image" was taken of tissue A to serve as baseline for the "post-image" taken of tissue B after mechanical stress. This was a theoretically accurate comparison that could be made, but future studies should take advantage of OCT's non-invasive nature. Because OCT does not damage the tissue, the specimen slated for mechanical testing should be pre-imaged and post-imaged. The results would be far more comparable then, as it is the exact same specimen.

Aside from better control during the experiment, another future direction is to better employ the OCT modality. OCT as an imaging technique for tendons and ligaments is still in its early stages, and this study was not able to employ the modality as we had hoped. The images we obtained were far from ideal. However, as this technology evolves and as proficiency with the technology grows, future studies should make more effort to find better images of OCT, take measurements concerning collagen crimp patterns, and compare them to angles obtained from histological methods. Should the results derived from OCT match the results derived from traditional histological methods, then OCT would be confirmed as a possible modality for biomechanical research. This might mean that OCT may become a more

universally used, which would provide more versatility in the experiments that could be conducted. Comparisons would be more valid as the same tissue could be analyzed before and after a certain treatment.

A newly developed OCT device, the laparoscopic OCT (LOCT), was initially used in the detection of human ovarian cancer (Hariri et al., 2009). With the same benefit of non-destructive imaging, the LOCT is capable of imaging depths up to 2mm with resolution approaching that of histological methods (10-20um). The diagnostic histopathological abilities of this new device are encouraging as to what new OCT devices can be engineered in the future. A 2mm depth is not sufficient for use in a clinical setting, as the ACL exceeds that depth from the surface of the knee. However, as OCT grows in resolution and in its ability to penetrate subsurface depths, it could very well become a viable option of ligament and tendon clinical tests and research *in vivo*.

Though our results suggested that the ST tissue had microstructural indications of failure, we can only make conclusions about morphology as a result of biomechanics if the stress protocol actually loads to failure. To show how high-stress loads impact tissue on a microstructural level, future studies should repeat this methodology but stress the tissue until failure before making observations about collagen morphology.

Additionally, while angles of the crimp fibril are a compelling argument, other morphological indicators should be analyzed. Future studies should employ more sensitive imaging modalities. Although we used BLM to obtain images of collagen crimping, many previous studies have opted to use polarized light microscopy (PLM)

or scanning electron microscopy (SEM) instead. We did discuss potentially using either PLM or SEM, but due to financial costs and practicality, opted for BLM instead.

One particular study that utilized PLM and SEM was focused on determining the structure of connective tissue within various skeletal muscles of rats (Jarvinen, Jozsa, Kannus, Jarvinen, & Jarvinen, 2002). PLM and SEM were used to study the crimp angles in collagen fibers after prolonged periods of muscle disuse. The results of this study showed that the crimp angles decreased by 10% in the muscles after the disuse period compared to the normal situation (Jarvinen et al., 2002). The crimp lengths and angles were measured using PLM, whereas the collagen fibrils were imaged in-depth using SEM.

Franchi et al. (2007A) examined crimps in rat Achilles tendons using light microscopy, PLM, SEM, and transmission electron microscopy (TEM). With normal light microscopy, the researchers found that the crimping in relaxed tendons looked more like straight bundles in a parallel arrangement. However, crimps in the same tissue looked like traditional, wave-like crimps when viewed under polarized light microscopy (Franchi et al., 2007A).

When the crimps were visualized using SEM, parallel bundles of collagen fibrils with knots were observed. The researchers described these knots as twisting or bending parts of fibrils, which also slightly resembled waveforms. TEM resulted in similar images of crimps as SEM (Franchi et al., 2007A). Overall, all the different types of microscopy used by these researchers depicted traditional, wave-like crimps. The sensitivity and detail that can be captured via electron microscopy (EM) will

allow for cataloguing of features we were not able to notice, such as these knots. Additionally, light microscopy's magnification only allowed us visuals on the fibril level, whereas EM would allow for crimp at the collagen molecule level, which would provide even more insight into the morphology of these tissues.

These other imaging modalities can also add more precision to our results. Kannus (2000) claimed that although the wavy configuration of crimps in collagen fibrils is evident using light microscopy, SEM is a much better technique. A study by Jarvinen, Jarvinen, Kannus, Jozsa, & Jarvivnen (2004) examined crimps in the collagen fibrils of ruptured tendons and found that crimp angles were smaller in ruptured tendons than in normal, healthy ones. The researchers compared crimp angles and wavelengths of the tendons using PLM. SEM, however, allowed them to get a better and more magnified view (Jarvinen et al., 2004). Most of the previous studies used PLM for measurements of crimp angle and wavelength and then SEM for a more in-depth crimp and morphology analysis. Therefore, using PLM followed by SEM would probably have allowed us to obtain the most thorough images of our tissue and best visualize the crimping within the grafts.

Other morphological features are collagen, fibril, and fiber organization. As postulated for the ST tissue, extensive collagen molecule sliding may have caused the recoil in crimp. To be more confident in that implication, organization of the tissue on several levels should also be quantified in the future. Additionally, since tissue organization also plays a large role in the way a tissue responds to stress, this data must also be accounted for in making clinical recommendations on a morphological basis.

Finally, there are several synthetic ACL grafts available on the market today. While such grafts exhibit great short-term results, their long-term clinical success is limited by their poor abrasion resistance, fatigue failure, and lack of integration with host tissue (Laurencin & Freeman, 2005). In order to solve these problems, engineers are working to design grafts consisting of biodegradable scaffolds that provide architecture to which cells attach and proliferate (Cooper, Lu, Ko, Freeman, & Laurencin, 2005). The design of the scaffold is very important in ensuring that the final structure of the engineered graft is mechanically sound. An understanding of the mechanical significance of the crimping patterns in natural tissue could be applied in designing these scaffolds.

## SUMMARY

In summary, the aim of this study was to elucidate the effect of collagen organization on the rate of tension loss following ACL reconstruction surgery. Both biomechanical testing and brightfield microscopy imaging were used to compare graft performance. As predicted, there was an exponential decrease in tension of all graft types following CPM, indicating that the rapid degradation may affect graft function after reconstruction. However, no graft type was capable of resisting tension loss significantly differently than the others. This study offers motivation for future researchers to investigate the potential of pre-tensioning grafts prior to reconstruction surgery in order to improve graft performance.

The imaging results suggest that BPTB grafts may perform better after reconstruction, based solely on morphological differences. BPTB grafts most closely mimicked the native ACL when comparing normalized changes in crimp angle

between the unstressed and stressed conditions. Furthermore, an increase in crimp angle in the ST grafts implies that they approach failure more quickly, although we cannot draw any concrete conclusions as the tissues were not stressed to failure in our experiment. By combining biomechanical testing and imaging to study the effect of collagen organization on tension loss in ACL grafts, this study provides new knowledge about the structure-function relationship of the graft tissues relevant to ACL reconstruction surgeries.

# APPENDIX A. METHODOLOGY OVERVIEW
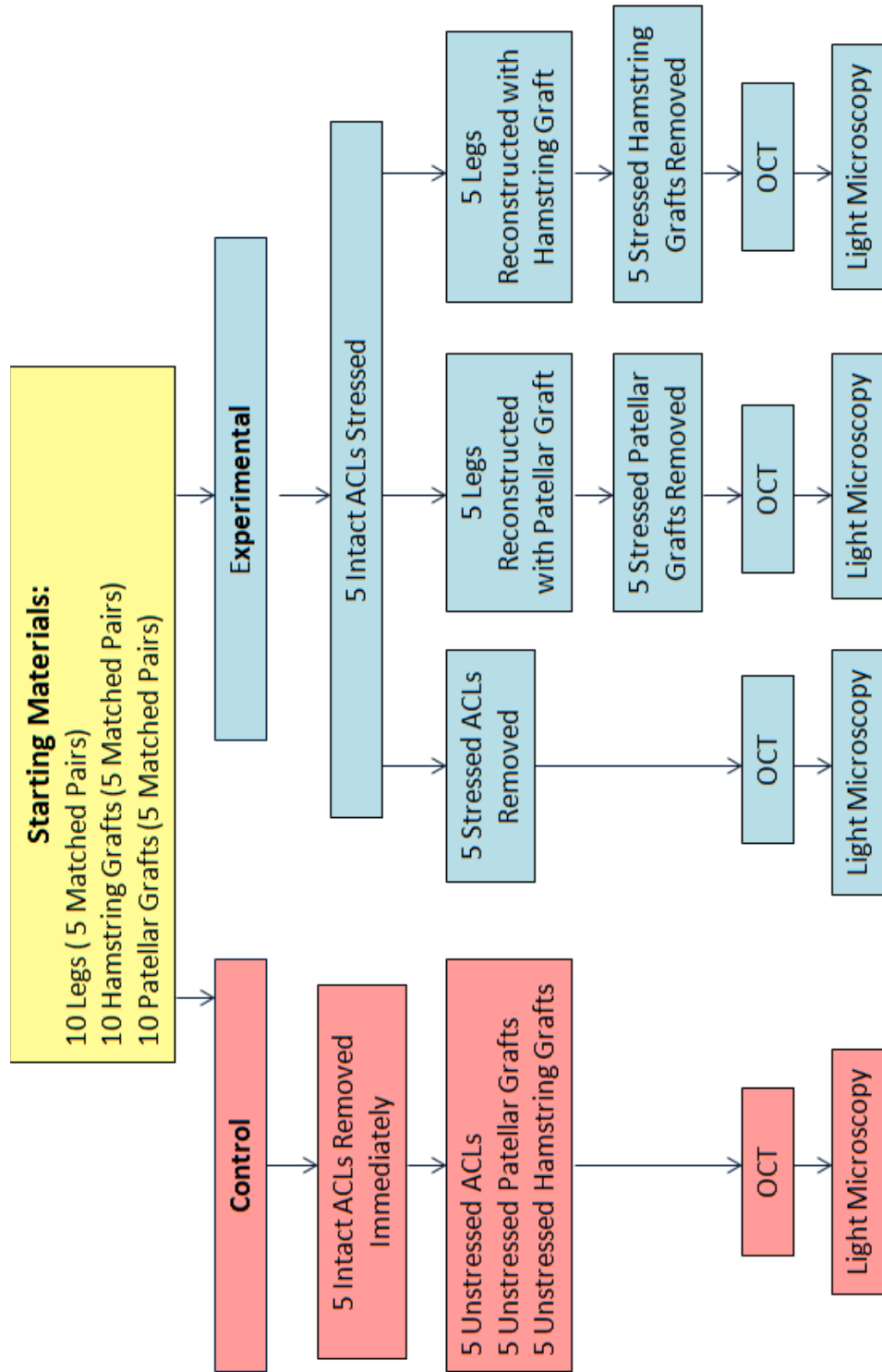
# APPENDIX B. CADAVER SPECIMEN DEMOGRAPHICS

*Table 1*.  Demographics of Cadaveric Legs.  The data details the
> 1) specimen number,
> 2) donor sex, male (M) or female (F),
> 3) donor age, and
> 4) cause of death.

ACL specimens were also harvested from these legs.

| Specimen Number | Sex | Age | Cause of Death |
|---|---|---|---|
| 11-1603 | M | 90 | CARDIAC ARHTHMIA; ANOIC BRAIN INJURY |
| 11-1617 | M | 74 | ASPIRATION PNEUMONIA |
| 11-1624 | M | 77 | RECTAL CANCER |
| 11-1625 | M | 94 | SEPTICEMIA |
| 11-1574 | F | 83 | CARDIAC ARREST; COMPLICATON OF CALDIFIC AORTIC STENOSIS |
| 11-498 | F | 84 | BILIARY CARCINOMA (LIVER CANCER), DIABETES, HYPERTENSION |

# APPENDIX C.  MUSCULOSKELETAL TISSUE FOUNDATION GRAFT TISSUE DEMOGRAPHICS

*Table 1.*  MTF Graft Tissue Demographics.  The data details the:
1) Donor ID number
2) Donor age
3) Donor sex: male (M) or female (F); note that MTF did not provide information about sex for the last three specimens
4) Donor race: Caucasian (C), Hispanic (H), Black (B), or Asian (A)
5) Donor height in inches
6) Donor weight in pounds
7) Type of tissue donated; note that for each type of tissue, a matched pair, i.e. the left and right legs' specimens, was donated
8) Rejection reason, or the reason why these grafts were not fit for surgical methods in a medical setting; note that MTF listed some reasons as "pending"
9) Cause of death; note that MTF listed some reasons as "pending"

| Donor Number | Age | Sex | Race | Ht | Wt (lb) | Type of Tissue | Rejection Reason | Cause of Death |
|---|---|---|---|---|---|---|---|---|
| 0171007737 | 56 | M | C | 66" | 178 | G BPTB | Clostridium x3 | Myocardial Infarction |
| 0171007609 | 56 | M | C | 68" | 360 | G BPTB | Psoriatic Arthritis | Chronic Pulmonary Aspergillosis |
| 0941007416 | 38 | M | H | 71" | 368 | BPTB | Massive Contamination with Group A Strep | Pending |
| 0831007928 | 57 | F | B | 66" | 188 | BPTB | Multiple Cultures Positive for Yeast | Anoxia |
| 0891007380 | 56 | M | C | 72" | 260 | G ST BPTB | Pending | Myocardial Infarction |
| 0561107999 | 42 | F | C | 63" | 137 | G ST BPTB | Renal Cell Carcinoma | Anoxia |
| 0171006990 | 51 | M | C | 61" | 225 | G ST BPTB | Clear Cell Carcinoma of Kidney | Pending |
| 0216007769 | 76 | M | C | 70" | 234 | BPTB | Clostridium | Respiratory |

| | | | | | | | x7 | Failure |
|---|---|---|---|---|---|---|---|---|
| 0211006981 | 29 | F | C | 68" | 247 | G | Acute Pneumonia | Anoxia |
| 0041102815 | 48 | - | C | 69" | 170 | G ST | Cultures & Enterococcus | Respiratory Arrest |
| 0171102805 | 51 | - | C | 69" | 281 | G ST | Cultures & Enterococcus | Myocardial Infarction |
| 0651100059 | 53 | - | A | 77" | 149 | G ST | History of Osteomyelitis | Chronic Pulmonary Aspergillosis |

# APPENDIX D.  SEMITENDINOSUS/GRACILIS GRAFT SURGICAL CONSTRUCTION

The following figures (1-7) pictorially describe the surgical construction of the ST/G graft as completed by the orthopedic surgeon.  Refer to the Methodology section describing the procedure for more comprehensive detail about the process.

*Note*: Are figures are attributed to Arthrex (2010).

Transtibial

Medial Portal

2



3

Medial Portal
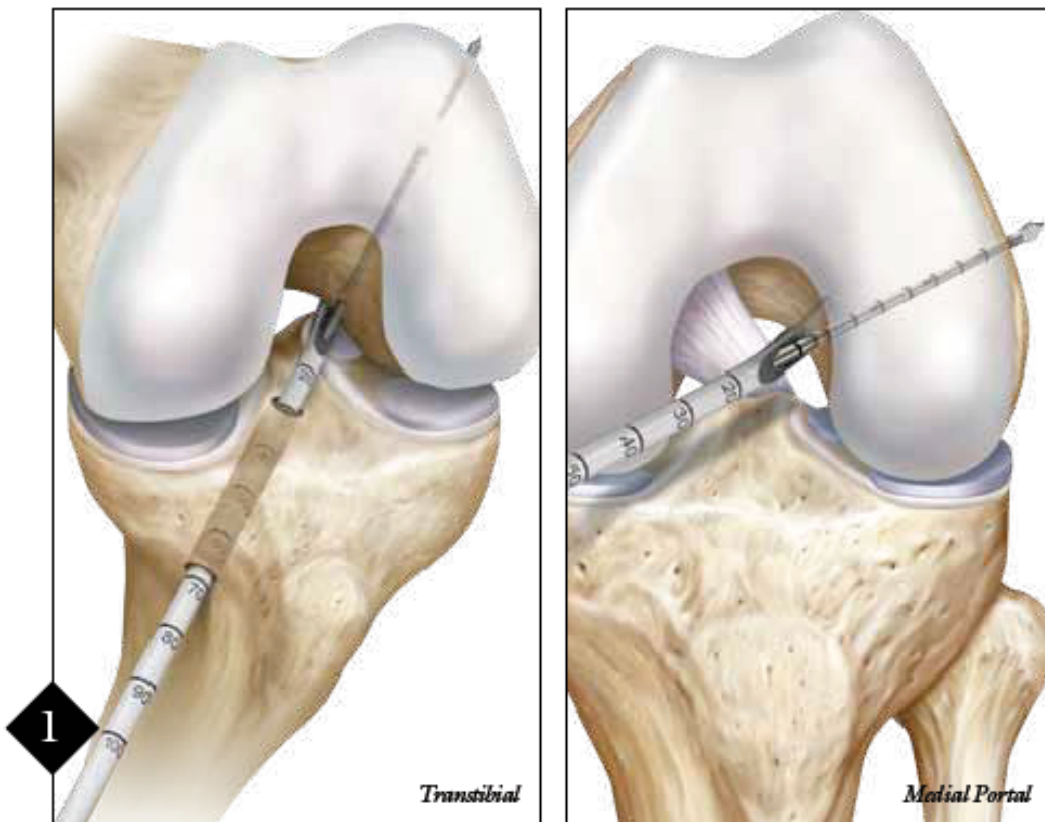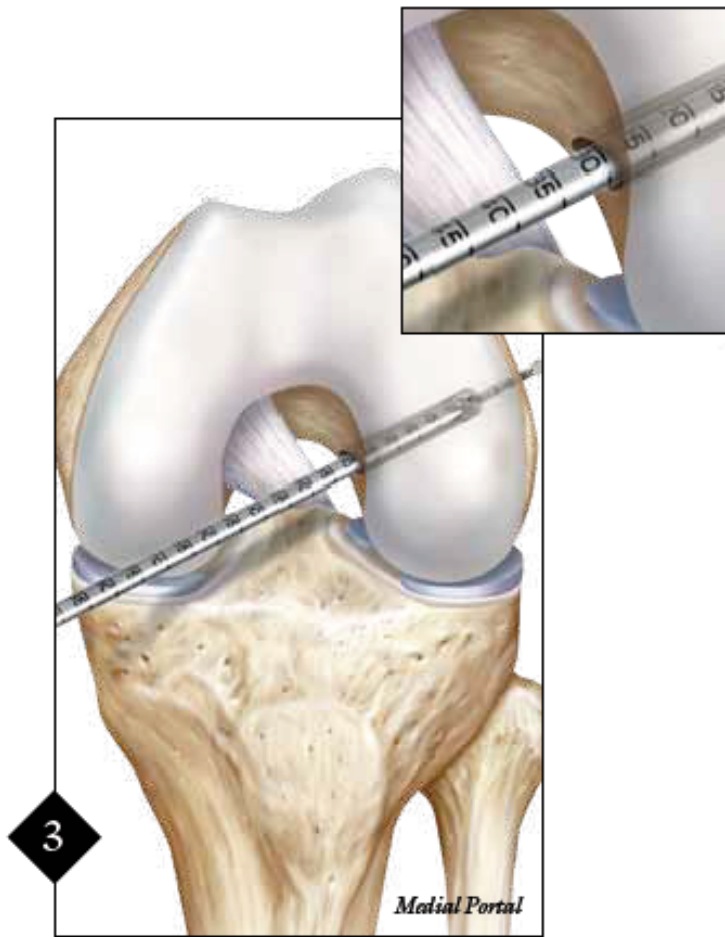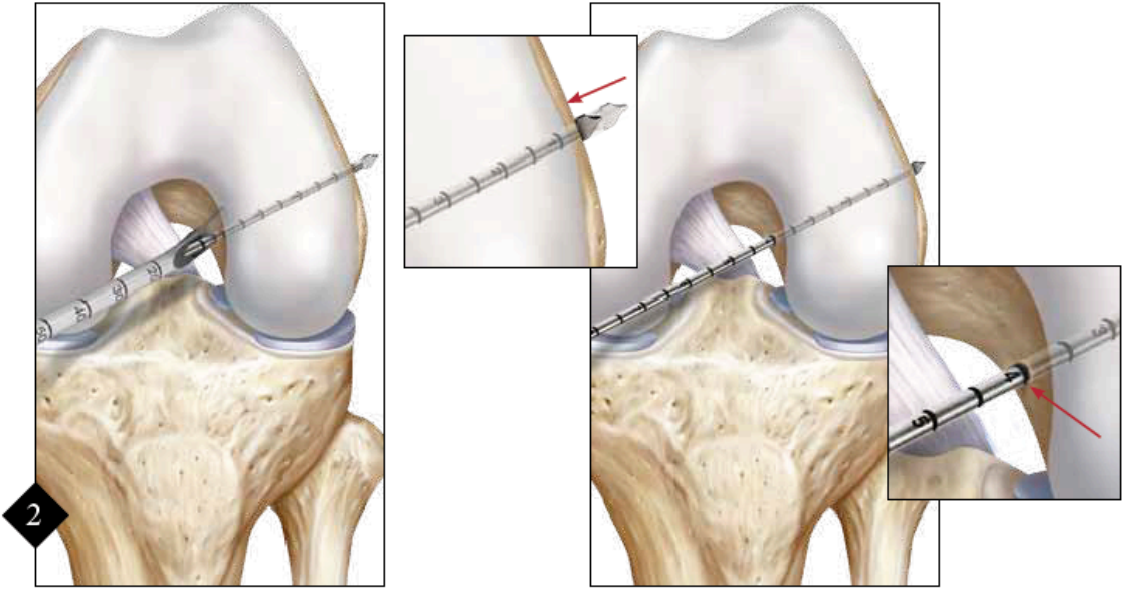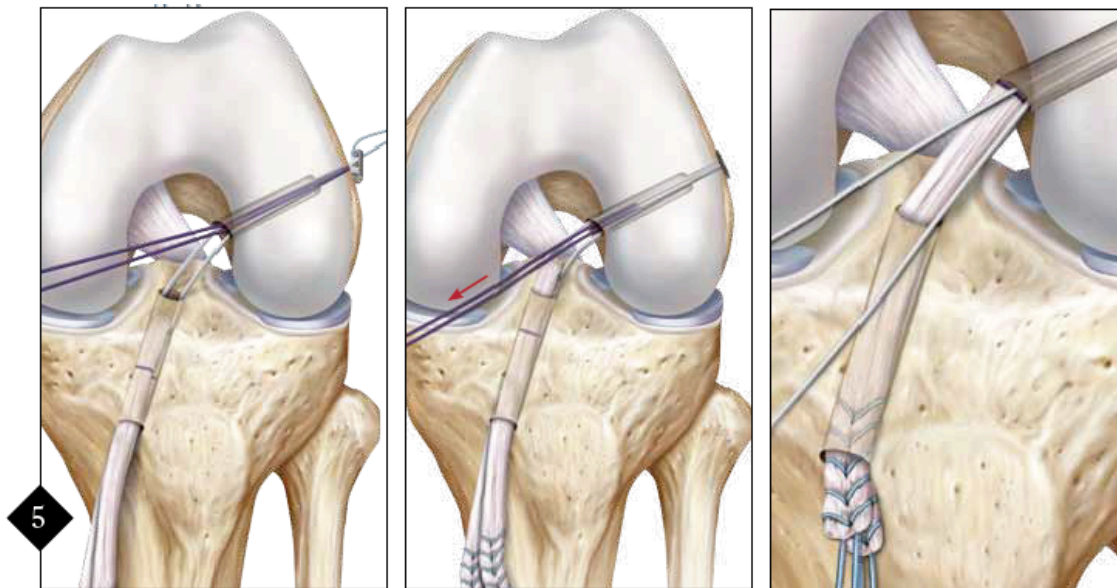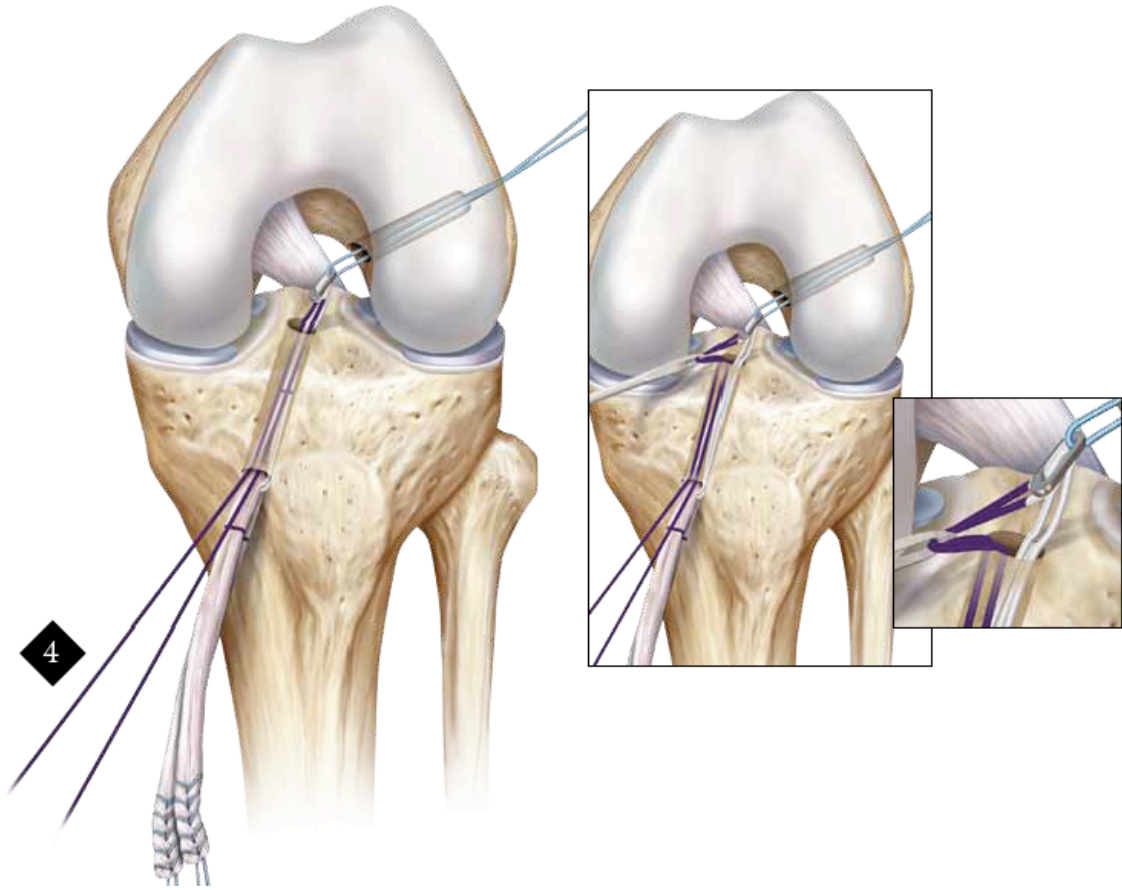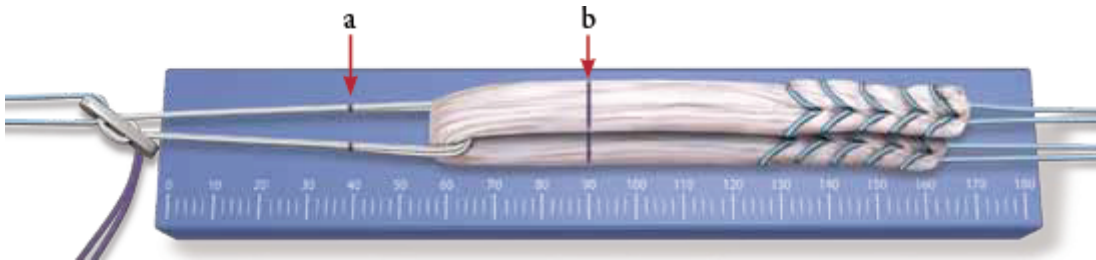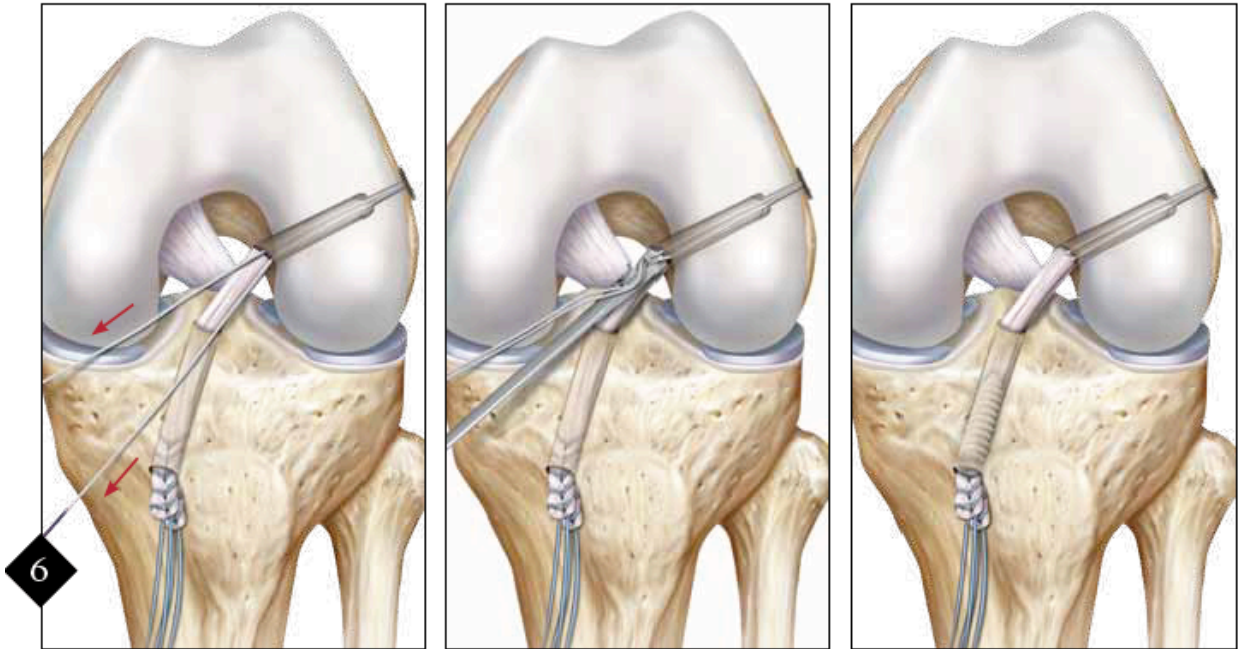
# APPENDIX E.  BONE-PATELLAR TENDON-BONE GRAFT SURGICAL CONSTRUCTION

The following figures (1-11) pictorially describe the surgical construction of the BPTB graft as completed by the orthopedic surgeon.  Refer to the Methodology section describing the procedure for more comprehensive detail about the process.

*Note:* All figures are attributed to Garrett (2011).
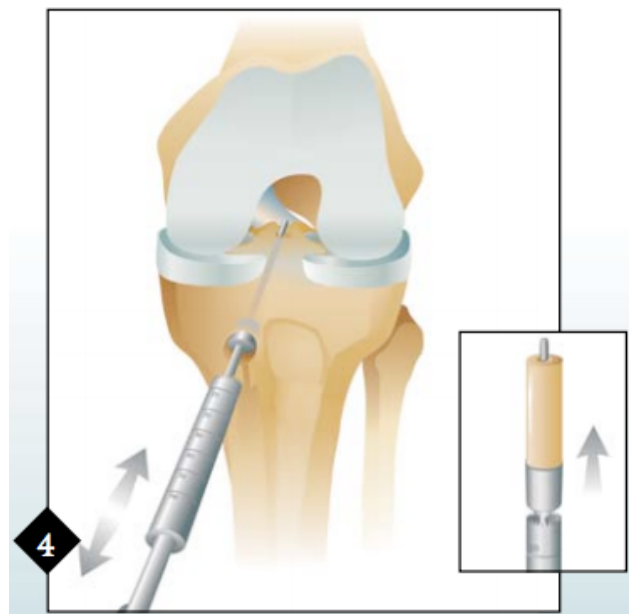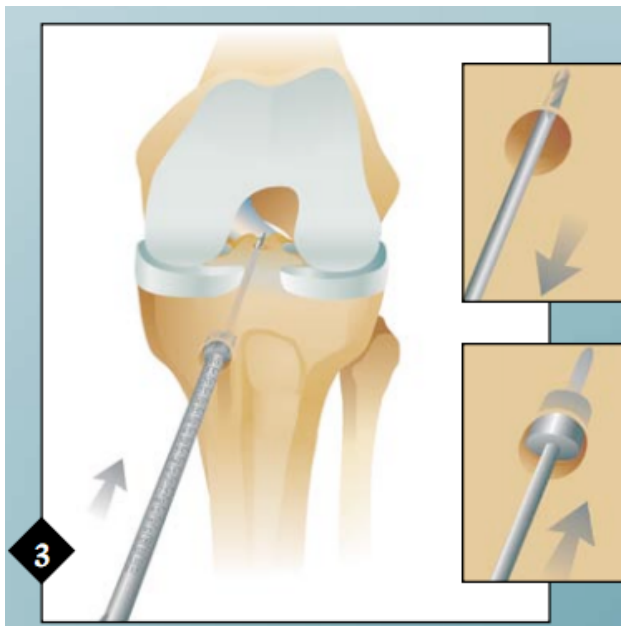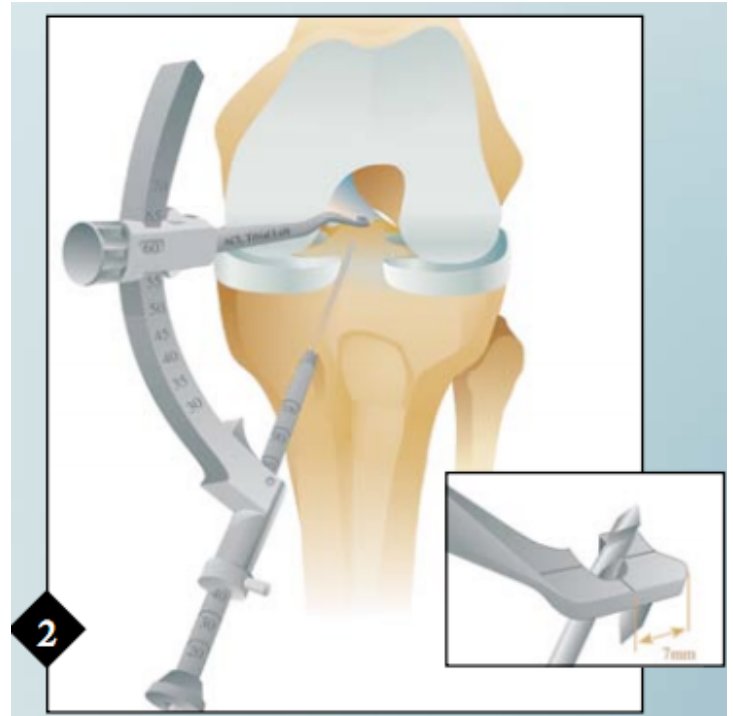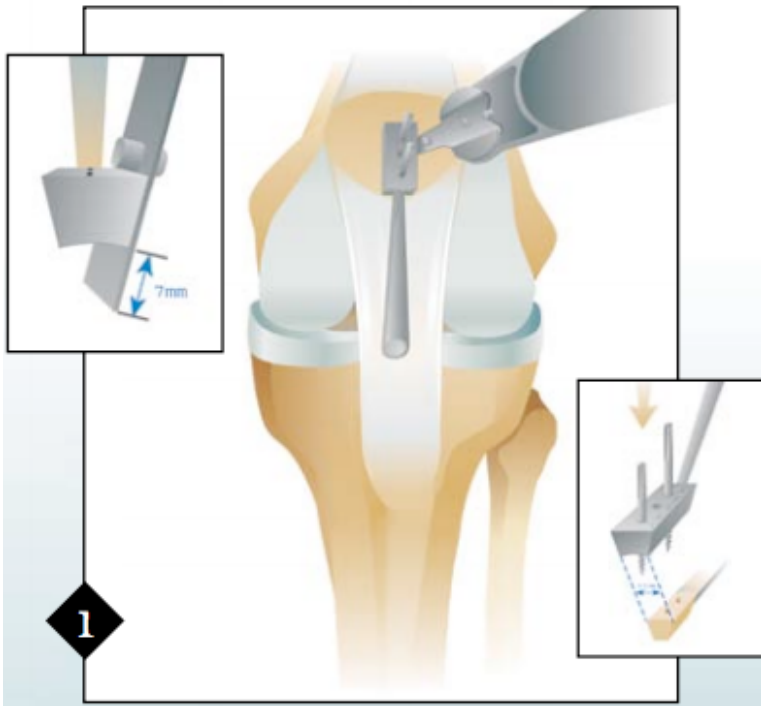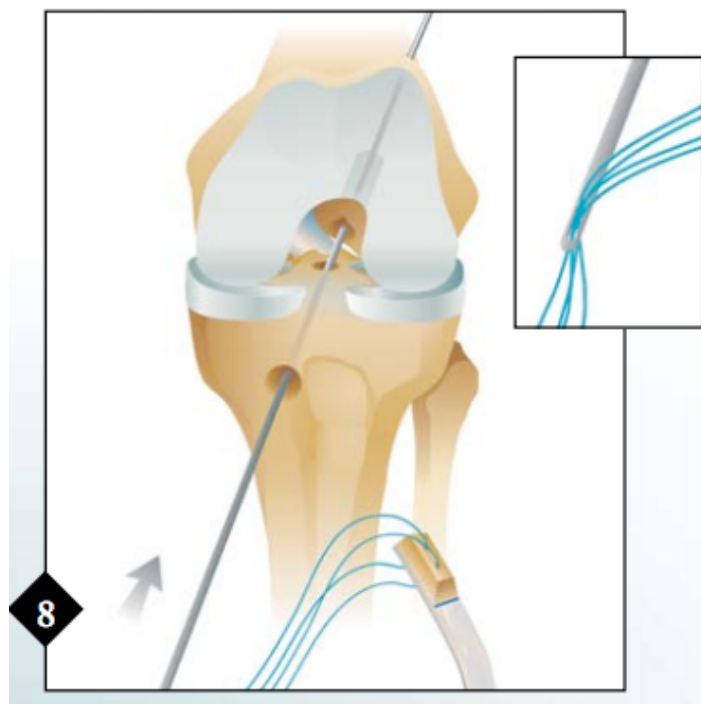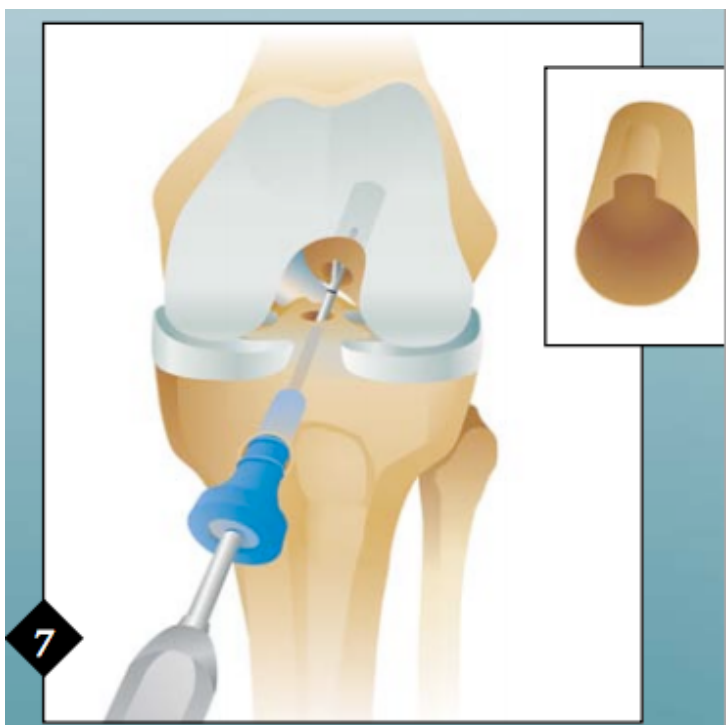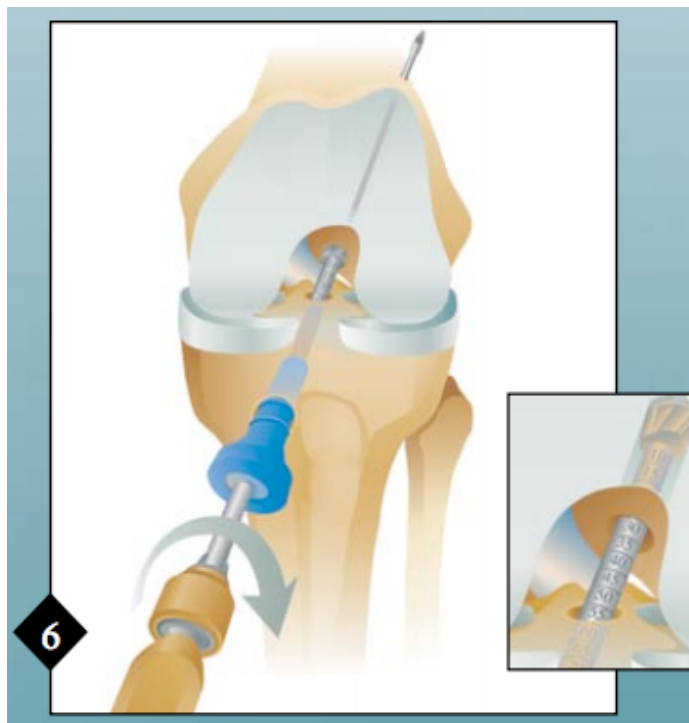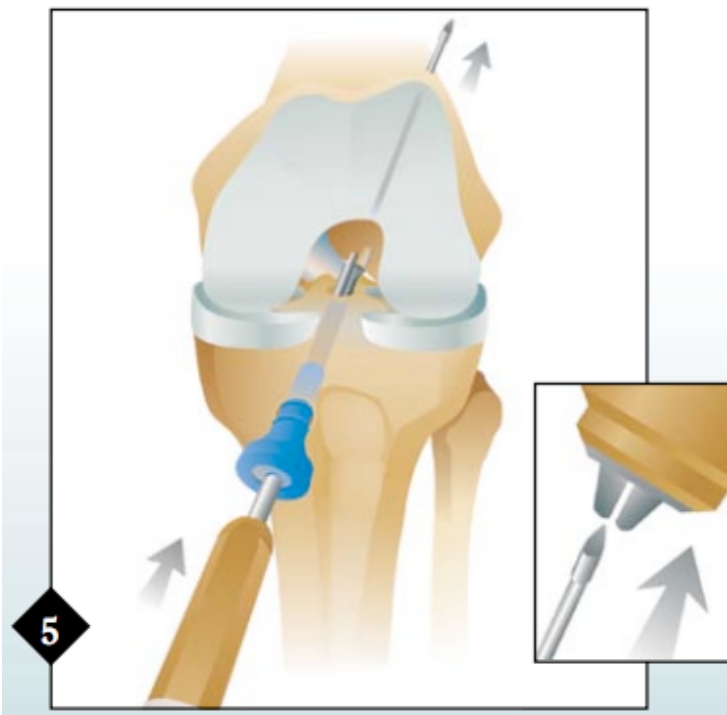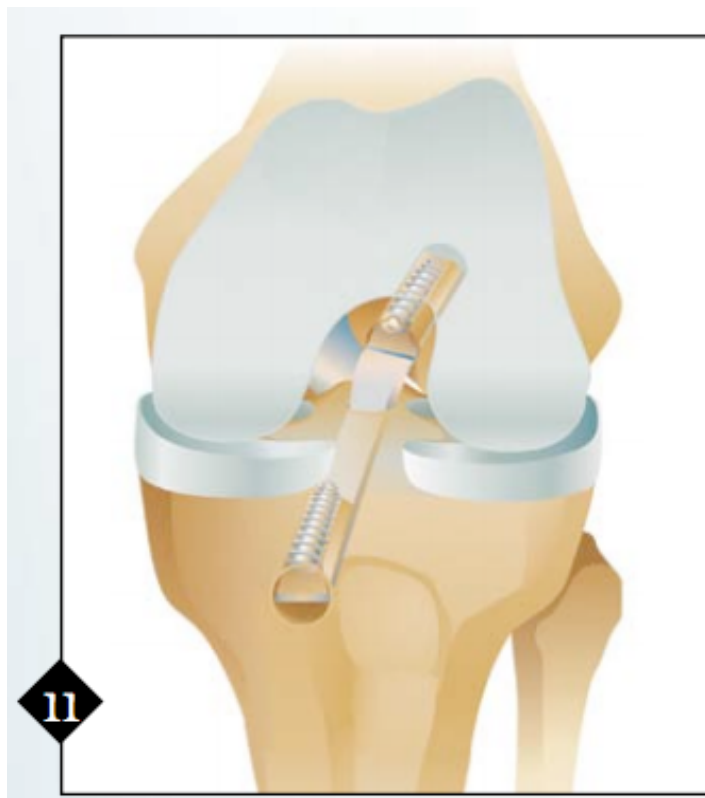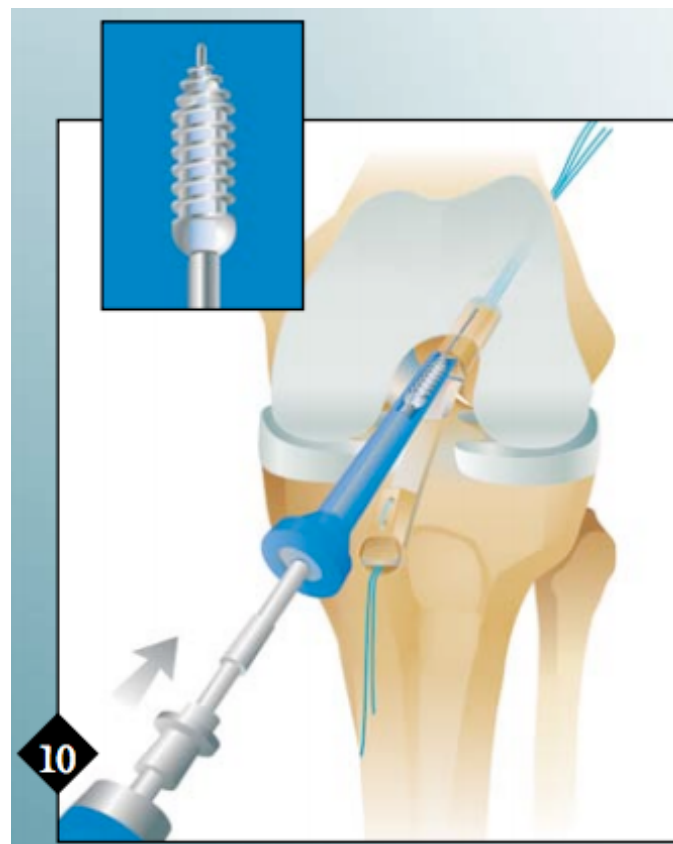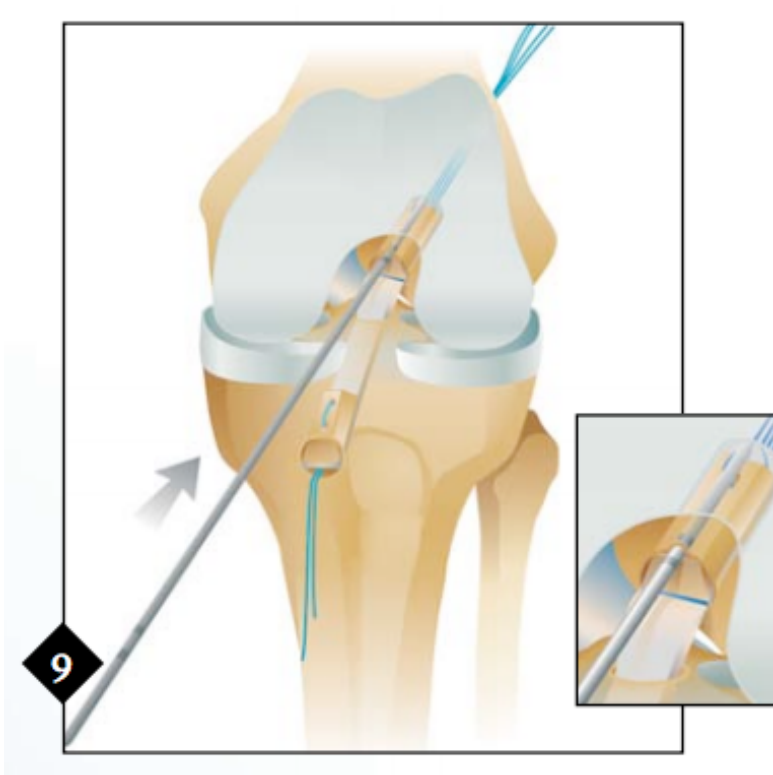
# APPENDIX F. STANDARD OPERATING PROCEDURES

## *REMOVAL OF EXTRANEOUS TISSUE*

Materials
- Bone saw
- Forceps
- Scalpel, blade size 10-11
- Scissors
- Sandpaper

Procedure
1. Measure and mark the distances of 10 and 20cm distal to the tibial tubercle
2. Use scalpel and slice through flesh to the bone at the 20cm mark in preparation for step 3.
3. Using a bone saw, cut the bone all the way through at the 20cm mark.
4. Remove the flesh distal to the knee from the 10cm mark and down completely in order to fully expose bone.
5. Be sure to clean the bone well (use sandpaper), remove any tissue (to allow for easier potting in bone cement later). Remove liquid from bone marrow.
6. Measure distance from center of the knee joint to the end of the now cut tibia, and mark this measured length from the center of the knee joint to the proximal end of the femur.
7. Repeat step 2 and 3 at this mark made in step 5.
8. Measure and mark 10cm from the now cut femur. Repeat steps 4 and 5 at this mark.

## *BONE POTTING*

Materials
- Mold (5 pieces)
- Tape
- Measuring cup (plastic)
- Bosworth Fastray Liquid and Power
- Hollow aluminum tube (length should be slightly longer than width of the assembled mold but still shorter than the solid metal rod)
- Solid metal rod

Procedure
1. Put together the five piece mold with tape, making sure that the walls with the holes face opposite sides. The holes should be closer to the closed end of the mold (as opposed to the end you will be pouring the bone cement in).
2. Place the hollow aluminum tube through the two holes in order to measure and cut the tube to the correct length.

3. Slide the solid metal rod into the tube, which is then placed into the two holes of the assembled mold.
4. Secure the prepared cadaver leg specimen and hold the bone end in the mold in the desired location.
5. Mix 12 scoops (29.6cc/scoop) of the Bosworth Fastray Powder with the liquid at a ratio of 1 scoop to 15 mL. You want to mix 4 scoops at a time in the cup.
6. Once the mixture is fully mixed, pour it into the mold. The bone cement takes approximately 20 min to fully solidify. Take care, the mixture heats up as it solidifies.
7. Remove the mold pieces from the solidified bone cement but removing the tape holding the assembled mold and popping off the walls. (You may need to use a hammer for some stubborn pieces).
8. To pot the other end, connect the previously potted end to the MTS machine and lower into the assembled mold. Repeat steps 1-7.

## PARAPATELLAR ARTHROTOMY

Materials
- Scalpel, blade size 10-11
- Clamps (pick ups)
- Suture kit
- Tweezers/Forceps
- Scissors

Procedure
1. Make an anterior midline incision approximately 15-20 cm in length,
   a. starting on the medial border of the quadriceps tendon (about 3-5cm from top of patella),
   b. continuing parallel to the medial border of the patella,
   c. ending at the medial border of the patellar tendon (about 5-10 cm from bottom of patella)
2. Cut through the skin and subcutaneous tissue to expose the patella, patellar tendon, quadriceps tendon, and vastus medialis oblique. Take special care to avoid damaging ACL.
3. Remove the infrapatellar fat pad.
4. Shift the patella to the lateral side of the leg to fully expose the intact ACL.

## MATERIALS TESTING SYSTEM FOR ACL EXTENSION-FLEXION TEST

Materials:
- MTS machine attachments for potted leg
- AIFP Tension Transducer

Procedure

1. Turn on the Chiller system that is located in the Mechanical corridor directly behind our lab. The key should be left at the MTS machine. The chiller system ensures that the Hydraulic Power Unit (HPU) does not overheat. To turn on the chiller, simply flip the switch on the front control panel.
2. Start up the MTS machine **Station Manager** from the icon on the desktop.
3. Select "ftse_2"
4. Check mark the box **Exclusive Control** in order to be able to click on any options and to set up the test
5. Reset the **Interlock 1** in the Station Manager main window.
6. At the bottom right hand corner of this window, you will see HPU and HSM1 with three boxes to the right. The furthest left box (with one bar) will be selected. As long as the chiller is turned on, you can click the middle box (2 bars) for HPU, and then the rightmost box (3 Bars). Now, repeat for HSM 1. This process is necessary for a slow system startup. Basically, this is to reduce the strain on the building electrical supply.
7. Click on the folder icon under **Basic TestWare** and open up the program labeled "acl-extensionflexion.tst"
8. Reset **Current** and **Total** counters for the number of cycles to zero.
9. Open the **Manual Command** window, check mark **Enable Manual Command**, and select **Axial** as the channel and **Displacement** as the control mode.
10. Set the axial displacement such that the axial mover is not fully extended and then zero the axial displacement in the **Signal Auto Offset** window.
11. Using the black knob on the front of the MTS machine load frame, you can move the cross bar up and down, effectively changing your workspace.
    a. Roughly adjust it such that the knee is at 20° of flexion (where a straight leg is zero degrees of flexion). If you need to adjust finely with the axial displacement command on the computer, remember to zero the axial displacement again.
    b. Measure flexion with the center of the goniometer (compass) over the lateral epicondyle of femur, with the proximal arm over the lateral midline of the femur (referencing greater trochanter), and with the dital arm over the lateral midline of the fibula (referencing the lateral malleolus and fibular head).
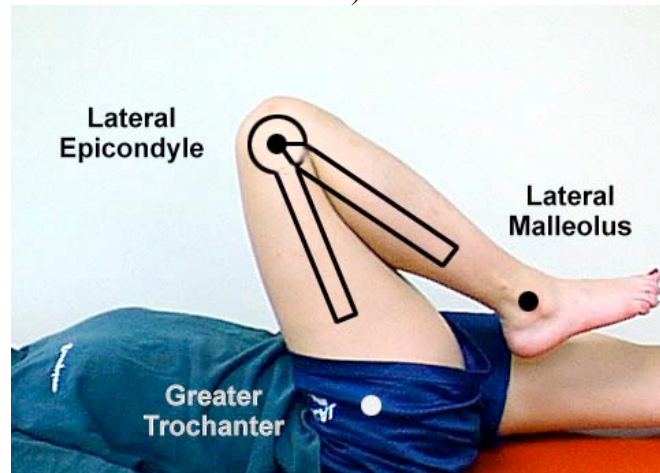
12. On the computer, set the **Axial Displacement** such that the knee is at 70° of flexion. Record the axial displacement, *d*.
13. Click on the icon with a hand with a pencil to edit the program.
    a. Set the target amplitude equal to *d*/2
    b. Set the target set point equal to –*d*/2
    c. Choose a save location and type in a **new filename** for the data to be saved to.
14. Uncheck-mark **Enable Manual Command** for the Axial Displacement
15. Open the **Scope** (icon with sine wave on a graph).
16. When ready, click the **Play** ▷ button to begin the test.


## TISSUE PROCESSING

Taking Out the Tissue
1. Press button with 3 arrows (2 down and 1 up) to open the tissue processor
2. Open the clear handles to each side- they will be hard to pull apart at first
3. The tissue (in the metal cylinder) should move up automatically
4. Remove the hanging metal cylinder containing the cassettes, and take the cassettes out

Putting New Tissue In
1. Get top and bottom tissue from fridge (Alicia's batch will be labeled Batch 2)
2. Take the tissue out with tweezers (the tweezers are placed in one of the plastic containers with an orange top, and we put the container in our little box of staining materials by the desks)
3. Place tissue in cassettes- 2 pieces of tissue per 1 cassette, so 2 cassettes in total (cassettes can be found right next to the gloves)
4. Hit the Prog (program) button
5. You'll see a blinking cursor
6. Get the blinking cursor on the P (2nd line, should say either P1 or P2) using the arrow buttons
7. Get the P setting to P2 by pressing the – or + buttons
8. Maneuver left and right arrows so the blinking cursor is on the hours setting (should read 1h00 or something like that)
9. Press the button with a rounded dotted line (that looks like it's rotating clockwise) to get the metal cylinder that you put the tissue in to correspond to the container that has 70% etOH (the other containers have a greater/smaller concentration of etOH, so make sure the cylinder is rotated so it ends up right above the container containing 70% etOH)

Changing the Settings
1. Press the Prog button again
2. Use the left arrow to move the blinking cursor up to where you see a U followed by a number (the number following U is the container number; paraffin is in containers 11 and 12)

127

3. Next to the U, you'll see a number, so press + or – until you get to U11 to change the processing time in paraffin by going to the 1h00 (or whichever time the processor is set to...you'll be able to tell where this part is) and pressing + or – until you get to the number of hours/minutes you want (Alicia, I think your processing time is 1 hour for each paraffin container)
4. Do the same as step 3 for U12, since paraffin is in both U11 and U12
5. Press the Prog button again
6. Press the down arrow- the processor should close and come down at this point
7. Press start to set up the time you want the processor to start (if the time part doesn't show up right away, press the button that has a clock on it, and this should come up)- the first number should be either a 0 or a 1 (0 means it will start today and 1 means it will start tomorrow) and the second set of numbers will be the actual time that you'll set
8. Press the clock button again, and instead of "start", the screen should say "end" (keep on pressing the clock button until you see "end" if you don't see it the first time)- enter the time you want the processor to stop
9. Close the tissue processor, and it should start as soon as you close it


## COLLAGEN STAINING (LIQUID STAIN)

*Note:* Procedure modified from Polysciences (2010).

1. Obtain slides with specimen and arrange on slide rack
    a. Slide rack is found under staining fume hood
2. Deparaffinize in two consecutive washes of 5' in Citrosolve
3. Rehydration
    a. Dip slides on slide rack slowly 12 times in 100% ethanol tank (use 200 proof bottle). Repeat.
    b. Dip slides on slide rack slowly 12 times in 95% ethanol tank (use 195 proof bottle). Repeat.
    c. Dip slides on slide rack slowly 12 times in 70% ethanol tank. Repeat.
    ***Note: Graded Ethanol and Citrosolve can be found underneath the fume hood. Make sure to fill each tank to the line before beginning rehydration steps.
4. Nuclear Staining
    a. 36 slow dips in distilled water. Approximately 2-3'
    b. Hematoxylin for 8'
    c. Tap water rinse for 9'
        i. Can either run slides under gentle stream of tap water for 9' or do two-three changes of tap water
5. Solution A for 2'
6. Distilled water rinse for approximately 3'
7. Solution B for 110'
8. Solution C for 2'

9. Dehydration
   a. 12 dips in 70% ethanol
   b. 12 dips in 95% ethanol. Repeat.
   c. 12 dips in 100% ethanol. Repeat.
10. Two consecutive 5' washes in Citrosolve
11. Take slides out of Citrosolve and wipe off excess Citrosolve around the specimen
12. Wash in Xylene for 1' and then wipe off excess Xylene around the specimen
13. Apply small amount of Permount on slide (do not cover specimen)
14. Apply coverslip and store
    a. Avoid bubbles/artifacts on specimen as best as possible


## COLLAGEN STAINING (POWDER STAIN)

*Note:* Procedure modified from Kiernan (2011).

1. Make Picrosirius Red solution
   a. Add 0.5g of staining powder to 500ml of saturated aqueous picric acid
2. Make acidified water
   a. Add 2.5ml of acetic acid to 500ml of distilled water
3. Obtain slides with specimen and arrange on slide rack
   a. Slide rack is found under staining fume hood
4. Deparaffinize in two consecutive washes of 5' in Citrosolve
5. Rehydration
   a. Dip slides on slide rack slowly 12 times in 100% ethanol tank (use 200 proof bottle). Repeat.
   b. Dip slides on slide rack slowly 12 times in 95% ethanol tank (use 195 proof bottle). Repeat.
   c. Dip slides on slide rack slowly 12 times in 70% ethanol tank. Repeat.
   <span style="color:blue">***Note: Graded Ethanol and Citrosolve can be found underneath the fume hood. Make sure to fill each tank to the line before beginning rehydration steps.</span>
6. Nuclear Staining
   a. 36 slow dips in distilled water. Approximately 2-3'
   b. Hematoxylin for 8'
   c. Tap water rinse for 10'
      i. Can either run slides under gentle stream of tap water for 9' or do two-three changes of tap water
7. Stain slides with Picrosirius Red solution for 60'
8. Wash twice with the acidified water
9. Dehydration
   a. 12 dips in 70% ethanol

       b. 12 dips in 95% ethanol. Repeat.

       c. 12 dips in 100% ethanol. Repeat.

10. Wash in Xylene for 1' and then wipe off excess Xylene around the specimen
11. Apply small amount of Permount on slide (do not cover specimen)
12. Apply coverslip and store

       a. Avoid bubbles/artifacts on specimen as best as possible


## BRIGHTFIELD LIGHT MICROSCOPY

1. Turn on Olympus 1X2-UCB (bottom left switch), the ASI box, and the joystick
2. Turn top wheel on microscope to setting 1 for brightfield
3. Turn bottom wheel on microscope to setting 6 for QCapture Pro (color images) or 1 for SlideBook (black and white images)
4. Open QCapture Pro software from desktop
5. Click on video camera and ensure that toolbar appears
6. Click on "Live Preview" from the toolbar
7. Start at 10X magnification and use Tshift to turn on light
8. Use the button on the left of microscope front panel to switch between eyepiece view and camera view
9. Adjust light intensity using Focus+ and Focus- or using the microscope front panel lightbulb button
10. Focus the image using focus knob on right or left side of microscope (use F/C button below knob to switch from coarse to fine focus)
11. Change XY coordinates by moving slide or turning on the joystick (power switch on back of joystick box)
12. On the QImaging digital camera preview, hit "Snap" to acquire image
13. Increase magnification to 40X and repeat steps 7-11
14. Save images to Gemstone folder on desktop
15. Exit QCapture
16. Turn off all boxes and recover the microscope with the blue cover

# APPENDIX G. AIFP RAW DATA FILTERING MATLAB CODE

### *READMTSDATALEGS.M*

```matlab
function mtsdata = readMTSdataLEGS(filelocation, newfilename)

fid=fopen(filelocation); %Clavicle_JW3L.dat
if fid < 0
    disp('file does not exist');
end
mydata = textscan(fid, '%s %s %s %*s %*s %*s %*s %*s %*s');
fclose(fid);

a = mydata(1);
b = mydata(2);
c = mydata(3);

time = a{1};
axDisp = b{1};
dvrt = c{1};

%to remove the headers
time = removeHeaderCells(strmatch('MTS', time), time);
time = removeHeaderCells(strmatch('Data', time), time);
time = removeHeaderCells(strmatch('Station', time), time);
time = removeHeaderCells(strmatch('Test', time), time);
time = removeHeaderCells(strmatch('Time', time), time);
time = removeHeaderCells(strmatch('Sec', time), time);
axDisp = removeHeaderCells(strmatch('Header', axDisp),
axDisp);
axDisp = removeHeaderCells(strmatch('Acquisition', axDisp),
axDisp);
axDisp = removeHeaderCells(strmatch('Name', axDisp), axDisp);
axDisp = removeHeaderCells(strmatch('File', axDisp), axDisp);
axDisp = removeHeaderCells(strmatch('Axial', axDisp), axDisp);
axDisp = removeHeaderCells(strmatch('mm', axDisp), axDisp);
dvrt = removeHeaderCells(strmatch('Time', dvrt), dvrt);
dvrt = removeHeaderCells(strmatch('Timed', dvrt), dvrt);
dvrt = removeHeaderCells(strmatch('ftse', dvrt), dvrt);
dvrt = removeHeaderCells(strmatch('Name', dvrt), dvrt);
dvrt = removeHeaderCells(strmatch('Displacement', dvrt),
dvrt);
dvrt = removeHeaderCells(strmatch('V', dvrt), dvrt);
allData = [time axDisp dvrt];
%xlswrite('alldata.xlsx', allData)
%alldata = cell2mat(allData)
%dvrt=cell2mat(dvrt);
```

```matlab
P=findvalleys(time, dvrt, 1, -5, 30, 30, 3);
xlswrite(newfilename, P)

end %function mtsdata


function indicesOfHundredCycles =
getIndicesHundredCycles(datacolumn)
[m n] = size(datacolumn);
totalNumCycles = str2double(datacolumn(m));
numHundredCycles = floor(totalNumCycles/100);
z = zeros(numHundredCycles+1,2);
for i=0:numHundredCycles
    index = 1;
    if i>0
        index = i*100;
    end
    temp = strmatch(int2str(index), datacolumn, 'exact');
    [row col] = size(temp);
    z(i+1, 1) = temp(1);
    z(i+1, 2) = row;
end

indicesOfHundredCycles = z;
end

function headlessData = removeHeaderCells(indicesOfHeader,
datacolumn)

for i=1:size(indicesOfHeader)
    index = indicesOfHeader(i)-(i-1);
    datacolumn(index);
    datacolumn(index)=[];
end %end of for loop
datacolumn(cellfun(@isempty,datacolumn))=[];
headlessData = datacolumn;

end %function headlessData
```

### FINDPEAKS.M

```matlab
function
P=findpeaks(x,y,SlopeThreshold,AmpThreshold,smoothwidth,peakgr
oup,smoothtype)
% function
P=findpeaks(x,y,SlopeThreshold,AmpThreshold,smoothwidth,peakgr
oup,smoothtype)
% Function to locate the positive peaks in a noisy x-y time
series data
% set.  Detects peaks by looking for downward zero-crossings
% in the first derivative that exceed SlopeThreshold.
```

132

```matlab
% Returns list (P) containing peak number and position,
% height, and width of each peak. Arguments "slopeThreshold",
% "ampThreshold" and "smoothwidth" control peak sensitivity.
% Higher values will neglect smaller features. "Smoothwidth"
is
% the width of the smooth applied before peak detection;
larger
% values ignore narrow peaks. "Peakgroup" is the number points
% around the top part of the peak that are taken for
measurement.
% The argument "smoothtype" determines the smooth algorithm:
%    If smoothtype=1, rectangular (sliding-average or boxcar)
%    If smoothtype=2, triangular (2 passes of sliding-average)
%    If smoothtype=3, pseudo-Gaussian (3 passes of sliding-
average)
% See http://terpconnect.umd.edu/~toh/spectrum/Smoothing.html
and
%
http://terpconnect.umd.edu/~toh/spectrum/PeakFindingandMeasure
ment.htm
% T. C. O'Haver, 1995.  Version 4,  Last revised September,
2011
if nargin~=7;smoothtype=1;end  % smoothtype=1 if not specified
in argument
if smoothtype>3;smoothtype=3;end
if smoothtype<1;smoothtype=1;end
smoothwidth=round(smoothwidth);
peakgroup=round(peakgroup);
d=fastsmooth(deriv(y),smoothwidth,smoothtype);
n=round(peakgroup/2+1);
P=[0 0 0 0];
vectorlength=length(y);
peak=1;
AmpTest=AmpThreshold;
for j=smoothwidth:length(y)-smoothwidth,
    if sign(d(j)) > sign (d(j+1)), % Detects zero-crossing
        if d(j)-d(j+1) > SlopeThreshold*str2double(y(j)), % if
slope of derivative is larger than SlopeThreshold
            if str2double(y(j)) > AmpTest,  % if height of
peak is larger than AmpThreshold

xx=zeros(size(peakgroup));yy=zeros(size(peakgroup));
                for k=1:peakgroup, % Create sub-group of
points near peak
                    groupindex=j+k-n+1;
                    if groupindex<1, groupindex=1;end
                    if groupindex>vectorlength,
groupindex=vectorlength;end

xx(k)=str2double(x(groupindex));yy(k)=str2double(y(groupindex)
);
                end
```

```matlab
                [coef,S,MU]=polyfit(xx,log(abs(yy)),2);   % Fit
parabola to log10 of sub-group with centering and scaling
                c1=coef(3);c2=coef(2);c3=coef(1);
                PeakX=-((MU(2).*c2/(2*c3))-MU(1));   % Compute
peak position and height of fitted parabola
                PeakY=exp(c1-c3*(c2/(2*c3))^2);

MeasuredWidth=norm(MU(2).*2.35703/(sqrt(2)*sqrt(-1*c3)));
                % if the peak is too narrow for least-squares
technique to work
                % well, just use the max value of y in the
sub-group of points near peak.
                if peakgroup<5,
                    PeakY=max(yy);
                    pindex=val2ind(yy,PeakY);
                    PeakX=xx(pindex(1));
                end
                % Construct matrix P. One row for each peak
                % detected, containing the peak number, peak
                % position (x-value) and peak height (y-
value).
                P(peak,:) = [round(peak) str2double(x(j))
str2double(y(j)) MeasuredWidth];
                peak=peak+1;
            end
        end
    end
end
% ------------------------------------------------------------
----------
function [index,closestval]=val2ind(x,val)
% Returns the index and the value of the element of vector x
that is closest to val
% If more than one element is equally close, returns vectors
of indicies and values
% Tom O'Haver (toh@umd.edu) October 2006
% Examples: If x=[1 2 4 3 5 9 6 4 5 3 1], then val2ind(x,6)=7
and val2ind(x,5.1)=[5 9]
% [indices values]=val2ind(x,3.3) returns indices = [4 10] and
values = [3 3]
dif=abs(x-val);
index=find((dif-min(dif))==0);
closestval=x(index);

function d=deriv(a)
% First derivative of vector using 2-point central difference.
%  T. C. O'Haver, 1988.
n=length(a);
d(1)=str2double(a(2))-str2double(a(1));
d(n)=str2double(a(n))-str2double(a(n-1));
for j = 2:n-1;
  d(j)=(str2double(a(j+1))-str2double(a(j-1))) ./ 2;
```

```matlab
end

function SmoothY=fastsmooth(Y,w,type,ends)
% fastbsmooth(Y,w,type,ends) smooths vector Y with smooth
%  of width w. Version 2.0, May 2008.
% The argument "type" determines the smooth type:
%   If type=1, rectangular (sliding-average or boxcar)
%   If type=2, triangular (2 passes of sliding-average)
%   If type=3, pseudo-Gaussian (3 passes of sliding-average)
% The argument "ends" controls how the "ends" of the signal
% (the first w/2 points and the last w/2 points) are handled.
%   If ends=0, the ends are zero.  (In this mode the elapsed
%     time is independent of the smooth width). The fastest.
%   If ends=1, the ends are smoothed with progressively
%     smaller smooths the closer to the end. (In this mode the
%     elapsed time increases with increasing smooth widths).
% fastsmooth(Y,w,type) smooths with ends=0.
% fastsmooth(Y,w) smooths with type=1 and ends=0.
% Example:
% fastsmooth([1 1 1 10 10 10 1 1 1 1],3)= [0 1 4 7 10 7 4 1 1
0]
% fastsmooth([1 1 1 10 10 10 1 1 1 1],3,1,1)= [1 1 4 7 10 7 4
1 1 1]
%  T. C. O'Haver, May, 2008.
if nargin==2, ends=0; type=1; end
if nargin==3, ends=0; end
  switch type
    case 1
       SmoothY=sa(Y,w,ends);
    case 2
       SmoothY=sa(sa(Y,w,ends),w,ends);
    case 3
       SmoothY=sa(sa(sa(Y,w,ends),w,ends),w,ends);
  end

function SmoothY=sa(Y,smoothwidth,ends)
w=round(smoothwidth);
SumPoints=sum(Y(1:w));
s=zeros(size(Y));
halfw=round(w/2);
L=length(Y);
for k=1:L-w,
   s(k+halfw-1)=SumPoints;
   SumPoints=SumPoints-Y(k);
   SumPoints=SumPoints+Y(k+w);
end
s(k+halfw)=sum(Y(L-w+1:L));
SmoothY=s./w;
% Taper the ends of the signal if ends=1.
  if ends==1,
    startpoint=(smoothwidth + 1)/2;
    SmoothY(1)=(Y(1)+Y(2))./2;
```

135

```
    for k=2:startpoint,
        SmoothY(k)=mean(Y(1:(2*k-1)));
        SmoothY(L-k+1)=mean(Y(L-2*k+2:L));
    end
    SmoothY(L)=(Y(L)+Y(L-1))./2;
end
```

# APPENDIX H. MECHANICAL CONTINUOUS PASSIVE MOTION TESTING GRAPHS OF RESULTS

*Figure 1.* Intact ACL. This figure shows the % tension loss relative to the total tension loss of intact ACL during mechanical CPM testing. Logarithmic curves were fitted to the data and $R^2$ values indicate fit. The legend indicates the cadaver knee specimen numbers and their corresponding fitted curves. Specimens 1574L and 1624R show unexpected behavior, most likely due to AIFP sensor misalignment and thus, were excluded in analysis.
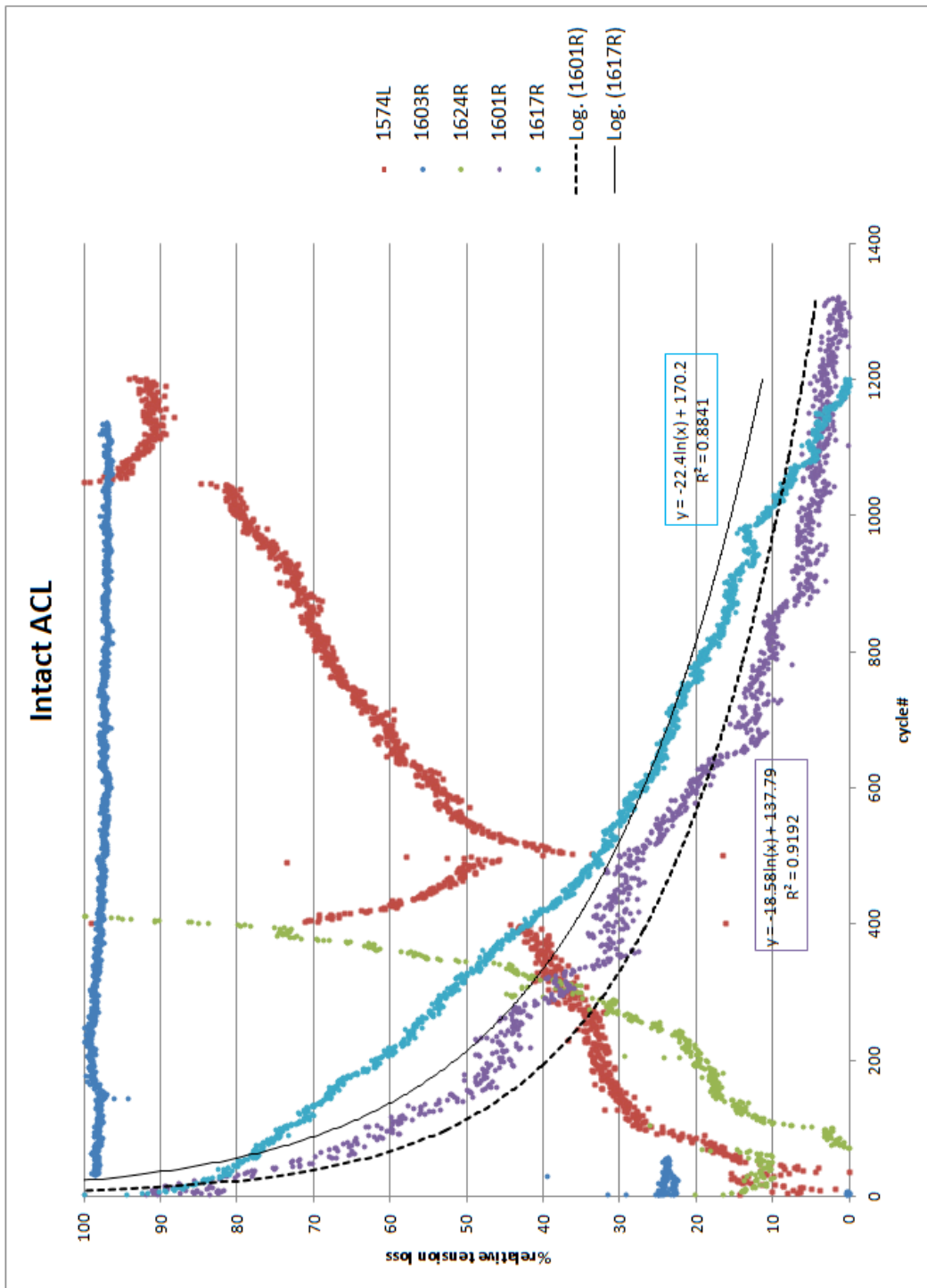
*Figure 2.* ST/G. This figure shows the % tension loss relative to the total tension loss of ST/G grafts during mechanical CPM testing. Logarithmic curves were fitted to the data and R$^2$ values indicate fit. The legend indicates the cadaver knee specimen numbers and their corresponding fitted curves. Specimen 1625L has an unexpected behavior, most likely due to failed testing, and was thus ignored in later analysis of ST/G data.
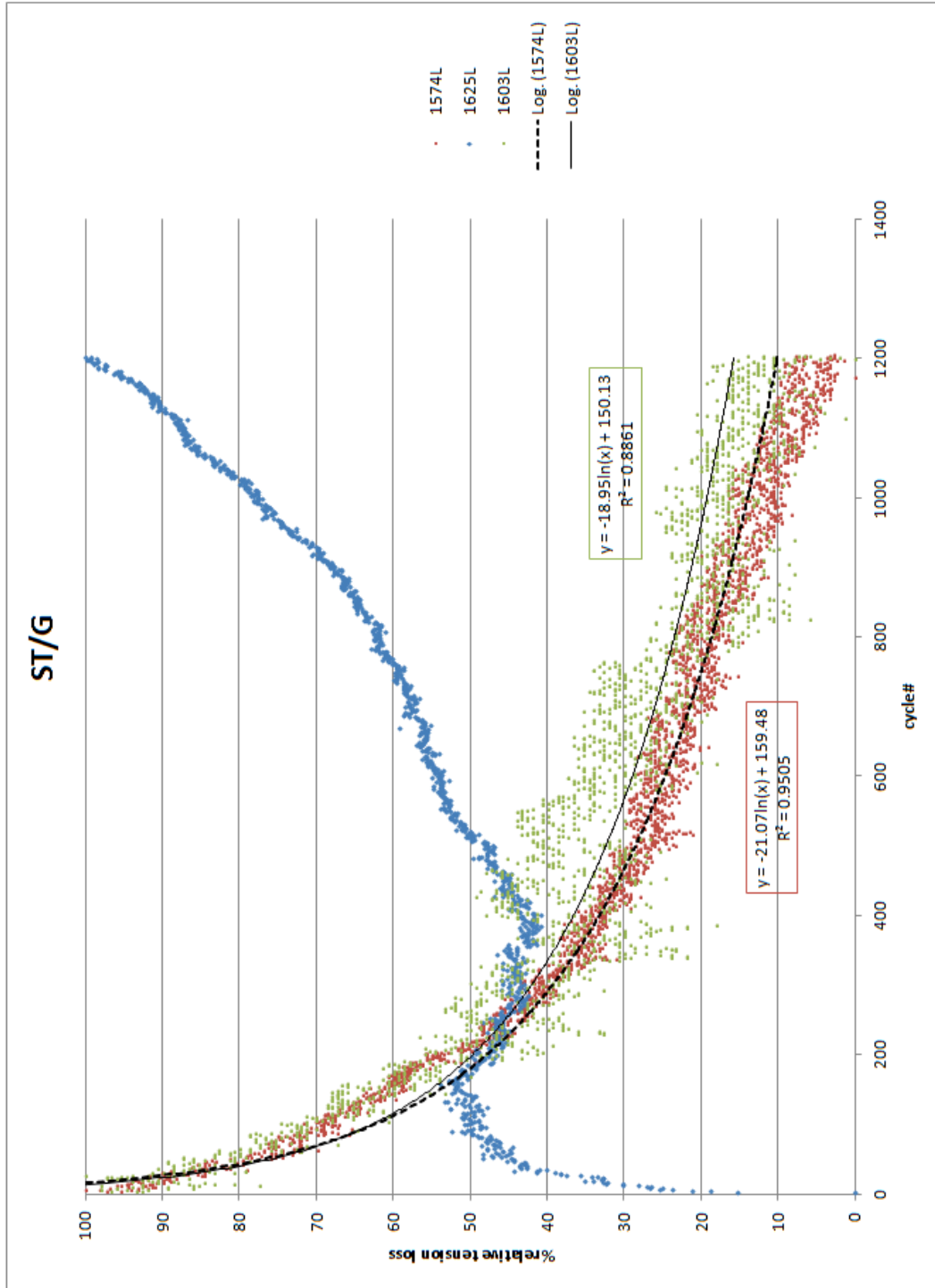
Figure 3. BPTB. This figure shows the % tension loss relative to the total tension loss of BPTB grafts during mechanical CPM testing. Logarithmic curves were fitted to the data and $R^2$ values indicate fit. The legend indicates the cadaver knee specimen numbers and their corresponding fitted curves.
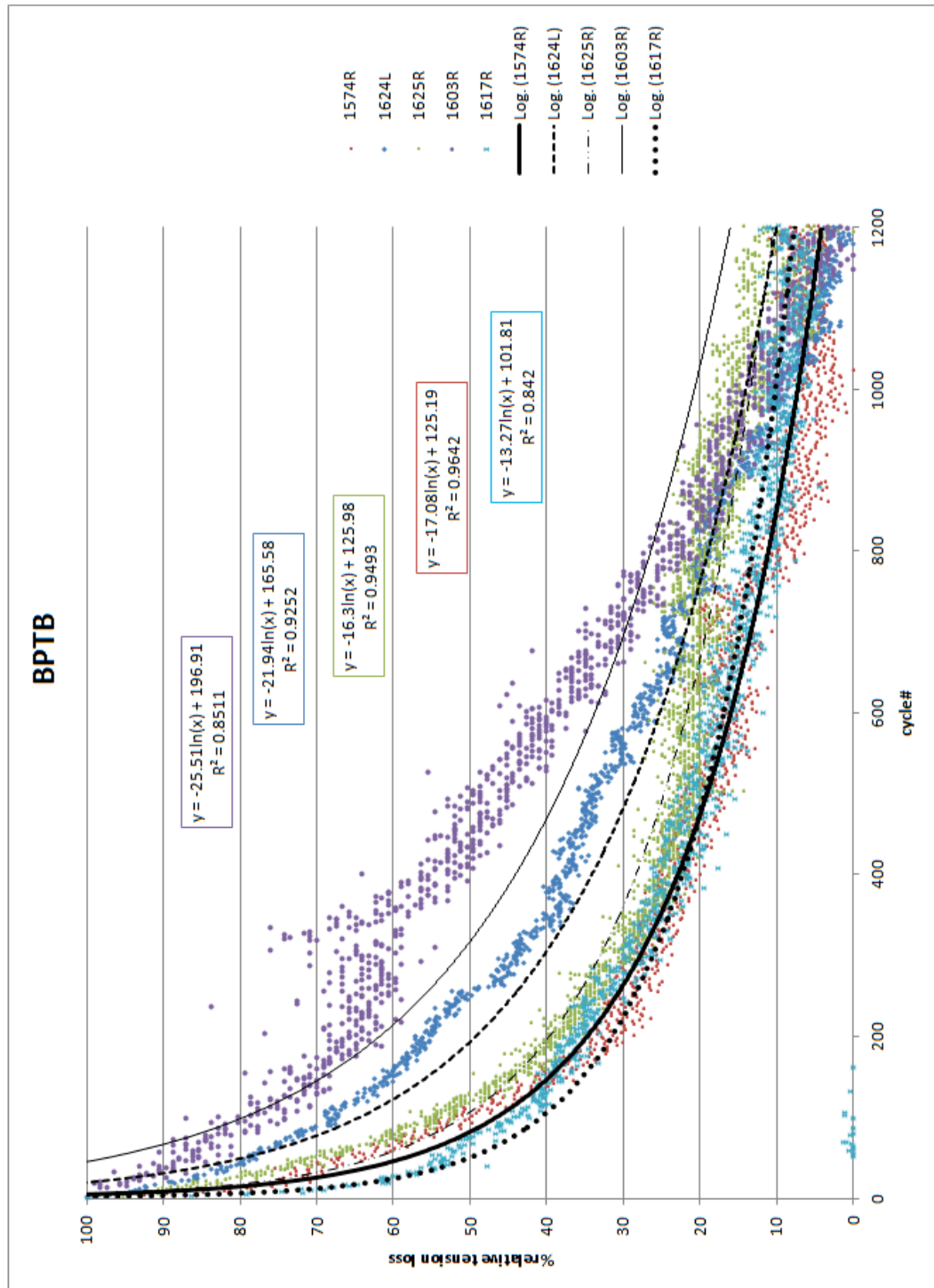
*Figure 4.* ACL. This figure shows the real tension transducer output during mechanical CPM testing of intact ACL. The legend indicates the cadaver knee specimen numbers.
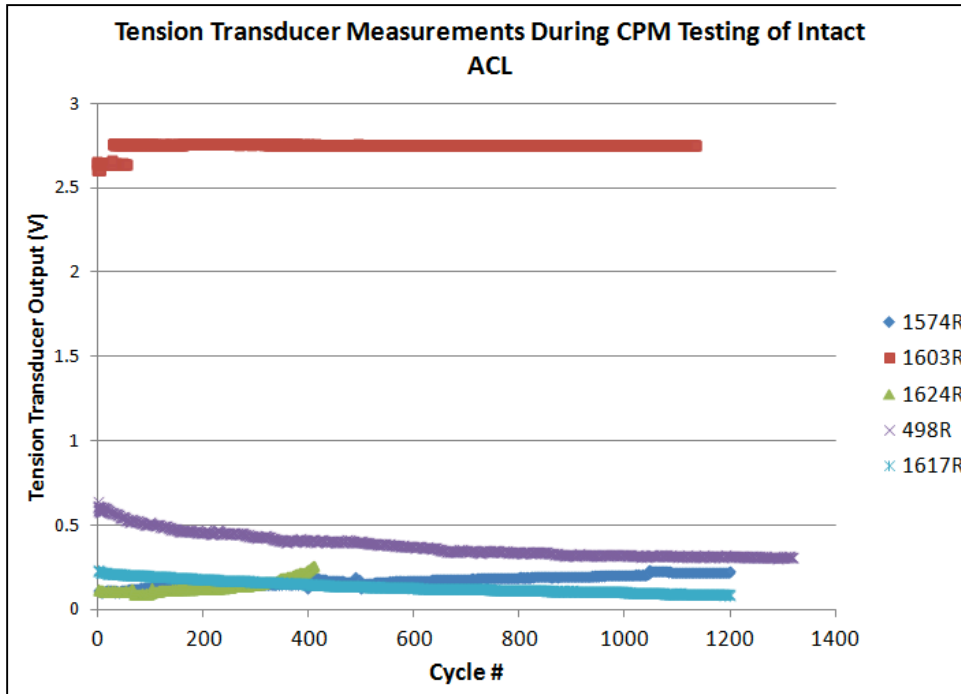


*Figure 5.* BPTB. This figure shows the real tension transducer output during mechanical CPM testing of BPTB grafts. The legend indicates the cadaver knee specimen numbers.
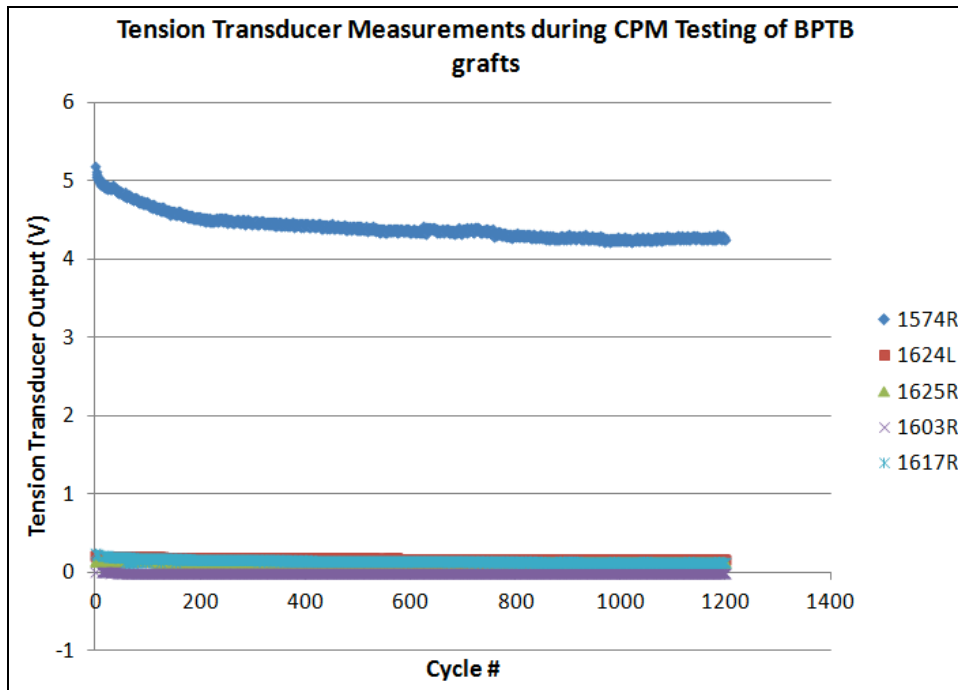
*Figure 6.* ST/G. This figure shows the real tension transducer output during mechanical CPM testing of ST/G grafs. The legend indicates the cadaver knee specimen numbers.
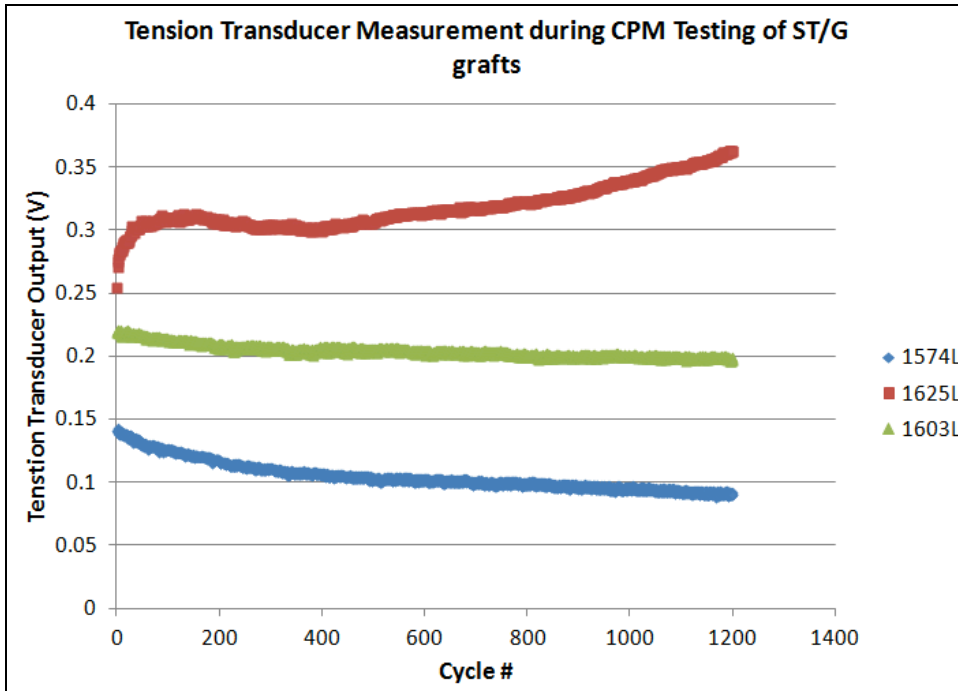
# APPENDIX I. TISSUE TREATMENT

*Table 1.* ACL Tissue Treatment. A history of how each ACL specimen was treated:

1) Leg Number indicates the leg from which the ACL derived from—its specimen ID and whether it was from the left (L) or right (R) leg.
2) Treatment is whether the ACL tissue was stressed or unstressed—if one leg was unstressed, its partner was stressed.
3) MTS Testing indicates the date in which the tissue, only those classified under the Stressed treatment, underwent continuous passive motion.
4) Fixation Start indicates the date in which the whole ACL tissue was placed in formalin.
5) Fixation Cut indicates the date in which the whole ACL tissue was cut into 1cm length fragments.
6) Tissue Processing indicates the date in which 2-3 1cm fragments of the ACL underwent dehydration/paraffin-embedding washes in the LEICA TP 1020, the automated tissue processor. Some tissues had two dates for Tissue Processing if it had been badly shredding during sectioning and required more fixation time.
7) OCT indicates the date wherein some tissues were analyzed via OCT. Not all tissues were imaged using this technique due to time constraints.

| Leg Number | | Graft Number | Treatment | MTS Testing | Fixation Start | Fixation Cut | Tissue Processing | | OCT |
|---|---|---|---|---|---|---|---|---|---|
| 1574 | L | | Unstressed | | 10/5/2011 | 11/14/2011 | 12/5/2011 | 12/15/2011 | 11/11/2011 |
| 1603 | L | | Unstressed | | 10/5/2011 | 10/31/2011 | 11/28/2011 | | |
| 1617 | L | | Unstressed | | 10/5/2011 | 10/31/2011 | 11/28/2011 | 1/30/2012 | |
| 1624 | L | | Unstressed | | 10/5/2011 | 11/14/2011 | 12/7/2011 | | 11/11/2011 |
| 1625 | L | | Unstressed | | 10/5/2011 | 10/31/2011 | 11/7/2011 | | 10/13/2011 |
| 1574 | R | | Stressed | 10/5/2011 | 10/5/2011 | 11/14/2011 | 12/5/2011 | 12/15/2011 | 11/11/2011 |
| 1603 | R | | Stressed | 1/19/2012 | 1/19/2012 | 1/27/2012 | 2/12/2012 | | |
| 1617 | R | | Stressed | 1/19/2012 | 1/19/2012 | 1/27/2012 | 2/12/2012 | | |
| 1624 | R | | Stressed | 10/5/2011 | 10/5/2011 | 11/14/2011 | 12/7/2011 | | 11/11/2011 |
| 1625 | R | | Stressed | 10/5/2011 | 10/5/2011 | 10/31/2011 | 11/7/2011 | | 10/13/2011 |

*Table 2.* BPTB Tissue Treatment. A history of how each BPTB specimen was treated.

1) Leg Number, the ID of the leg, only applies to the BPTB that were reconstructed in a leg and then stressed with the MTS machine.
2) Graft Number indicates the ID number of the BPTB tissue and from which leg, left or right, it was from.
3) Treatment is whether the BPTB tissue was stressed or unstressed—if one leg was unstressed, its partner was stressed.
4) MTS Testing indicates the date in which the tissue, only those classified under the Stressed treatment, underwent continuous passive motion.
5) Fixation Start indicates the date in which the whole BPTB tissue was placed in formalin.
6) Fixation Cut indicates the date in which the whole BPTB tissue was cut into 1cm length fragments.
7) Tissue Processing indicates the date in which 2-3 1cm fragments of the BPTB underwent dehydration/paraffin-embedding washes in the LEICA TP 1020, the automated tissue processor. Some tissues had two dates for Tissue Processing if it had been badly shredding during sectioning and required more fixation time.
8) OCT indicates the date wherein some tissues were analyzed via OCT. Not all tissues were imaged using this technique due to time constraints.

| Leg Number | | Graft Number | | Treatment | MTS Testing | Fixation Start | Fixation Cut | Tissue Processing | | OCT |
|---|---|---|---|---|---|---|---|---|---|---|
| ███ | | 7416 | R | Unstressed | ███ | 10/5/2011 | 11/4/2011 | 11/28/2011 | | 10/13/2011 |
| ███ | | 7928 | L | Unstressed | ███ | 10/5/2011 | 10/31/2011 | 11/7/2011 | | |
| ███ | | 7999 | R | Unstressed | ███ | 10/5/2011 | 11/14/2011 | 12/5/2011 | 12/15/2011 | 11/11/2011 |
| ███ | | 7380 | L | Unstressed | ███ | 2/18/2012 | 2/27/2012 | 3/12/2012 | | |
| ███ | | 0690 | L | Unstressed | ███ | 2/18/2012 | 2/27/2012 | 3/12/2012 | | |
| 1624 | L | 7416 | L | Stressed | 1/19/2012 | 1/19/2012 | 1/27/2012 | 2/12/2012 | | |
| 1625 | R | 7928 | R | Stressed | 1/19/2012 | 1/19/2012 | 1/27/2012 | 2/12/2012 | | |
| 1574 | R | 7999 | L | Stressed | 11/4/2011 | 11/4/2011 | 11/14/2011 | 12/5/2011 | 12/15/2011 | 11/11/2011 |
| 1603 | R | 7380 | R | Stressed | 2/18/2012 | 2/18/2012 | 2/27/2012 | 3/12/2012 | | |
| 1617 | R | 0690 | R | Stressed | 2/18/2012 | 2/18/2012 | 2/27/2012 | 3/12/2012 | | |

*Table 3.* ST/G Tissue Treatment. A history of how each ST/G specimen was treated.

1) Leg Number, the ID of the leg, only applies to the ST/G that were reconstructed in a leg and then stressed with the MTS machine.
2) Tissue indicates the type of tissue in question, whether it is semitendinosus (ST) or gracilis (G). Some ST/G grafts contained a double bundle of solely semitendinosus and others required the gracilis tissue as well. When the tissue was immersed in the formalin, the bundle was un-sutured so that though

the graft contained both tissues, they were processed separately. Beyond tissue ID, gracilis tissues were not processed any further.

3) Graft Number indicates the ID number of the ST/G tissue and from which leg, left or right, it was from.
4) Treatment is whether the ST/G tissue was stressed (S) or unstressed (U)—if one leg was unstressed, its partner was stressed. Gracilis tissues indicated below are always stressed, as they were part of the double-bundle graft.
5) MTS Testing indicates the date in which the tissue, only those classified under the Stressed treatment, underwent continuous passive motion.
6) Fixation Start indicates the date in which the whole ST/G tissue was placed in formalin.
7) Fixation Cut indicates the date in which the whole ST/G tissue was cut into 1cm length fragments.
8) Tissue Processing indicates the date in which 2-3 1cm fragments of the ST/G underwent dehydration/paraffin-embedding washes in the LEICA TP 1020, the automated tissue processor. Some tissues had two dates for Tissue Processing if it had been badly shredding during sectioning and required more fixation time.
9) OCT indicates the date wherein some tissues were analyzed via OCT. Not all tissues were imaged using this technique due to time constraints.

| Leg Number | | Tissue | Graft Number | | Treat-ment | MTS Testing | Fixation Start | Fixation Cut | Tissue Processing | | OCT |
|---|---|---|---|---|---|---|---|---|---|---|---|
| ███ | | ST | 2805 | L | U | ███ | 10/5/2011 | 11/14/2011 | 12/7/2011 | | 11/11/2011 |
| ███ | | ST | 2815 | R | U | ███ | 10/5/2011 | 10/31/2011 | 11/28/2011 | | |
| ███ | | ST | 6990 | L | U | ███ | 10/5/2011 | 10/31/2011 | 11/21/2011 | | 10/13/2011 |
| ███ | | ST | 7380 | R | U | ███ | 10/5/2011 | 10/31/2011 | 11/28/2011 | | |
| ███ | | ST | 7999 | L | U | ███ | 10/5/2011 | 10/31/2011 | 11/28/2011 | | |
| 1625 | L | ST | 2805 | R | S | 11/4/2011 | 11/4/2011 | 11/14/2011 | 12/7/2011 | | 11/11/2011 |
| 1624 | R | ST | 2815 | L | S | 11/4/2011 | 11/4/2012 | 11/14/2012 | -- | | |
| 1617 | L | ST | 6990 | R | S | 11/4/2011 | 11/4/2011 | 11/14/2011 | 12/5/2011 | 12/15/2011 | 11/11/2011 |
| 1603 | L | ST | 7380 | L | S | 1/19/2012 | 1/19/2012 | 1/27/2012 | 2/12/2012 | | |
| 1574 | L | ST | 7999 | R | S | 1/19/2012 | 1/19/2012 | 1/27/2012 | 2/12/2012 | | |
| ███ | | | | | | | | | | | |
| 1625 | L | G | 2815 | L | S | | | | | | |
| 1624 | R | G | 7999 | R | S | | | | | | |
| 1574 | L | G | 6990 | R | S | | | | | | |

# APPENDIX J. COLLAGEN CRIMP ANGLE RAW DATA

*Table 1*.  ACL Collagen Crimp Angle Raw Data.  The individual data-points for each ACL specimen:

  1) Leg Number indicates the leg from which the ACL specimen was derived from—the specimen ID and whether it was from the left (L) or right (R) leg.
  2) Treatment indicates whether the ACL tissue was stressed (S) or unstressed (U).
  3) Angles contains the 15 data-points collected by three randomly selected experimenters, five data-points collected by each experimenter.
  4) Avg is the average of all these data-points.

| Leg Number | | Treat-ment | Angles | | | | | | | | | | | | | |
|---|---|---|---|---|---|---|---|---|---|---|---|---|---|---|---|---|
| 1574 | L | U | 12.2 | 11.3 | 18.2 | 12.5 | 14.0 | 6.5 | 6.3 | 13.4 | 7.9 | 15.4 | 31.2 | 26.7 | 32.6 | 2 |
| 1603 | L | U | 21.6 | 15.3 | 18.3 | 19.6 | 18.1 | 13.1 | 19.8 | 11.8 | 14.4 | 16.3 | 26.6 | 25.9 | 29.7 | 2 |
| 1617 | L | U | 28.8 | 14.3 | 10.9 | 21.7 | 15.5 | 24.9 | 13.3 | 16.7 | 20.2 | 68.4 | 30.6 | 45.3 | 26.2 | 3 |
| 1624 | L | U | 16.0 | 25.1 | 27.2 | 17.9 | 18.9 | 22.7 | 33.7 | 18.3 | 17.5 | 23.2 | 22.8 | 28.1 | 20.6 | 2 |
| 1625 | L | U | 16.8 | 17.7 | 18.3 | 15.5 | 15.3 | 23.8 | 17.2 | 9.4 | 14.5 | 7.2 | 28.8 | 27.2 | 25.2 | 2 |
| 1574 | R | S | 11.1 | 18.1 | 9.8 | 14.7 | 17.6 | 13.2 | 15.5 | 19.7 | 11.8 | 14.6 | 26.6 | 17.1 | 23.6 | 2 |
| 1603 | R | S | 19.4 | 20.6 | 16.3 | 17.5 | 12.3 | 19.9 | 15.7 | 17.7 | 11.8 | 17.9 | 18.2 | 18.4 | 12.4 | 1 |
| 1617 | R | S | 10.8 | 11.1 | 13.0 | 18.4 | 14.8 | 21.9 | 26.6 | 15.7 | 18.5 | 17.7 | 10.9 | 14.4 | 15.5 | 1 |
| 1624 | R | S | 18.8 | 15.9 | 16.2 | 14.5 | 15.6 | 14.0 | 38.6 | 17.1 | 16.8 | 8.8 | 16.5 | 18.9 | 17.5 | 1 |
| 1625 | R | S | 23.9 | 29.1 | 19.4 | 23.9 | 33.4 | 23.5 | 17.8 | 23.9 | 23.3 | 12.7 | 18.2 | 13.9 | 15.9 | 1 |

*Table 2*.  BPTB Collagen Crimp Angle Raw Data.  The individual data-points for each BPTB specimen:

  1) Leg Number indicates the leg (the specimen ID and whether it was the left (L) or right (R) leg) that the BPTB graft was reconstructed in, thus it only applies to BPTB specimen that underwent the stressed treatment.
  2) Graft Number indicates the ID number of the BPTB tissue and from which leg, left or right, it was from.
  3) T indicates whether the BPTB tissue was stressed (S) or unstressed (U).
  4) Angles contains the 15 data-points collected by three randomly selected experimenters, five data-points collected by each experimenter.

| Leg Number | Graft Number | | T | Angles | | | | | | | | | | | | |
|---|---|---|---|---|---|---|---|---|---|---|---|---|---|---|---|---|
| ■■■■■ | 7416 | R | U | 8.3 | 8.3 | 7.2 | 12.6 | 10.9 | 8.5 | 8.2 | 7.5 | 10.2 | 9.3 | 26.6 | 28.9 | 36.0 |
| ■■■■■ | 7928 | L | U | 9.9 | 9.2 | 6.7 | 15.4 | 10.4 | 12.4 | 10.1 | 12.5 | 9.6 | 10.0 | 27.8 | 21.6 | 30.9 |
| ■■■■■ | 7999 | R | U | 5.6 | 15.1 | 10.2 | 8.4 | 9.1 | 11.6 | 14.2 | 10.2 | 11.8 | 9.5 | 30.5 | 30.2 | 26.3 |
| ■■■■■ | 7380 | L | U | 13.1 | 16.2 | 22.9 | 11.7 | 19.6 | 14.4 | 11.6 | 9.9 | 10.1 | 7.1 | 17.5 | 18.3 | 24.5 |
| ■■■■■ | 0690 | L | U | 10.9 | 17.3 | 17.5 | 13.2 | 16.4 | 7.0 | 11.1 | 12.0 | 14.7 | 13.0 | 22.8 | 18.5 | 24.7 |

| Leg | | Graft | | T | | | | | | | | | | | | | |
|---|---|---|---|---|---|---|---|---|---|---|---|---|---|---|---|---|---|
| 1624 | L | 7416 | L | S | | | | | | | | | | | | | |
| 1625 | R | 7928 | R | S | 7.9 | 9.6 | 8.1 | 13.4 | 11.3 | 9.7 | 12.8 | 14.9 | 6.0 | 9.3 | 14.5 | 16.8 | 15.8 |
| 1574 | R | 7999 | L | S | 10.7 | 26.4 | 11.0 | 18.8 | 22.8 | 6.1 | 8.5 | 7.6 | 6.7 | 6.4 | 18.8 | 15.1 | 16.9 |
| 1603 | R | 7380 | R | S | 6.1 | 7.0 | 7.6 | 6.8 | 4.8 | 12.1 | 20.8 | 11.8 | 12.5 | 16.2 | 9.7 | 20.4 | 15.6 |
| 1617 | R | 0690 | R | S | 16.3 | 18.8 | 14.2 | 25.1 | 16.8 | 18.1 | 23.5 | 21.5 | 37.4 | 15.7 | 13.8 | 14.4 | 14.1 |

*Table 3.* ST Collagen Crimp Angle Raw Data. The individual data-points for each ST specimen:

1) Leg Number indicates the leg (the specimen ID and whether it was the left (L) or right (R) leg) that the ST graft was reconstructed in, thus it only applies to ST specimen that underwent the stressed treatment.
2) Graft Number indicates the ID number of the ST tissue and from which leg, left or right, it was from.
3) T indicates whether the ST tissue was stressed (S) or unstressed (U).
4) Angles contains the 15 data-points collected by three randomly selected experimenters, five data-points collected by each experimenter.

| Leg Number | | Graft Number | | T | Angles | | | | | | | | | | | | |
|---|---|---|---|---|---|---|---|---|---|---|---|---|---|---|---|---|---|
| | | 2805 | L | U | 9.1 | 6.7 | 13.7 | 16.5 | 12.4 | 5.1 | 7.4 | 9.3 | 11.9 | 8.8 | 8.9 | 9.1 | 10.5 |
| | | 2815 | R | U | 10.1 | 8.1 | 10.0 | 11.1 | 9.9 | 10.9 | 18.1 | 9.0 | 10.0 | 6.6 | 13.1 | 18.8 | 12.7 |
| | | 6990 | L | U | 6.4 | 11.3 | 14.3 | 14.9 | 8.7 | 19.3 | 21.0 | 11.3 | 16.8 | 16.3 | 11.3 | 7.1 | 19.8 |
| | | 7380 | R | U | 9.7 | 9.9 | 10.5 | 11.7 | 14.9 | 11.4 | 6.4 | 7.8 | 9.9 | 8.8 | 17.9 | 11.3 | 13.1 |
| | | 7999 | L | U | 7.6 | 9.8 | 7.2 | 10.0 | 10.9 | 16.0 | 12.4 | 8.6 | 6.0 | 8.4 | 11.7 | 7.2 | 13.5 |
| 1625 | L | 2805 | R | S | 20.4 | 20.5 | 15.3 | 23.2 | 13.9 | 8.9 | 9.3 | 13.1 | 7.9 | 11.6 | 20.9 | 23.1 | 13.2 |
| 1624 | R | 2815 | L | S | | | | | | | | | | | | | |
| 1617 | L | 6990 | R | S | 16.9 | 12.4 | 18.9 | 9.5 | 20.3 | 10.7 | 14.4 | 16.8 | 10.3 | 9.6 | 27.2 | 13.0 | 24.6 |
| 1603 | L | 7380 | L | S | 15.0 | 23.8 | 24.9 | 18.0 | 17.3 | 12.7 | 14.5 | 9.5 | 8.4 | 9.4 | 27.4 | 25.9 | 21.1 |
| 1574 | L | 7999 | R | S | 7.8 | 8.3 | 11.2 | 7.8 | 10.0 | 9.8 | 11.8 | 10.4 | 8.7 | 6.8 | 18.1 | 23.7 | 17.0 |

Missing data for BPTB 7416L was due to limitations in producing sectioned tissue for imaging analysis. Missing data for ST 2815L was due to its irregular stress protocol, making it incomparable to the rest of the tissue.

# APPENDIX K: IMAGING ANALYSIS STATISTICS

**KEY:**
*Tissue*= Stressed (1) vs. Unstressed (2)
*Type*= ACL (1) vs. BPTB (2) vs. ST/G (3)
*Dependent Variable*= Crimp Angle
*Note: Significance threshold used was p<0.05*

## ACL Means (Stressed vs. Unstressed)

**Case Processing Summary**

| | Cases | | | | | |
|---|---|---|---|---|---|---|
| | Included | | Excluded | | Total | |
| | N | Percent | N | Percent | N | Percent |
| CrimpAngle * Tissue | 150 | 100.0% | 0 | .0% | 150 | 100.0% |

**Report**

CrimpAngle

| Tissue | Mean | N | Std. Deviation |
|---|---|---|---|
| 1.00 | 17.6231 | 75 | 5.19277 |
| 2.00 | 21.1459 | 75 | 9.25833 |
| Total | 19.3845 | 150 | 7.68675 |

## ACL Oneway ANOVA (Stressed vs. Unstressed)

**ANOVA**

CrimpAngle

| | Sum of Squares | df | Mean Square | F | Sig. |
|---|---|---|---|---|---|
| Between Groups | 465.387 | 1 | 465.387 | 8.260 | .005 |
| Within Groups | 8338.436 | 148 | 56.341 | | |
| Total | 8803.822 | 149 | | | |

## BPTB Means (Stressed vs. Unstressed)

**Case Processing Summary**

| | Cases | | | | | |
|---|---|---|---|---|---|---|
| | Included | | Excluded | | Total | |
| | N | Percent | N | Percent | N | Percent |
| CrimpAngle * Tissue | 135 | 99.3% | 1 | .7% | 136 | 100.0% |

| Tissue | Mean | N | Std. Deviation |
|--------|------|---|----------------|
| 1.00 | 14.0590 | 60 | 6.20143 |
| 2.00 | 16.1165 | 75 | 7.92795 |
| Total | 15.2021 | 135 | 7.25917 |

## BPTB Oneway ANOVA (Stressed vs. Unstressed)

**ANOVA**

CrimpAngle

| | Sum of Squares | df | Mean Square | F | Sig. |
|--------|----------------|-----|-------------|-------|------|
| Between Groups | 141.118 | 1 | 141.118 | 2.712 | .102 |
| Within Groups | 6920.090 | 133 | 52.031 | | |
| Total | 7061.207 | 134 | | | |

## ST Means (Stressed vs. Unstressed)

**Case Processing Summary**

| | Cases | | | | | |
|--------|-------|---------|-------|---------|-------|---------|
| | Included | | Excluded | | Total | |
| | N | Percent | N | Percent | N | Percent |
| CrimpAngle * Tissue | 135 | 100.0% | 0 | .0% | 135 | 100.0% |

**Report**

CrimpAngle

| Tissue | Mean | N | Std. Deviation |
|--------|------|---|----------------|
| 1.00 | 15.5146 | 60 | 5.76944 |
| 2.00 | 11.3245 | 75 | 3.71294 |
| Total | 13.1867 | 135 | 5.16105 |

## ST Oneway ANOVA (Stressed vs. Unstressed)

**ANOVA**

CrimpAngle

| | Sum of Squares | df | Mean Square | F | Sig. |
|--------|----------------|-----|-------------|--------|------|
| Between Groups | 585.228 | 1 | 585.228 | 26.084 | .000 |
| Within Groups | 2984.059 | 133 | 22.437 | | |
| Total | 3569.287 | 134 | | | |

## ACL vs. BPTB vs. ST Means

**Case Processing Summary**

| | Cases | | | | | |
|---|---|---|---|---|---|---|
| | Included | | Excluded | | Total | |
| | N | Percent | N | Percent | N | Percent |
| CrimpAngle * Type | 420 | 99.8% | 1 | .2% | 421 | 100.0% |

**Report**

CrimpAngle

| Type | Mean | N | Std. Deviation |
|---|---|---|---|
| 1.00 | 19.3845 | 150 | 7.68675 |
| 2.00 | 15.2021 | 135 | 7.25917 |
| 3.00 | 13.1867 | 135 | 5.16105 |
| Total | 16.0480 | 420 | 7.29632 |

## ACL vs. BPTB vs. ST Oneway ANOVA

**ANOVA**

CrimpAngle

| | Sum of Squares | df | Mean Square | F | Sig. |
|---|---|---|---|---|---|
| Between Groups | 2871.657 | 2 | 1435.828 | 30.808 | .000 |
| Within Groups | 19434.317 | 417 | 46.605 | | |
| Total | 22305.973 | 419 | | | |

## *Post Hoc Tests*

**Multiple Comparisons**

Dependent Variable: CrimpAngle

| | (I) Type | (J) Type | Mean Difference (I-J) | Std. Error | Sig. | 95% Confidence Interval | |
|---|---|---|---|---|---|---|---|
| | | | | | | Lower Bound | Upper Bound |
| Tukey HSD | 1.00 | 2.00 | 4.18244* | .80989 | .000 | 2.2775 | 6.0874 |
| | | 3.00 | 6.19775* | .80989 | .000 | 4.2928 | 8.1027 |
| | 2.00 | 1.00 | -4.18244* | .80989 | .000 | -6.0874 | -2.2775 |
| | | 3.00 | 2.01531* | .83093 | .042 | .0609 | 3.9698 |
| | 3.00 | 1.00 | -6.19775* | .80989 | .000 | -8.1027 | -4.2928 |
| | | 2.00 | -2.01531* | .83093 | .042 | -3.9698 | -.0609 |
| Scheffe | 1.00 | 2.00 | 4.18244* | .80989 | .000 | 2.1929 | 6.1720 |
| | | 3.00 | 6.19775* | .80989 | .000 | 4.2082 | 8.1873 |
| | 2.00 | 1.00 | -4.18244* | .80989 | .000 | -6.1720 | -2.1929 |
| | | 3.00 | 2.01531 | .83093 | .054 | -.0259 | 4.0565 |
| | 3.00 | 1.00 | -6.19775* | .80989 | .000 | -8.1873 | -4.2082 |
| | | 2.00 | -2.01531 | .83093 | .054 | -4.0565 | .0259 |

*. The mean difference is significant at the .05 level.

*Homogeneous Subsets*

**CrimpAngle**

| | Type | N | Subset for alpha = .05 | | |
|---|---|---|---|---|---|
| | | | 1 | 2 | 3 |
| Tukey HSD[a,b] | 3.00 | 135 | 13.1867 | | |
| | 2.00 | 135 | | 15.2021 | |
| | 1.00 | 150 | | | 19.3845 |
| | Sig. | | 1.000 | 1.000 | 1.000 |
| Scheffe[a,b] | 3.00 | 135 | 13.1867 | | |
| | 2.00 | 135 | | 15.2021 | |
| | 1.00 | 150 | | | 19.3845 |
| | Sig. | | 1.000 | 1.000 | 1.000 |

Means for groups in homogeneous subsets are displayed.

a. Uses Harmonic Mean Sample Size = 139.655.

b. The group sizes are unequal. The harmonic mean of the group sizes is used. Type I error levels are not guaranteed.

# Stressed vs. Unstressed Means

**Case Processing Summary**

| | Cases | | | | | |
|---|---|---|---|---|---|---|
| | Included | | Excluded | | Total | |
| | N | Percent | N | Percent | N | Percent |
| CrimpAngle * Tissue | 420 | 99.8% | 1 | .2% | 421 | 100.0% |

**Report**

CrimpAngle

| Tissue | Mean | N | Std. Deviation |
|---|---|---|---|
| 1.00 | 15.8777 | 195 | 5.86056 |
| 2.00 | 16.1956 | 225 | 8.35385 |
| Total | 16.0480 | 420 | 7.29632 |

# Stressed vs. Unstressed Oneway ANOVA

**ANOVA**

CrimpAngle

| | Sum of Squares | df | Mean Square | F | Sig. |
|---|---|---|---|---|---|
| Between Groups | 9.112 | 1 | 9.112 | .168 | .682 |
| Within Groups | 20268.613 | 373 | 54.339 | | |
| Total | 20277.724 | 374 | | | |

150

# Overall Means

**Case Processing Summary**

| | Cases | | | | | |
| --- | --- | --- | --- | --- | --- | --- |
| | Included | | Excluded | | Total | |
| | N | Percent | N | Percent | N | Percent |
| CrimpAngle * Tissue | 420 | 99.8% | 1 | .2% | 421 | 100.0% |
| CrimpAngle * Type | 420 | 99.8% | 1 | .2% | 421 | 100.0% |

**CrimpAngle * Tissue**

CrimpAngle

| Tissue | Mean | N | Std. Deviation |
| --- | --- | --- | --- |
| 1.00 | 15.8777 | 195 | 5.86056 |
| 2.00 | 16.1956 | 225 | 8.35385 |
| Total | 16.0480 | 420 | 7.29632 |

**CrimpAngle * Type**

CrimpAngle

| Type | Mean | N | Std. Deviation |
| --- | --- | --- | --- |
| 1.00 | 19.3845 | 150 | 7.68675 |
| 2.00 | 15.2021 | 135 | 7.25917 |
| 3.00 | 13.1867 | 135 | 5.16105 |
| Total | 16.0480 | 420 | 7.29632 |

# Univariate Analysis of Variance

**Between-Subjects Factors**

| | | N |
| --- | --- | --- |
| Tissue | 1.00 | 195 |
| | 2.00 | 225 |
| Type | 1.00 | 150 |
| | 2.00 | 135 |
| | 3.00 | 135 |

**Levene's Test of Equality of Error Variances**[a]

Dependent Variable: CrimpAngle

| F | df1 | df2 | Sig. |
| --- | --- | --- | --- |
| 10.385 | 5 | 414 | .000 |

Tests the null hypothesis that the error variance of the dependent variable is equal across groups.

a. Design: Intercept+Tissue+Type+Tissue * Type

**Tests of Between-Subjects Effects**

Dependent Variable: CrimpAngle

| Source | Type III Sum of Squares | df | Mean Square | F | Sig. | Partial Eta Squared | Noncent. Parameter | Observed Power[a] |
|---|---|---|---|---|---|---|---|---|
| Corrected Model | 4063.388[b] | 5 | 812.678 | 18.443 | .000 | .182 | 92.215 | 1.000 |
| Intercept | 105859.416 | 1 | 105859.416 | 2402.390 | .000 | .853 | 2402.390 | 1.000 |
| Tissue | 22.303 | 1 | 22.303 | .506 | .477 | .001 | .506 | .109 |
| Type | 2712.800 | 2 | 1356.400 | 30.782 | .000 | .129 | 61.565 | 1.000 |
| Tissue * Type | 1155.985 | 2 | 577.992 | 13.117 | .000 | .060 | 26.234 | .997 |
| Error | 18242.585 | 414 | 44.064 | | | | | |
| Total | 130472.093 | 420 | | | | | | |
| Corrected Total | 22305.973 | 419 | | | | | | |

a. Computed using alpha = .05

b. R Squared = .182 (Adjusted R Squared = .172)

## Estimated Marginal Means

### 1. Grand Mean

Dependent Variable: CrimpAngle

| Mean | Std. Error | 95% Confidence Interval | |
|---|---|---|---|
| | | Lower Bound | Upper Bound |
| 15.964 | .326 | 15.324 | 16.604 |

### 2. Type

Dependent Variable: CrimpAngle

| Type | Mean | Std. Error | 95% Confidence Interval | |
|---|---|---|---|---|
| | | | Lower Bound | Upper Bound |
| 1.00 | 19.384 | .542 | 18.319 | 20.450 |
| 2.00 | 15.088 | .575 | 13.958 | 16.218 |
| 3.00 | 13.420 | .575 | 12.289 | 14.550 |

### 3. Tissue

Dependent Variable: CrimpAngle

| Tissue | Mean | Std. Error | 95% Confidence Interval | |
|---|---|---|---|---|
| | | | Lower Bound | Upper Bound |
| 1.00 | 15.732 | .478 | 14.793 | 16.672 |
| 2.00 | 16.196 | .443 | 15.326 | 17.066 |

### 4. Tissue * Type

Dependent Variable: CrimpAngle

| Tissue | Type | Mean | Std. Error | 95% Confidence Interval | |
|---|---|---|---|---|---|
| | | | | Lower Bound | Upper Bound |
| 1.00 | 1.00 | 17.623 | .767 | 16.116 | 19.130 |
| | 2.00 | 14.059 | .857 | 12.374 | 15.744 |
| | 3.00 | 15.515 | .857 | 13.830 | 17.199 |
| 2.00 | 1.00 | 21.146 | .767 | 19.639 | 22.653 |
| | 2.00 | 16.117 | .767 | 14.610 | 17.623 |
| | 3.00 | 11.324 | .767 | 9.818 | 12.831 |

## Post Hoc Tests

### Type

**Multiple Comparisons**

Dependent Variable: CrimpAngle

| | (I) Type | (J) Type | Mean Difference (I-J) | Std. Error | Sig. | 95% Confidence Interval Lower Bound | 95% Confidence Interval Upper Bound |
|---|---|---|---|---|---|---|---|
| Tukey HSD | 1.00 | 2.00 | 4.1824* | .78750 | .000 | 2.3301 | 6.0348 |
| | | 3.00 | 6.1978* | .78750 | .000 | 4.3454 | 8.0501 |
| | 2.00 | 1.00 | -4.1824* | .78750 | .000 | -6.0348 | -2.3301 |
| | | 3.00 | 2.0153* | .80796 | .035 | .1148 | 3.9158 |
| | 3.00 | 1.00 | -6.1978* | .78750 | .000 | -8.0501 | -4.3454 |
| | | 2.00 | -2.0153* | .80796 | .035 | -3.9158 | -.1148 |
| Scheffe | 1.00 | 2.00 | 4.1824* | .78750 | .000 | 2.2478 | 6.1170 |
| | | 3.00 | 6.1978* | .78750 | .000 | 4.2631 | 8.1324 |
| | 2.00 | 1.00 | -4.1824* | .78750 | .000 | -6.1170 | -2.2478 |
| | | 3.00 | 2.0153* | .80796 | .046 | .0304 | 4.0002 |
| | 3.00 | 1.00 | -6.1978* | .78750 | .000 | -8.1324 | -4.2631 |
| | | 2.00 | -2.0153* | .80796 | .046 | -4.0002 | -.0304 |

Based on observed means.

*. The mean difference is significant at the .05 level.

### Homogeneous Subsets

**CrimpAngle**

| | Type | N | Subset 1 | Subset 2 | Subset 3 |
|---|---|---|---|---|---|
| Tukey HSD[a,b,c] | 3.00 | 135 | 13.1867 | | |
| | 2.00 | 135 | | 15.2021 | |
| | 1.00 | 150 | | | 19.3845 |
| | Sig. | | 1.000 | 1.000 | 1.000 |
| Scheffe[a,b,c] | 3.00 | 135 | 13.1867 | | |
| | 2.00 | 135 | | 15.2021 | |
| | 1.00 | 150 | | | 19.3845 |
| | Sig. | | 1.000 | 1.000 | 1.000 |

Means for groups in homogeneous subsets are displayed.
Based on Type III Sum of Squares
The error term is Mean Square(Error) = 44.064.

a. Uses Harmonic Mean Sample Size = 139.655.

b. The group sizes are unequal. The harmonic mean of the group sizes is used. Type I error levels are not guaranteed.

c. Alpha = .05.

# Stressed Means (ACL vs. BPTB vs. ST/G)

**Case Processing Summary**

| | Cases | | | | | |
|---|---|---|---|---|---|---|
| | Included | | Excluded | | Total | |
| | N | Percent | N | Percent | N | Percent |
| CrimpAngle * Type | 195 | 100.0% | 0 | .0% | 195 | 100.0% |

**Report**

CrimpAngle

| Type | Mean | N | Std. Deviation |
|---|---|---|---|
| 1.00 | 17.6231 | 75 | 5.19277 |
| 2.00 | 14.0590 | 60 | 6.20143 |
| 3.00 | 15.5146 | 60 | 5.76944 |
| Total | 15.8777 | 195 | 5.86056 |

# Stressed Oneway ANOVA

**ANOVA**

CrimpAngle

| | Sum of Squares | df | Mean Square | F | Sig. |
|---|---|---|---|---|---|
| Between Groups | 434.856 | 2 | 217.428 | 6.703 | .002 |
| Within Groups | 6228.304 | 192 | 32.439 | | |
| Total | 6663.160 | 194 | | | |

## *Post Hoc Tests*

**Multiple Comparisons**

Dependent Variable: CrimpAngle

| | (I) Type | (J) Type | Mean Difference (I-J) | Std. Error | Sig. | 95% Confidence Interval | |
|---|---|---|---|---|---|---|---|
| | | | | | | Lower Bound | Upper Bound |
| Tukey HSD | 1.00 | 2.00 | 3.56411* | .98650 | .001 | 1.2340 | 5.8942 |
| | | 3.00 | 2.10851 | .98650 | .085 | -.2216 | 4.4386 |
| | 2.00 | 1.00 | -3.56411* | .98650 | .001 | -5.8942 | -1.2340 |
| | | 3.00 | -1.45560 | 1.03986 | .343 | -3.9118 | 1.0006 |
| | 3.00 | 1.00 | -2.10851 | .98650 | .085 | -4.4386 | .2216 |
| | | 2.00 | 1.45560 | 1.03986 | .343 | -1.0006 | 3.9118 |
| Scheffe | 1.00 | 2.00 | 3.56411* | .98650 | .002 | 1.1305 | 5.9978 |
| | | 3.00 | 2.10851 | .98650 | .105 | -.3251 | 4.5422 |
| | 2.00 | 1.00 | -3.56411* | .98650 | .002 | -5.9978 | -1.1305 |
| | | 3.00 | -1.45560 | 1.03986 | .377 | -4.0209 | 1.1097 |
| | 3.00 | 1.00 | -2.10851 | .98650 | .105 | -4.5422 | .3251 |
| | | 2.00 | 1.45560 | 1.03986 | .377 | -1.1097 | 4.0209 |

*. The mean difference is significant at the .05 level.

*Homogeneous Subsets*

**CrimpAngle**

| | Type | N | Subset for alpha = .05 1 | Subset for alpha = .05 2 |
|---|---|---|---|---|
| Tukey HSD[a,b] | 2.00 | 60 | 14.0590 | |
| | 3.00 | 60 | 15.5146 | 15.5146 |
| | 1.00 | 75 | | 17.6231 |
| | Sig. | | .318 | .093 |
| Scheffe[a,b] | 2.00 | 60 | 14.0590 | |
| | 3.00 | 60 | 15.5146 | 15.5146 |
| | 1.00 | 75 | | 17.6231 |
| | Sig. | | .352 | .113 |

Means for groups in homogeneous subsets are displayed.

a. Uses Harmonic Mean Sample Size = 64.286.

b. The group sizes are unequal. The harmonic mean of the group sizes is used. Type I error levels are not guaranteed.

# Unstressed Means (ACL vs. BPTB vs. ST/G)

**Case Processing Summary**

| | Cases Included N | Cases Included Percent | Cases Excluded N | Cases Excluded Percent | Cases Total N | Cases Total Percent |
|---|---|---|---|---|---|---|
| CrimpAngle * Type | 225 | 100.0% | 0 | .0% | 225 | 100.0% |

**Report**

CrimpAngle

| Type | Mean | N | Std. Deviation |
|---|---|---|---|
| 1.00 | 21.1459 | 75 | 9.25833 |
| 2.00 | 16.1165 | 75 | 7.92795 |
| 3.00 | 11.3245 | 75 | 3.71294 |
| Total | 16.1956 | 225 | 8.35385 |

# Unstressed Oneway ANOVA

**ANOVA**

CrimpAngle

| | Sum of Squares | df | Mean Square | F | Sig. |
|---|---|---|---|---|---|
| Between Groups | 3617.970 | 2 | 1808.985 | 33.426 | .000 |
| Within Groups | 12014.281 | 222 | 54.118 | | |
| Total | 15632.251 | 224 | | | |

155

## Post Hoc Tests

**Multiple Comparisons**

Dependent Variable: CrimpAngle

| | (I) Type | (J) Type | Mean Difference (I-J) | Std. Error | Sig. | 95% Confidence Interval Lower Bound | 95% Confidence Interval Upper Bound |
|---|---|---|---|---|---|---|---|
| Tukey HSD | 1.00 | 2.00 | 5.02939* | 1.20131 | .000 | 2.1948 | 7.8639 |
| | | 3.00 | 9.82143* | 1.20131 | .000 | 6.9869 | 12.6560 |
| | 2.00 | 1.00 | -5.02939* | 1.20131 | .000 | -7.8639 | -2.1948 |
| | | 3.00 | 4.79204* | 1.20131 | .000 | 1.9575 | 7.6266 |
| | 3.00 | 1.00 | -9.82143* | 1.20131 | .000 | -12.6560 | -6.9869 |
| | | 2.00 | -4.79204* | 1.20131 | .000 | -7.6266 | -1.9575 |
| Scheffe | 1.00 | 2.00 | 5.02939* | 1.20131 | .000 | 2.0689 | 7.9899 |
| | | 3.00 | 9.82143* | 1.20131 | .000 | 6.8610 | 12.7819 |
| | 2.00 | 1.00 | -5.02939* | 1.20131 | .000 | -7.9899 | -2.0689 |
| | | 3.00 | 4.79204* | 1.20131 | .000 | 1.8316 | 7.7525 |
| | 3.00 | 1.00 | -9.82143* | 1.20131 | .000 | -12.7819 | -6.8610 |
| | | 2.00 | -4.79204* | 1.20131 | .000 | -7.7525 | -1.8316 |

*. The mean difference is significant at the .05 level.

## Homogeneous Subsets

**CrimpAngle**

| | Type | N | Subset for alpha = .05 — 1 | Subset for alpha = .05 — 2 | Subset for alpha = .05 — 3 |
|---|---|---|---|---|---|
| Tukey HSD[a] | 3.00 | 75 | 11.3245 | | |
| | 2.00 | 75 | | 16.1165 | |
| | 1.00 | 75 | | | 21.1459 |
| | Sig. | | 1.000 | 1.000 | 1.000 |
| Scheffe[a] | 3.00 | 75 | 11.3245 | | |
| | 2.00 | 75 | | 16.1165 | |
| | 1.00 | 75 | | | 21.1459 |
| | Sig. | | 1.000 | 1.000 | 1.000 |

Means for groups in homogeneous subsets are displayed.

a. Uses Harmonic Mean Sample Size = 75.000.

# Percent Comparison (ACL vs. BPTB vs. ST/G) Means

*Note: DV=Average Crimp Angle Percent Change* ((Stressed-Unstressed)/Unstressed)

**Case Processing Summary**

| | Cases Included N | Cases Included Percent | Cases Excluded N | Cases Excluded Percent | Cases Total N | Cases Total Percent |
|---|---|---|---|---|---|---|
| PercentChange * Type | 13 | 100.0% | 0 | .0% | 13 | 100.0% |

156

**Report**

PercentChange

| Type | Mean | N | Std. Deviation |
|------|------|---|----------------|
| 1.00 | -14.3780 | 5 | 18.63728 |
| 2.00 | -12.8825 | 4 | 19.01461 |
| 3.00 | 40.6600 | 4 | 22.34154 |
| Total | 3.0169 | 13 | 31.83758 |

# Percent Comparison (ACL vs. BPTB vs. ST/G) Oneway ANOVA

**ANOVA**

PercentChange

| | Sum of Squares | df | Mean Square | F | Sig. |
|---|----------------|-----|-------------|--------|------|
| Between Groups | 8192.088 | 2 | 4096.044 | 10.314 | .004 |
| Within Groups | 3971.492 | 10 | 397.149 | | |
| Total | 12163.580 | 12 | | | |

## *Post Hoc Tests*

**Multiple Comparisons**

Dependent Variable: PercentChange

| | (I) Type | (J) Type | Mean Difference (I-J) | Std. Error | Sig. | 95% Confidence Interval Lower Bound | Upper Bound |
|---|----------|----------|-----------------------|------------|------|-------------|-------------|
| Tukey HSD | 1.00 | 2.00 | -1.49550 | 13.36851 | .993 | -38.1425 | 35.1515 |
| | | 3.00 | -55.03800* | 13.36851 | .005 | -91.6850 | -18.3910 |
| | 2.00 | 1.00 | 1.49550 | 13.36851 | .993 | -35.1515 | 38.1425 |
| | | 3.00 | -53.54250* | 14.09165 | .009 | -92.1719 | -14.9131 |
| | 3.00 | 1.00 | 55.03800* | 13.36851 | .005 | 18.3910 | 91.6850 |
| | | 2.00 | 53.54250* | 14.09165 | .009 | 14.9131 | 92.1719 |
| Scheffe | 1.00 | 2.00 | -1.49550 | 13.36851 | .994 | -39.7903 | 36.7993 |
| | | 3.00 | -55.03800* | 13.36851 | .007 | -93.3328 | -16.7432 |
| | 2.00 | 1.00 | 1.49550 | 13.36851 | .994 | -36.7993 | 39.7903 |
| | | 3.00 | -53.54250* | 14.09165 | .011 | -93.9087 | -13.1763 |
| | 3.00 | 1.00 | 55.03800* | 13.36851 | .007 | 16.7432 | 93.3328 |
| | | 2.00 | 53.54250* | 14.09165 | .011 | 13.1763 | 93.9087 |

*. The mean difference is significant at the .05 level.

## Homogeneous Subsets

**PercentChange**

| | Type | N | Subset for alpha = .05 | |
|---|---|---|---|---|
| | | | 1 | 2 |
| Tukey HSD[a,b] | 1.00 | 5 | -14.3780 | |
| | 2.00 | 4 | -12.8825 | |
| | 3.00 | 4 | | 40.6600 |
| | Sig. | | .993 | 1.000 |
| Scheffe[a,b] | 1.00 | 5 | -14.3780 | |
| | 2.00 | 4 | -12.8825 | |
| | 3.00 | 4 | | 40.6600 |
| | Sig. | | .994 | 1.000 |

Means for groups in homogeneous subsets are displayed.

a. Uses Harmonic Mean Sample Size = 4.286.

b. The group sizes are unequal. The harmonic mean of the group sizes is used. Type I error levels are not guaranteed.

# APPENDIX L: BIOMECHANICS STATISTICS

**KEY:**
*Type=* ACL (1) vs. BPTB (2) vs. ST/G (3)
*Dependent Variable=* Logarithmic Decay Coefficient
*\*Note: Significance threshold used was p<0.05*

## ACL vs. BPTB vs. ST/G
## Means

**Case Processing Summary**

|  | Cases | | | | | |
|---|---|---|---|---|---|---|
|  | Included | | Excluded | | Total | |
|  | N | Percent | N | Percent | N | Percent |
| Coeff * Type | 9 | 100.0% | 0 | .0% | 9 | 100.0% |

**Report**

Coeff

| Type | Mean | N | Std. Deviation |
|---|---|---|---|
| 1.00 | 20.4900 | 2 | 2.70115 |
| 2.00 | 18.8100 | 5 | 4.85512 |
| 3.00 | 20.0100 | 2 | 1.49907 |
| Total | 19.4500 | 9 | 3.68562 |

## ACL vs. BPTB vs. ST/G Oneway ANOVA

**ANOVA**

Coeff

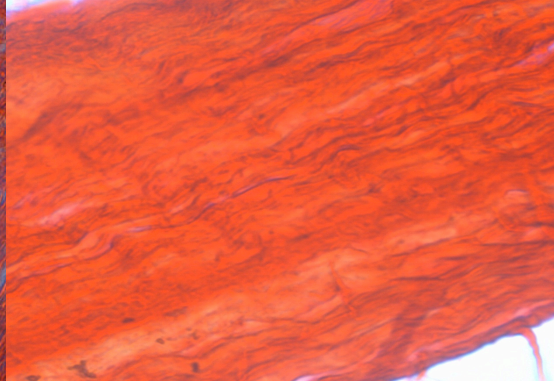|  | Sum of Squares | df | Mean Square | F | Sig. |
|---|---|---|---|---|---|
| Between Groups | 4.838 | 2 | 2.419 | .140 | .872 |
| Within Groups | 103.832 | 6 | 17.305 |  |  |
| Total | 108.671 | 8 |  |  |  |

# APPENDIX M: BRIGHTFIELD MICROSCOPY IMAGES

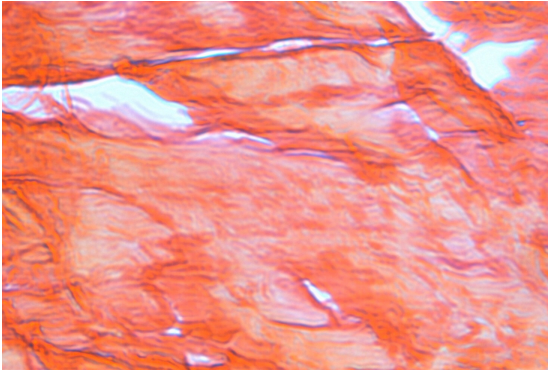## *ACL IMAGES*

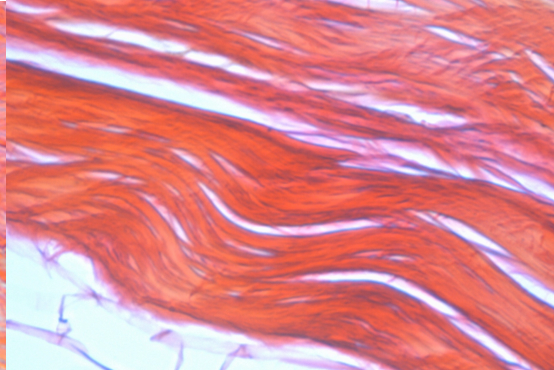Example Bad Image: ACL 1625R:          Example Good Image: ACL 1574L
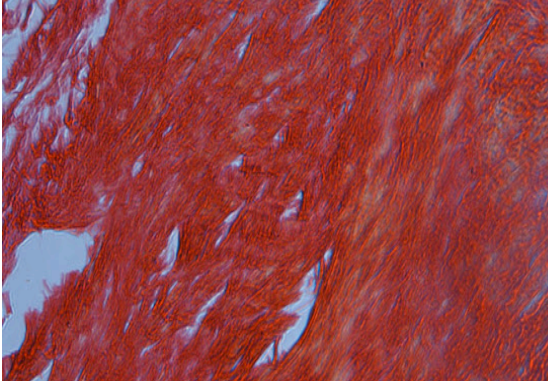


## *ST IMAGES*

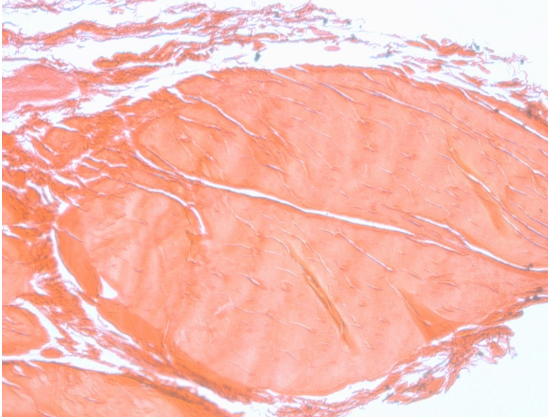Example Bad Image: ST 6990L:          Example Good Image: ST 2805R
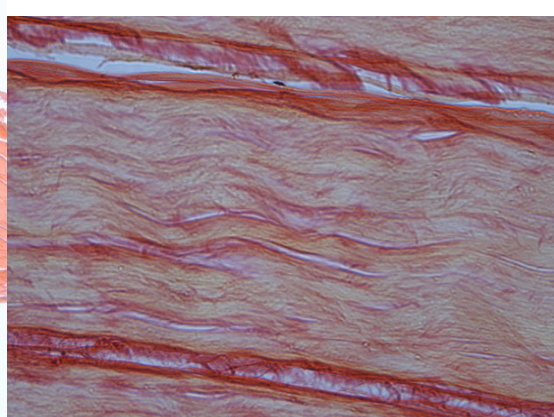


## *BPTB IMAGES*

Example Bad Image: BPTB 7999L:          Example Good Image: BPTB 7978L

# APPENDIX N: GLOSSARY

<u>Allograft</u>: tissue or organ transplanted from a cadaver organism of the same species.

<u>Arthroscopically Implanted Force Probe® (AIFP®)</u>: a small force transducer that is designed to be implanted into soft tissue. It is made of stainless steel that forms a spring structure that deforms when mechanically loaded and measures the local force present in the tissue (Microstrain, 2011).

<u>Autograft</u>: a graft of tissue transplanted from one part of an individual's body to another part of the body (AAOS, 2009).

<u>Anterior Cruciate Ligament (ACL)</u>: this ligament connects the tibia and femur, from the lateral femoral condyle to the intercondyloid eminence of the tibia.

<u>Biphasic</u>: describes a system with two phases. Biological soft tissues, such as ligaments and tendons, are described as biphasic due to the solid and liquid components.

<u>Bone-Patellar Tendon-Bone (BPTB) Graft</u>: an ACL graft where a section from the middle of the patellar tendon is excised along with two pieces of bone on the top and bottom of the patellar tendon. The tendon is shaped by the surgeon to ensure it will properly fit into the bone tunnel in the ACL and is then secured into the knee using interference screws (Wheeless, 2011).

<u>Brightfield Light Microscopy</u>: mode of microscopy in which samples are illuminated from below by white light and observed from above.

<u>Capsuloligamentous Structures</u>: smaller ligament-like entities grouped around joints, which provide structural support.

<u>Collagen</u>: the most common protein found in mammals, which may have various functions such as tissue assembly and maintenance, tissue scaffolding, cell adhesion, angiogenesis, etc (Franchi et al., 2008).

<u>Continuous Passive Motion (CPM)</u>: a treatment protocol intended to help recovery after joint surgery, by moving the joint passively with a motorized device, recovery is accelerated by decreasing soft tissue stiffness and increasing range of motion (The Center, 1999).

<u>Crimping</u>: arrangement of collagen fibers in a planar zig-zag pattern (Franchi et al., 2008).

<u>Fascicle</u>: a bundle or cluster.

<u>Graft Site Morbidity</u>: refers to any consequences resulting from harvesting a graft

from the patient's own body, such as chronic pain, scarring, or bleeding.

Interference Screw: a screw that serves as an anchoring point for a flexible transplant in bone.

Lachman Test: a diagnostic test used in clinical examination of suspected ACL tears.

Laxity: the quality or state of being lax or loose.

Ligament: a band of fibrous collagen tissue that attaches bones or cartilages (Franchi et al., 2008).

Materials testing system (MTS machine): an instrument that facilitates a variety of mechanical testing (compression, tension, torsion, etc).

Medial Collateral Ligament (MCL): a broad, flat ligament located on the medial side of the knee, often torn in conjunction with the ACL.

Muscoskeletal Transplant Foundation (MTF): non-profit service organization for donor muscoskeletal tissue.

One-Leg Hop Test: diagnostic test in which the patient hops on one leg for a distance that is then measured.

Optical Coherence Tomography (OCT): non-invasive imaging modality that utilizes long wavelengths of light to penetrate a scattering medium in order to obtain 3D images.

Posterior Cruciate Ligament (PCL): this ligament connects the tibia to the femur and crosses with the ACL inside the joint.

Semitendinosus and Gracilis (STG) Hamstring Graft: a graft composed of the semitendinosus and gracilis tendons from the hamstring.

Signal Conditioning Card: an electronic device that receives an analog input from a sensor and convert it to a measurable signal. In a force transducer the signal conditioning card will use a voltage source to covert the change in resistance in the force probe to a measurable voltage difference (National Instruments, 2010).

Stress Relaxation: stress applied to the tissue changes under a constant situation of strain.

Stress-Strain: a graph that shows the response of a material to increasing force. The plot includes stress (a measure of force applied over area) versus strain (the percent change in length of the material) (Roylance, 2001).

Tendon: a band of fibrous collagen tissue that attaches a muscle to a bone (Franchi et al. 2008).

Tensile Strength: the amount of force necessary to pull a material until it breaks (Engineers Edge).

Tension Transducer:  a force probe that converts mechanically sensed force into electric signals that can be used for measurement, they often use a variable resistor that changes resistance based on the force applied to it, this change in resistance is then converted to a voltage reading which can be correlated to force values (Cleveland Motion Controls).

Trim Pot: a trim-pot is an adjustable variable resistor, which is placed directly on a circuit board; it can be adjusted to change the set point or sensitivity of a measurement (Hewes, 2011).

Ultra-High Molecular-Weight (UHMW) Polyethylene: a thermoplastic that has very high toughness, wear resistance, and chemical resistance.  It is also very easy to machine (Ridout Plastics, 2012). Valgus Collapse: abnormal positioning of a limb that is twisted or bent inwards toward the midline.

Viscoelastic Creep: strain in the tissue changes while the stress applied to the tissue remains constant.

Viscoelasticity: property of a material that exhibits a different stress-strain relationship when it is being loaded as compared to when it is being unloaded.

# REFERENCES

AAOS. (2009). Bone and tissue transplantation. Retrieved from http://orthoinfo.aaos.org/topic.cfm?topic=a00115

Ahmed, A. M., & McLean, C. (2002). In vitro measurement of the restraining role of the anterior cruciate ligament during walking and stair ascent. *Journal of Biomechanical Engineering-Transactions of the ASME, 124*(6), 768-779.

Amiel, D., Frank, C., Harwood, F., Fronek, J., & Akeson, W. (1983). Tendons and ligaments: A morphological and biochemical comparison. *Journal of Orthopaedic Research*, *1*(3), 257–265.

Amiel, D., Kleiner, J. B., Roux, R. D., Harwood, F. L., & Akeson, W. H. (1986). The phenomenon of "ligamentization": Anterior cruciate ligament reconstruction with autogenous patellar tendon. *Journal of Orthopaedic Research, 4*(2), 162-172.

Amis, A. A., & Jakob, R. P. (1998). Anterior cruciate ligament graft positioning, tensioning and twisting. *Knee Surgery, Sports Traumatology, Arthroscopy, 6*(5), S2-S12.

Anderson, A. F., Snyder, R., & Lipscomb, A. B. (2001). Anterior cruciate ligament reconstruction: A prospective randomized study of three surgical methods. *The American Journal of Sports Medicine, 29*(3), 272-279.

Andrews, P. M., Chen, Y., Onozato, M. L., Huang, S. W., Adler, D. C., Huber, R. A., Jiang, J., Barry, S. E., Cable, A. E., & Fujimoto, J. G. (2008). High-resolution optical coherence tomography imaging of the living kidney. *Laboratory Investigation, 88*(4), 441-449.

Arnoczky, S. P. (1982). Anatomy of the anterior cruciate ligament. *Clinical Orthopaedics and Related Research, 172*(1), 19-25.

Arnold, M. R., Lie, D. T. T., Verdonschot, N., de Graaf, R., Amis, A. A., & van Kampen, A. (2005). The remains of anterior cruciate ligament graft tension after cyclic knee motion. *American Journal of Sports Medicine, 33*(4), 536-542.

Arthrex. (2010). ACL reconstruction with ACL Tightrope®: Surgical technique. Retrieved from www.arthrex.com/myarthrex/surgicaltechniques/index.cfm

Beynnon, B. D., Johnson, R. J., Fleming, B. C., Kannus, P., Kaplan, M., Samani, J., Renstrïm, P. (2002). Anterior cruciate ligament replacement: Comparison of bone-patellar tendon-bone grafts with two-strand hamstring grafts: A prospective, randomized study. *The Journal of Bone and Joint Surgery, 84*(9), 1503-1513.

Biau, D. J., Katsahian, S., Kartus, J., Harilainen, A., Feller, J. A., Sajovic, M., Ejerhed, L., Zaffagnini, S., Röpke, M., & Nizard, R. (2009). Patellar tendon versus hamstring tendon autografts for reconstructing the anterior cruciate ligament: a meta-analysis based on individual patient data. *The American Journal of Sports Medicine, 37*(12), 2470-2478.

Biau, D. J., Tournoux, C., Katsahian, S., Schranz, P. J., & Nizard, R. S. (2006). Bone-patellar tendon-bone autografts versus hamstring autografts for reconstruction of anterior cruciate ligament: Meta-analysis. *British Medical Journal*, *332*(7548), 995-998.

Blevins, F. T., Hecker, A. T., Bigler, G. T., Boland, A. L., & Hayes, W. C. (1994). The effects of donor age and strain rate on the biomechanical properties of bone-patellar tendon-bone allografts. *The American Journal of Sports Medicine, 22*(3), 328-33.

Blythe, A., Tasker, T., & Zioupos, P. (2006). ACL graft constructs: *In-vitro* fatigue testing highlights the occurrence of irrecoverable lengthening and the need for adequate (pre)conditioning to avert the recurrence of knee instability. *Technology and Health Care, 14*(1), 335-347.

Boden, B. P., Dean, G. S., Feagin, J. A., & Garrett, W. E. Jr. (2000). Mechanisms of anterior cruciate ligament injury. *Orthopedics, 23*(6), 573-578.

Boden, B. P., Sheehan, F. T., Torg, J. S., & Hewett, T. E. (2010). Noncontact anterior cruciate ligament injuries: Mechanisms and risk factors. *The Journal of the American Academy of Orthopaedic Surgeons, 18*(9), 520-527.

Bontempi, M. (2009). Probabilistic model of ligaments and tendons: Quasistatic linear stretching. *Physical Review E: Statistical, Nonlinear, and Soft Matter Physics, 79*(3), 030903-1-030903-4.

Chandrashekar, N., Hashemi, J., Slauterbeck, J., & Beynnon, B. D. (2008). Low-load behaviour of the patellar tendon graft and its relevance to the biomechanics of the reconstructed knee. *Clinical Biomechanics, 23*(7), 918-925.

Chen, Y., Aguirre, A.D., Ruvinskaya, L., Devor, A., Boas, D.A., Fujimoto, J.G. (2009). Optical coherence tomography (OCT) reveals depth-resolved dynamics during functional brain activation. *Journal of Neuroscience Methods, 178*(1), 162-173.

Clark, J. W. (2010). *Medical instrumentation: Application and design*. J. G. Webster, (Ed.). Hoboken, NJ: John Wiley & Sons.

Clavert, P., Kempf, J.-F., Bonnomet, F., Boutemy, P., Marcelin, L., & Kahn, J.-L. (2007). Effects of freezing/thawing on the biomechanical properties of human tendons. *Surgical and Radiologic Anatomy*, *23*(4), 259-262.

Cleveland Motion Controls. Tension load cells and tension transducers. Retrieved from http://www.cmccontrols.com/tension-load-cell.asp

Cooper, J. A., Lu, H. H., Ko, F. K., Freeman, J. W., & Laurencin, C. T. (2005). Fiber-based tissue-engineered scaffold for ligament replacement: design considerations and in vitro evaluation. *Biomaterials, 26*(13), 1523-1532.

Daniel, D. M., Stone, M. L., Dobson, B. E., Fithian, D. C., Rossman, D. J., & Kaufman, K. R. (1994). Fate of the ACL-injured patient: A prospective outcome study. *The American Journal of Sports Medicine, 22*(5), 632-644.

Dargel, J., Gotter, M., Mader, K., Penning, D., Koebke, J., & Schmidt-Wiethoff, R. (2007). Biomechanics of the anterior cruciate ligament and implications for surgical reconstruction. *Strategies in Trauma and Limb Reconstruction, 2*(1), 1-12.

Diamant, J., Keller, A., Baer, E., Litt, M., & Arridge, R. G. C. (1972). Collagen: Ultrastructure and its relation to mechanical properties as a function of ageing. *Proceedings of the Royal Society B: Biological Sciences*, *180*(60), 293-315.

Dugan, S. A. (2005). Sports-related knee injuries in female athletes: What gives? *American Journal of Physical Medicine and Rehabilitation, 84*(2), 122-130.

Engineers Edge. Strength of materials- mechanics of materials. Retrieved from http://www.engineersedge.com/strength_of_materials.htm

Eriksson, K., Anderberg P., Hamberg P., Olerud P., & Wredmark T. (2001). There are differences in early morbidity after ACL reconstruction when comparing patellar tendon and semitendinosus tendon graft: A prospective randomized study of 107 patients. *Scandinavian Journal of Medicine & Science in Sports*, *11*(3), 70-77.

Fercher, A. (1996). Optical coherence tomography. *Journal of Biomedical Optics*, *1*(2), 157-173.

Flahiff, C. M., Brooks, A. T., Hollis, J. M., Vander Schilden, J. L., & Nicholas, R. W. (1995). Biomechanical analysis of patellar tendon allografts as a function of donor age. *The American Journal of Sports Medicine, 23*(3), 354-58.

Fleming, B. C., Peura, G. D., & Beynnon, B.D. (2000). Factors influencing the output of an implantable force transducer. *Journal of Biomechanics, 33*(7), 889-893.

Fleming, B. C., Vajapeyam, S., Connolly, S. A., Magarian, E. M., & Murray, M. M. (2011). The use of magnetic resonance imaging to predict ACL graft structural properties. *Journal of Biomechanics*, *44*(16), 2843-2846.

Franchi, M., Fini, M., Quaranta, M., De Pasquale, V., Raspanti, M., Giaversi, G., Ottani, V., & Ruggeri, A. (2007A). Crimp morphology in relaxed and stretched rat Achilles tendon. *Journal of Anatomy, 210*(1), 1-7.

Franchi, M., Ottani, V., Stagni, R., & Ruggeri, A. (2010). Tendon and ligament fibrillar crimps give rise to left-handed helices of collagen fibrils in both planar and helical crimps. *Journal of Anatomy, 216*(3), 301-309.

Franchi, M., Quaranta, M., Macciocca, M., De Pasquale, V., Ottani, V., & Ruggeri, A. (2009). Structure relates to elastic recoil and functional role in quadriceps tendon and patellar ligament. *Micron, 40*(3), 370-377.

Franchi, M., Raspanti, M., Dell'Orbo, C., Quaranta, M., De Pasquale, V., Ottani, V., & Ruggeri, A. (2008). Different crimp patterns in collagen fibrils relate to the subfibrillar arrangement. *Connective Tissue Research*, *49*(2), 85-91.

Franchi, M., Trirè, A., Quaranta, M., Orsini, E., & Ottani, V. (2007B). Collagen structure of tendon relates to function. *The Scientific World Journal, 7*(1), 404-420.

Frank, C. B., & Jackson, D. W. (1997). "Current concepts review: The science of reconstruction of the anterior cruciate ligament." *Journal of Bone and Joint Surgery*, *79*(10), 1556-76.

Freeman, J. W. (2009). Tissue engineering options for ligament healing. *Bone and Tissue Regeneration Insights, 2*, 13-23.

Friederich, N. F., & O'Brien, W. R. (1998). Anterior cruciate ligament graft tensioning versus knee stability. *Knee Surgery, Sports Traumatology, Arthroscopy, 6*(1), S38-S42.

Fujimoto, J. G. (2003). Optical coherence tomography for ultrahigh resolution *in vivo* imaging. *Nature Biotechnology, 21*(11), 1361-1367.

Fukubayashi, T., Torzilli, P. A., Sherman, M. F., & Warren, R. F. (1982). An *in vitro* biomechanical evaluation of anterior-posterior motion of the knee. Tibial displacement, rotation, and torque. *Journal of Bone and Joint Surgery, American Version, 64*(2), 258-264.

Gao, S. S., Xia, A., Yuan, T., Raphael, P. D., Shelton, R. L., Applegate, B. E., & Oghalai, J. S. (2011). Quantitative imaging of cochlear soft tissues in wild-type and hearing-impaired transgenic mice by spectral domain optical coherence tomography. *Optics Express, 19*(16), 15415-15428.

Garrett, J. C. (2011). Transtibial ACL reconstruction system for BTB grafts: Surgical technique. Retrieved from http://www.arthrex.com/myarthrex/surgicaltechniques/index.cfm

Goh, K. L., Chen, Y., Chou, S. M., Listrat, A., Bechet, D., & Wess, T. J. (2010). Effects of frozen storage temperature on the elasticity of tendons from a small murine model. *Animal, 4*(9), 1613-1617.

Górios, C., Hernandez, A. J., Amatuzzi, M. M., Leivas, T. P., Pereira, C. A. M., Neto, R. B., & Pereira, E. D. S. (2001). Rigidity of the knee anterior cruciate ligament and grafts to reconstruct it with the patellar ligament and with the semitendinosus and gracilis muscles. *Acta Ortopédica Brasileira, 9*(2), 26-39.

Gottlob, C. A., Baker, C. L., Pellissier, J. M., & Colvin, L. (1999). Cost effectiveness of anterior cruciate ligament reconstruction in young adults. *Clinical Orthopaedics and Related Research, 367*, 272-282.

Hadjicostas, P. T., Soucacos, P. N., Koleganova, N., Piecha, G., Krohmer, G., & Berger, I. (2008). Comparative analysis of the microstructure of the hamstring tendons: an electron microscopic, histologic, and morphologic study. *Journal of Surgical Orthopaedic Advances, 17*(3), 153-158.

Hansen, K. A., Weiss, J. A., & Barton, J. K. (2002). Recruitment of tendon crimp with applied tensile strain. *Journal of Biomechanical Engineering-Transactions of the ASME, 124*(1), 72-77.

Hariri, L. P., Bonnema, G. T., Schmidt, K., Winkler, A. M., Korde, V., Hatch, K. D., Davis, J. R., Brewer, M. A., & Barton, J. K. (2009). Laparoscopic optical coherence tomography imaging of human ovarian cancer. *Gynecologic Oncology*, *114*(2), 188-194.

Hashemi, J., Chandrashekar, N., & Slauterbeck, J. (2005). The mechanical properties of the human patellar tendon are correlated to its mass density and are independent of sex. *Clinical Biomechanics, 20*(6), 645-52.

Herzog, W., Hasler, E. M., & Leonard, T. R. (1996). *In-situ* calibration of the implantable force transducer. *Journal of Biomechanics, 29*(12), 1649-1652.

Hewes, John. (2011). Variable resistors. Retrieved from http://www.kpsec.freeuk.com/components/vres.htm

Holzapfel, G. A. (2000). Biomechanics of soft tissue. Retrieved from http://biomechanics.stanford.edu/me338/me338_project02.pdf

Hospodar, M. S. J., & Miller, M. D. (2009). Controversies in ACL reconstruction: Bone-patellar Tendon-bone anterior cruciate ligament reconstruction remains the gold standard. *Sports Medicine and Arthroscopy Review, 17*(4), 242-246.

Huang, D., Swanson, E. A., Lin, C. P., Schuman, J. S., Stinson, W. G., Chang, W., Hee, M. R., Flotte, T., Gregory, K., Puliafito, C.A., et al. (1991A). Optical coherence tomography. *Science*, *254*(5035), 1178-1181.

Huang, D., Wang, J., Lin, C. P., Puliafito, C. A., & Fujimoto, J. G. (1991B). Micron-resolution ranging of cornea anterior chamber by optical reflectometry. *Lasers in Surgery and Medicine, 11*(5), 419–425.

Huang, H., Zhang, J., Sun, K., Zhang, X., & Tian, S. (2011). Effects of repetitive multiple freeze-thaw cycles on the biomechanical properties of human flexor digitorum superficialis and flexor pollicis longus tendons. *Clinical Biomechanics, 26*(4), 419-423.

Izatt, J. A., Hee, M. R., Swanson, E. A., Lin, C. P., Huang, D., Schuman, J. S., Puliafito, C. A., & Fujimoto, J. G. (1994). Micrometer-scale resolution imaging of the anterior eye *in vivo* with optical coherence tomography. *Archives of Ophthalmology, 112*(12), 1584-1589.

Jarvinen, T.A., Jarvinen, T.L., Kannus, P., Jozsa, L., & Jarvinen, M. (2004). Collagen fibres of the spontaneously ruptured human tendons display decreased thickness and crimp angle. *Journal of Orthopaedic Research, 22*(6), 1303-1309.

Jarvinen, T.A., Jozsa, L., Kannus, P., Jarvinen, T.L., & Jarvinen, M. (2002). Organization and distribution of intramuscular connective tissue in normal and immobilized skeletal muscles. *Journal of Muscle Research and Cell Motility, 23*(3), 245-254.

Jung, H.-J., Gautum, V., Fisher, M.B., Yang, G., Hsu, S., Bianchi, J., Ronholdt, C., & Woo, S.L.Y. (2011). The effects of multiple freeze-thaw cycles on the biomechanical properties of the human bone-patellar tendon-bone allograft. *Journal of Orthopaedic Research, 29*(8), 1193-1198.

Kannus, P. (2000). Structure of the tendon connective tissue. *Scandinavian Journal of Medicine & Science in Sports, 10*, 312-320.

Kakarlapudi, T. K., & Bickerstaff, D. R. (2000). Knee instability: isolated and complex. *British Journal of Sports Medicine, 34*(5), 395-400.

Kiernan, J.A. (2011). Sirius red staining protocol for collagen. Retrieved from http://www.ihcworld.com/_protocols/special_stains/sirius_red.htm

Kondo, E., Yasuda, K., Katsura, T., Hayashi, R., Kotani, Y. & Tohyama, H. (2012). Biomechanical and histological evaluations of the doubled semitendinosus tendon autograft after anterior cruciate ligament reconstruction in sheep. *American Journal of Sports Medicine*, *40*, 315-324.

Laurencin, C. T., & Freeman, J. W. (2005). Ligament tissue engineering: An evolutionary materials science approach. *Biomaterials, 26*(36), 7530-7536.

Li, S., Su, W., Zhao, J., Xu, Y., Bo, Z., Ding, X., Wei, Q. (2010). A meta-analysis of hamstring autografts versus bone–patellar tendon–bone autografts for reconstruction of the anterior cruciate ligament. *The Knee, 18*(5), 287–293.

Li, Q., Onozato, M. L., Andrews, P. M., Chen, C. W., Paek, A., Naphas, R., Yuan, S., Jiang, J., Cable, A,. & Chen, Y. (2009). Automated quantification of microstructural dimensions of the human kidney using optical coherence tomography (OCT). *Optics Express, 17*(18), 16000-16016.

Liu, S. H., Kabo, J. M., & Osti, L. (1995). Biomechanics of two types of bone-tendon-bone graft for ACL reconstruction. *Journal of Bone and Joint Surgery, American Version, 77-B*, 232-235.

Markolf, K. L., Wascher, D. C., & Finerman, G. A. (1993). Direct *in vitro* measurement of forces in the cruciate ligaments. Part II: The effect of section of the posterolateral structures. *Journal of Bone and Joint Surgery, American Version, 75*(3), 387-394.

Marumo, K., Saito, M., Yamagishi, T., & Fujii, K. (2005). The "ligamentization" process in human anterior cruciate ligament reconstruction with autogenous patellar and hamstring tendons: a biochemical study. *The American Journal of Sports Medicine, 33*(8), 1166-1173.

MicroStrain. (2011). Arthroscopically implantable force probe. Retrieved from http://www.microstrain.com/displacement/aifp

More, R. C., & Markolf, K. L. (1988). Measurement of stability of the knee and ligament force after implantation of a synthetic anterior cruciate ligament. In vitro measurement. *Journal of Bone and Joint Surgery, American Version, 70*(7), 1020-1031.

Morrison, J. B. (1970). "The mechanics of the knee joint in relation to normal walking." *Journal of Biomechanics, 3*(1), 51-61.

Munson, B.R., Young, D.F., Okiishi, T. H., & Huebsch, W.W. (2009). *Fundamentals of fluid mechanics* (6th ed.).  John Wiley & Sons, Inc.

National Instruments. (2010). What is signal conditioning?. Retrieved from http://zone.ni.com/devzone/cda/tut/p/id/10630

Nordin, M. & Frankel, V.H. (2001). *Basic biomechanics of the musculoskeletal system* (3rd ed.). J. Butler, (Ed.). Baltimore, MD: Lippincott Williams & Wilkins.

Noyes, F., Butler D., Grood , E., Zernicke, R., Hefzy, M. (1984). Biomechanical analysis of human ligament grafts used in knee-ligament repairs and reconstructions. *Journal of Bone and Joint Surgery*, *66*(3), 344-52.

O'Donoghue, D. H. (1950). Surgical treatment of fresh injuries to the major ligaments of the knee. *Journal of Bone and Joint Surgery, 32*(1), 721-738.

Olberding, J. E., & Suh, J. K. F. (2006). A dual optimization method for the material parameter identification of a biphasic poroviscoelastic hydrogel: Potential application to hypercompliant soft tissues. *Journal of Biomechanics, 39*(13), 2468-2475.

OptiFlex 3 knee continuous passive motion. (2012). Retrieved October 29, 2009 from http://www.southwestmedical.com/products/OptiFlex-3-Knee-Continuous-Passive-Motion-3582.html

Oza, A. L., Vanderby. R., Lakes, R.S. (2006). Creep and relaxation in ligament: Theory, methods and experiment. In G.A. Holzapfel & R.W. Ogden (Eds.), *Mechanics of biological tissue* (379-397). Germany: Springer.

Özkaya, N., & Nordin, M. (1999). *Fundamentals of biomechanics* (2nd ed.). D.L. Leger, (Ed.). New York, NY: Springer.

Paterno, M. V., Weed, A. M., & Hewett, T. E. (2012). A between sex comparison of anterior-posterior knee laxity after anterior cruciate ligament reconstruction with patellar tendon or hamstrings autograft: A systematic review. *Sports Medicine, 42*(2), 135-152.

Patterson-Kane, J.C., Firth, E.C., Goodship, A.E., & Parry, D.A.D. (1997). Age-related differences in collagen crimp patterns in the superficial digital flexor

tendon core region of untrained horses. *The Journal of the Australian Veterinary Association*, *75*(1), 39-44.

Patterson-Kane, J.C., Wilson, A.M., Firth, E.C., Parry, D.A.D., & Goodship, A.E. (1998). Exercise-related alterations in crimp morphology in the central regions of superficial digital flexor tendons from young thoroughbreds: A controlled study. *Equine Veterinary Journal*, *30*(1), 61-64.

Pinczewski, L., Roger, G., & Scranton Jr., P. E. (1998). Surgical technique for hamstring and patellar tendon grafts: Using the RCI interference screw. Retrieved from http://endo.smith-nephew.com/au/Standard.asp?NodeId=2554

Polysciences. (2010). Data sheet #837: FAQ: Picrosirius red stain kit. Retrieved from http://www.polysciences.com/Core/Display.aspx?pageId=98&productId=2744&categoryId=50

Purslow, P. P., Wess T. J., & Hukins, D. W. L. (1998). Collagen orientation and molecular spacing during creep and stress-relaxation in soft connective tissues. *Journal of Experimental Biology, 201*(1), 135-142.

QImaging. (2012). Product datasheet: QCapture pro 7™ software. Retrieved from http://www.qimaging.com/products/software/#qcappro

Quatman, C. E. & Hewett, T. E. (2009). The anterior cruciate ligament injury controversy: Is "valgus collapse" a sex-specific mechanism? *British Journal of Sports Medicine, 43*(5), 328-335.

Raspanti M., Manelli A., Franchi, M., & Ruggeri, A. (2005) The 3D structure of crimps in the rat Achilles tendon. *Matrix Biology, 24*(7), 503–507.

Rich, L., & Whittaker, P. (2005). Collagen and picrosirius red staining: A polarized light assessment of fibrillar hue and spatial distribution. *Brazilian Journal of Morphology Science, 22*(2), 97-104.

Ridout Plastics. (2012). UHMW: Sheet, rod, tube. Retrieved from http://www.eplastics.com/Plastic/UHMW

Roylance, D. (2001). Stress-strain curves. Retrieved from http://ocw.mit.edu/index.htm

Rupp, S., Sell, R., Kohn, D., & Müller, B. (2000). The influence of avascularity on the mechanical properties of human bone-patellar-tendon-bone grafts. *Journal of Bone and Joint Surgery, 82*(7), 1059-1064.

Screen, H. R., Lee, D. A., Bader, D. L., & Shelton, J. C. (2004). An investigation into the effects of the hierarchical structure of tendon fascicles on micromechanical properties. *Proceedings of the Institution of Mechanical Engineers. Part H, Journal of Engineering in Medicine, 218*(2), 109-119.

Sekiguchi, H., Post, W.R., Han, J.S., Ryu, J., & Kish, V. (1998). The effects of cyclic loading on tensile properties of a rabbit femur–anterior cruciate ligament–tibia complex (FATC). *The Knee, 5*(3), 215-220.

Shadwick, R.E. (1990). Elastic energy storage in tendons: Mechanical differences related to function and age. *Journal of Applied Physiology, 68*(3), 31033-31040

Shah, J. S., Jayson, M. I., & Hampson, W. G. (1977). Low-tension studies of collagen fibers from ligaments of the human spine. *Annals of the Rheumatic Diseases, 36*(2), 139-145.

Shah, J. S., Jayson, M. I. V., & Hampson, W. G. J. (1979). Mechanical implications of crimping in collagen fibres of human spinal ligaments. *Engineering in Medicine*, *8*(2), 95-102.

Shelbourne, K. D. & Nitz, P. A. (1991). The O'Donoghue triad revisited: Combined knee injuries involving anterior cruciate and medial collateral ligament tears. *American Journal of Sports Medicine, 19*(5), 474-477.

Simonian, P. T., Cole, B. J., & Bach, B. R. (Eds.). (2006). *Sports injuries of the knee: Surgical approaches*. New York, NY: Thieme Medical Publishers, Inc.

Sohrab, G., Smith, J. T., & West, H. S. Jr. (2011). ACL solutions. Retrieved from http://www.aclsolutions.com

Strocchi, R., de Pasquale, V., Gubellini, P., Facchini, A., Marcacci, M., Buda, R., Zaffagnini, S., & Ruggeri, A. (1992). The human anterior cruciate ligament: Histological and ultrastructural observations. *Journal of Anatomy, 180*(3), 515-519.

The Center for Orthopaedics and Sports Medicine. (1999). Continuous passive motion. Retrieved from http://www.arthroscopy.com/sp06001.htm

Tohyama, H., Beynnon, B. D., Fleming, B. C., Peura, G. D., Johnson, R. J., & Pope e, M.H. (1994). Evaluation of the arthroscopic force probe: A study of the factors that effect the measurement of tendon and ligament force in-vivo. *Transactions of the Orthopaedic Research Society, 19*, 644.

Toth, A. P. & Cordasco F. A. (2001). Anterior cruciate ligament injuries in the female athlete. *The Journal of Gender-Specific Medicine, 4*(4), 25-34.

Wascher, D. C., Markolf, K. L., Shapiro, M. S., & Finerman, G. A. (1993). Direct in vitro measurement of forces in the cruciate ligaments. Part I: The effect of multiplane loading in the intact knee. *Journal of Bone and Joint Surgery, 75*(3), 377-386.

Werner, M., Chott, A., Fabiano, A., & Battifora, H. (2000). Effect of formalin tissue fixation and processing on immunohistochemistry. *American Journal of Surgical Pathology, 24*(7), 1016-1019.

Wheeless, C. R. III. (2011). Biomechanics of ACL. Retrieved from http://www.wheelessonline.com/ortho/biomechanics_of_acl

Wolfgang, E., & Bernd, M. (2001). A linear viscoelastic biphasic model for soft tissues based on the theory of porous media. *Journal of Biomechanical Engineering, 123*(5), 418-424.

Woo, S. L. Y., Chan, S. S., & Yamaji, T. (1997). Biomechanics of knee ligament healing, repair and reconstruction. *Journal of Biomechanics, 30*(5), 431-439.

Woo, S. L. Y., Debski, R. E., Zeminski, J., Abramowitch, S. D., Saw, S. S. C., & Fenwick, J. A. (2000). Injury and repair of ligaments and tendons. *Annual Review of Biomedical Engineering, 2*, 83-118.

Woo, S. L-Y., Fox, R. J., Sakane, M., Livesay, G. A., Rudy, T. W., & Fu, F. H. (1998). Biomechanics of the ACL: Measurement of in situ forces in the ACL and knee kinematics. *The Knee, 5*(4)*,* 267-288.

Woo, S. L. Y., Kanamori, A., Zeminski, J., Yagi, M., Papageorgiou, C., & Fu, F. H. (2002). The effectiveness of reconstruction of the anterior cruciate ligament with hamstrings and patellar tendon - A cadaveric study comparing anterior

tibial and rotational loads. *Journal of Bone and Joint Surgery-American Volume, 84A*(6), 907-914.

Woo, S. L.-Y., Wu, C., Dede, O., Vercillo, F., & Noorani, S. (2006). Biomechanics and anterior cruciate ligament reconstruction. *Journal of Orthopaedic Surgery and Research, 1*(2), 1-9.